UNIVERSITY
OF TRENTO - Italy
DEPARTMENT OF INDUSTRIAL ENGINEERING

XXVIII cycle

Doctoral School in Materials Science and Engineering

Biomimetic and Bioinspired Biologically Active Materials

Thi Duy Hanh Le

Tutor
Claudio Migliaresi, prof.
Antonella Motta, prof.

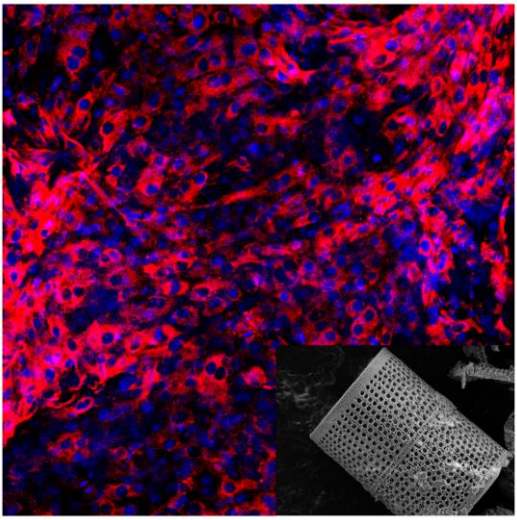

March 2016

BIOMIMETIC AND BIOINSPIRED BIOLOGICALLY ACTIVE MATERIALS

THI DUY HANH LE

E-mail: thiduyhanh.le@unitn.it

Approved by:

Prof. Claudio Migliaresi, Advisor
Department of Industrial Engineering,
University of Trento, Italy.

Prof. Antonella Motta, Co-advisor
Department of Industrial Engineering,
University of Trento, Italy.

Ph.D. Commission:

Prof. ssa Ilaria Cristofolini,
Department of Industrial Engineering
University of Trento, Italy.

Prof. Paolo Antonio Netti,
Dipartimento di Ingegneria Chimica,
dei Materiali, e della Produzione
industriale.
University of Naples Federico II, Italy.

Prof. Maurizio Vedani,
Dipartimento Meccanica
Politecnico of Milano,Italy.

University of Trento,

Department of Industrial Engineering

March 2016

University of Trento - Department of Industrial Engineering

Doctoral Thesis

Thi Duy Hanh Le - 2016
Published in Trento (Italy) – by University of Trento

ISBN: - - - - - - - - -

… To people who come into my life…by anyway..

Sometime, I forget to thank you…
But I cannot express how much I appreciate…

CONTENTS

List of figure

List of tables

ABSTRACT

Tissue engineering is an interdisciplinary field aimed to design and engineer an efficient system for tissue and organ regeneration, for instance, for bone healing, based on the combined use of scaffolds, cells, bioactive or signalling molecules.

An optimal tissue engineering procedure requires materials and scaffolds fulfilling several requirements, one of those being the ability to trigger and control the crosstalk with the biological environment both in vitro and in vivo, and to induce and control the extracellular matrix production and assembling.

Diatomite is one of the most abundant natural sources of hydrated amorphous silica resulting from the accumulation of diatom skeletons. Diatoms possess particular features in structure, morphology as well as composition. Interestingly, it has been recognized that the formation process of diatom skeleton is possibly related to that of human bone.

In this study, we wanted to utilize diatoms as silicon donor additives in scaffolds for bone tissue engineering, having been demonstrated the important role of silicon in bone formation.

In this first part of the project, we used several methods to eliminate impurities in the raw diatomite. Diatom microparticles (DMPs) and nanoparticles (DNPs) were successfully produced by fragmentation of purified diatoms under alkaline condition. Our result showed that both DMPs and DNPs were able to release silicon, as detected in-vitro by inductively coupled plasma optical emission spectrometry (ICP/OES). In addition, diatom microparticles and nanoparticles - derived from diatom skeletons - showed minimal or non-cytotoxic effects in-vitro as determined by lactate dehydrogenase assays on cell cultures.

These findings suggest that diatom particles derived from diatom skeleton as a silicon donor might have potential use for bone tissue engineering.

In the second part of this thesis, we studied the effect of diatom particles on some properties of silk fibroin/diatom particles scaffolds. To handle this task, a series of fibroin scaffolds loaded with different amounts and size of diatom particles (microparticles, nanoparticles and their combination) were fabricated by using the salt leaching

method. Diatom particles addition influenced scaffold morphology and mechanical properties, and its biological behaviour as assessed on human osteosarcoma cell line MG63 cultures. Scaffolds loaded with diatom particles strongly enhanced cell adhesion, metabolic activity and proliferation. Moreover, the possible beneficial effect of the addition of diatoms particles to silk fibroin on early bone formation was determined through collagen type I synthesis evaluation, osterix expression and alkaline phosphatase induction.

Cultures with human mesenchymal stem cells (hMSCs) demonstrated the silk/diatom particles scaffolds were able to induce the differentiation of progenitor cells.

In conclusion, our findings provided strong evidence for a potential use of diatom particles- derived from natural diatom skeleton in biological applications, in particular for bone tissue regeneration.

Chapter 1: General Introduction

1.1 General introduction on diatoms

Diatom is a single eukaryotic cell belonging microalgae groups, found in diverse environments such as fresh water, sea or even in moist soil or surfaces.

Diatom skeleton greatly varies in shape, ranging from box-shaped to cylindrical shape with different symmetric properties. More than 10^4 diatom species are identified in the environment including living cells and fossils [1], [2].

Diatom cell structure, indeed, is comprised of a true nucleus and many organelles, which include mitochondria and chloroplasts organelles (plastids) and the endoplasmic reticulum (ER). All soft parts of diatom cells are surrounded by a standard lipid bilayer membrane (plasmalemma) tightly enclosed by cell wall, so-called diatom frustule [3], [4].

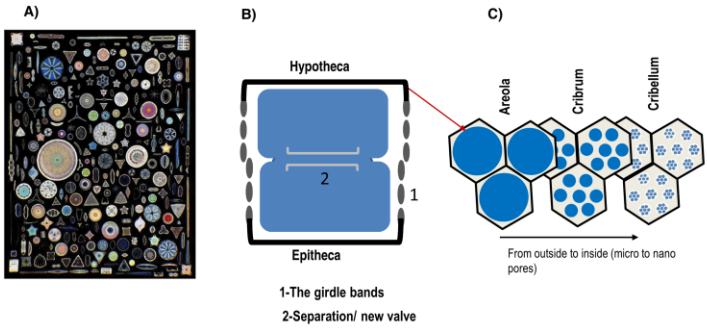

Figure 1-1: a) Diversity of diatom morphology in different sources including fossil, freshwater and marine environment [1], b) Diatom skeleton structure and c) the patterned porous structure of the gird bands.

Diatom frustule, i.e. the hard and porous cell siliceous wall or external layer of diatoms (Figure 1-1 B and C), is generally structured by two parts like a petri-dish, also termed as theca. Classically, epitheca defines the bigger valve or the parent valve while hypotheca is the smaller one.

Each theca in turn consists of a valve (upper and lower part, respectively) and several bands of silica (girdle bands) at the circumference of the cell [5],[6].
For many diatoms, frustule can be categorized in three major layers, named foramen (the most inward), the cribrum and the cribellum (most outward) [7].
Chemical composition of diatom frustule comprises both inorganic and organic components which are strongly associated each other. Hydrated amorphous silica, $SiO_2.nH_2O$, was identified as the major component of diatom frustule whilst organic components including silaffin proteins, long chain polyamines (LCPA), and polysaccharides have the role to strengthen the silica structure and protect diatom skeleton preventing the spontaneous dissolution in the environment [8]–[10].

1.2 Organic component of diatom cell wall

It is known that the scaffold of frustule is a hybrid of organic and inorganic materials but the formation, structure and function of organic matters during cell wall formation is not clear yet. Organic compounds, mainly proteins and Long chain polyamines, LCPA, form the diatom cell wall [11], [12].

1.2.1 Long chain polyamines

Long chain polyamines (LCPA) have generally a (N-methylated-) poly(propyleneimine) chain with up to 20 repeating units depending on the diatom species, presented in the Figure 1-2. Molecular mass of LCPA is commonly below 3.5 kDa [13].

1.2.2 Cell wall proteins

Diatom cell wall proteins can be categorized into three families: silaffins, frustulins, pleuralins.

1.2.2.1 Frustulins

Frustulin family has been identified as a calcium - binding glycoprotein, is categorized in α, β, γ and δ –frustulins with molecular masses at 75, 105, 150 and 200 kDa, respectively. However, the amino acid sequence data of β, γ and δ – frustulin state is similar to α-state. In diatom skeleton, frustulins are found in the outer surface of cell wall and function as a protector. The contribution of frustulins

to silicification of diatom frustule is not well understood, however frustulins may affect the shape of diatom by affecting the interaction between different proteins, especially in the case of pennate diatoms [14],[15].

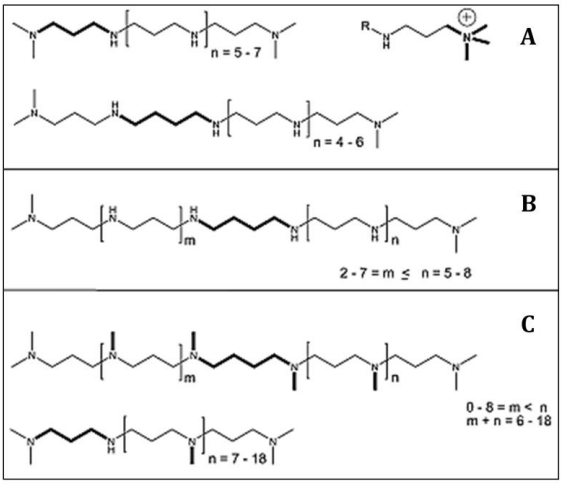

Figure 1-2: Chemical structures of some long-chain polyamines characteristic of three different diatom species a) T. Fseudonana, b) C. Fusiformis and c) S. Turris [16].

1.2.2.2 Pleuralins

Pleuralins, formerly known as HF-extractable protein (HEPs), have molecular weight of 130 and 150 kDa. Pleuralins possess high anionic charge in the range of -83 to -87 in physiological pH [17].
It has been known that both frustulins and pleuralins are not involved in silicification of diatom frustule through the silica deposition pathway. However, it has been postulated that pleuralins, located and tightly associated with silica at the overlapping region of two girdle bands, could be related with the on–off function of these connecting girdle bands during diatom cytokinesis. The strong interaction between pleuralins and silica may be also involved in this

phenomenon, although mechanism of the association is unclear [12],[17].

1.2.2.3 Silaffins

Silaffin is comprised of peptides with different functional molecular groups such as phosphate, sulphate, glucose, methyl, and others, as reported in Table 1-1 [9],[18].

Table 1-1 Numerous silaffin's maturation formed by precursor variants and different post- translational modification, adapted from [18]

Diatoms	**Silaffin**	**PMTs at positions**		**Induced Silica ability**	**Ref.**
		Lysine	**Hydroxyl of amino acids**		
C. Fusiformis	Sil 1A & 1B	Ethylations and polyamine modification at ε-amino group; Hydroxylation and phosphorylation at δ-position	Phosphorylation	Yes	[19], [20]
	Sil -2		Sulphfation, glycosylation and phosphorylation	No	[21]
T. *Pseudonana*	tpsil-1H, tpsil-2H	Methylations and polyamine modification at ε-amino group; hydroxylation and phosphorylation at δ-position	Sulphation, glycosylation and phosphorylation	No	[22], [23]
	tpsil-1L tpsil-2L			No	
E. *Zodiacu*		Methylations and polyamine modification at ε-amino group	Not analysed	Not analysed	[24]
C. Gracilis				Yes	[25]

A variety of silaffins have been identified, depending on diatom species and post-translational modification process (PMT). Diatom genes encoding for silaffin precursors are functionalized by a

complex maturation process. It was found that most silaffins are very rich in Lysine and Serine [19], [26].

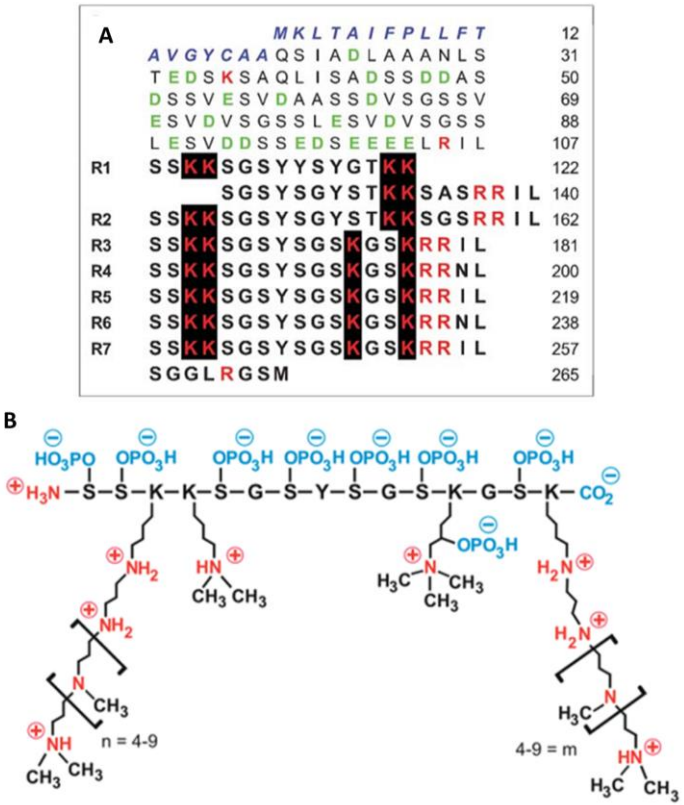

Figure 1-3: A) the primary structure of peptide precursors sil1p presenting the signal peptide (italics), highly acidic peptide sequence attached regular peptides (108- 271) is shown silaffin sequences. Abbreviation for amino acids is followed as A, Ala; C, Cys; D, Asp; E, Glu; F, Phe; G, Gly; I, Ile; K, Lys; L, Leu; M, Met; N, Asn; Q, Gln; R, Arg; S, Ser; T, Thr; V, Val; and Y, Tyr. B) The schematic chemical structure of Silaffin 1-A of C.fusiformis cell wall [19].

Silaffins are able to induce silica formation to construct diatom frustules. Nevertheless, the silica formation strongly depends on the chemical structure of silaffins. For example, the silaffin protein rich of phosphates in its structure fast induces silica precipitation in aqueous

solution of silicic acid whilst sulphate groups in sillafins are unable to form silica.
Not only silica formation, but also size and shape might be regulated by silaffins chemical structure in-vitro. The role of silaffins in silica formation will be discussed below.

1.3 The silica chemistry

General use of the term “silicon” in this case refers not only to the silicon element, but also comprises the various forms of unknown silicon compositions, whereas the name of silica refers to all the forms of SiO_2 as crystalline, amorphous or hydrated amorphous silica.
Silicon (Si) is one of most abundant elements in nature; however, it is extremely rare to find silicon in the elemental form. Silicon commonly exists as oxidized form in silica and silicates where elemental Si is regularly surrounded by four oxygen atoms to form tetrahedral coordination of crystalline silica, SiO_2. However, silica can also exist as hydrated amorphous structure naturally.

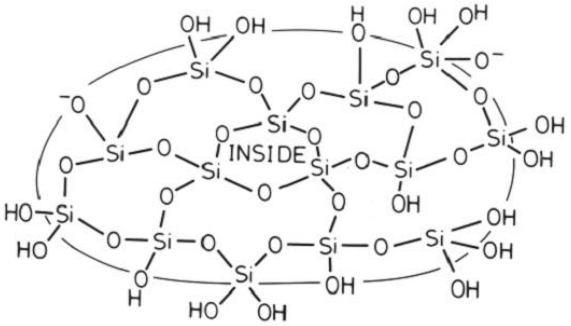

Figure 1-4: Schematic to show the range of functionalities possible for fundamental silica particles [27].

Silica can be produced from precursors by using the sol-gel technique. This is a complex process that includes many overlapping stages such as dissolution and condensation controlled by various factors such as formulation, temperature, pH, the presence of metallic ions or molecules. For instance, silicic acid, $Si(OH)_4$, formed by the

hydrolysis reaction, is indeed the basic unit of silica synthesis [27]–[29].

Silicic acid is the predominant form of soluble silicon in water with a wide range of solubility depending on conditions. Silicic acid, a weak acid with a pKa of 9.8, is universally found at low concentration in the environment. The solubility of silicic acid in water at room temperature is around 2 mM in neutral conditions [27], [30]. Silicic acid can condense to form solid colloids when the concentration is over its solubility. The self-condensation of silicic acid starts with the oligomerization to form dimers, as in the equation below.

$$2\mathrm{Si(OH)_4} \rightarrow \mathrm{(OH)_3Si-O-Si(OH)_3^-OH + H^+}$$

Further steps of self-condensation involve polymerization to form trimmers and cyclic oligomers, which tend to form siloxane branches. Siloxane branches easily transform into polysilicic acid as nuclei or colloidal nanosilica (Figure 1-4). Depending on specific conditions, nuclei can flocculate to form silica particles or polymerize to generate a gelling structure. Especially, pH condition and the presence of salt impact significantly on silica structure formation [30].

1.4 The understanding of diatom cell wall formation

The understanding of diatom cell wall formation has received great attention in many scientific fields since this process actually concerns biology, environment, geology, materials. The formation of cell occurs via two steps, first silicic acid transport and then silica synthesis and deposit to form a 3D structure.

1.4.1 Silicic acid transport

Soluble silicon in seawater contains around 97% of the neutral silicic acid form and about 3% of ionic form, $\mathrm{SiO(OH)_3^-}$,. Silicic acid from the environment can enter into diatom cells via specific proteins named silicic acid transporters (SiTs). Other transport molecules subsequently transport silicic acid inside the cells where silica precipitates, when its concentration exceeds solubility. Solubility strongly depends on the volume of cell. The significantly increased concentration of silicic acid results in the interaction of silicic acid with the GXQ amino acid (glycine, a subset of different amino acid, and glutamine) of SiT genes [31],[32]. Together with the increase of silicic acid concentration, biomolecules could also modify its affinity owing

to the interaction with silicic acid via the hydrogen bonding during the transportation [33],[34].

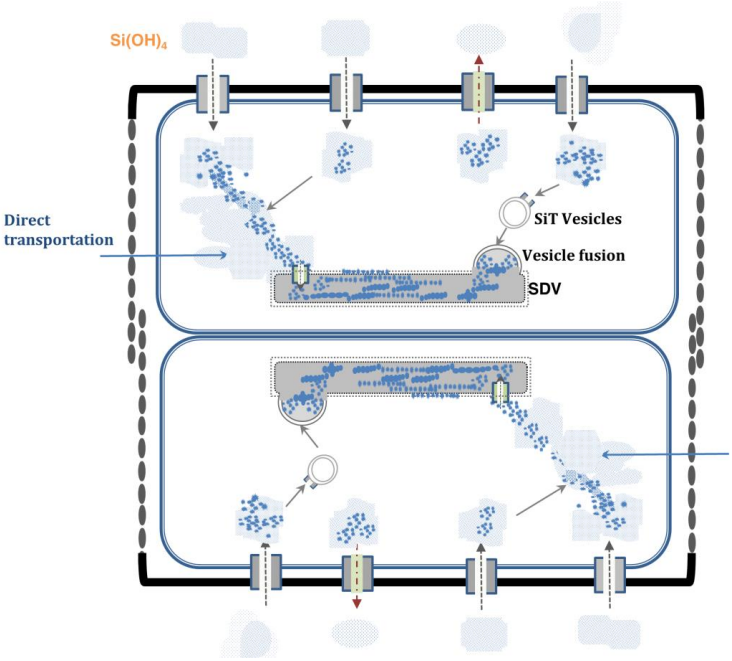

Figure 1-5: The proposal of different pathways of silicic acid uptake of transport in diatom intracellular, reproduced and adapted by [35]

However, mechanism of SiT proteins and transported silicic acid interaction has not been understood completely. It is concurred that different pathways of transporters may simultaneously exist and process silicic acid with variable functions such as modification soluble silicon form neutral $Si(OH)_4$ to ionized silicic acid $SiO(OH)_3^-$ or silicic acid polymerization (Figure 1-5) [36],[37].

Besides the organic influence, the coordination of inorganic nutrients like Na+, Ge^{4+}, Al^{3+}, Zn^{2+}, $Fe^{2/3+}$ and silicic acid uptake during the transportation probably influences the soluble silicon uptake capacity as well as its affinities [38],[39].

Another suggestion is that soluble silicon colloidal silica can coexist inside the cell during transportation although no clear proofs have been presented [35], [40].

1.4.2 Mechanism of diatom silica biogenesis

1.4.2.1 Silica precipitation

As for the presented silica chemistry, the equilibrium between solid and liquid phase in aqueous solution depends on several conditions, for instance charge, pH or the presence of some salts.

In fact, either silaffins or LCPA can induce silica precipitation rapidly from the silicic acid medium. For example, the rate of silica precipitation in presence of silaffins is around 10^6 times faster than silica formation from silicic acid [19]. In case of silaffins, phosphate groups in silaffins structures guide silicic acid condensation. In other words, the silica precipitation gradually increases with the number of phosphate groups. In fact, dephospholyrated silaffins are not able to induce silica formation in-vitro. The post – translational modification of silaffins could be critical to control silica formation [19], [20].

Silica formation by biosilicification has been proposed to occur by the self-assembly via electrostatic interaction of the zwitterionic molecules, for instance silaffins with the presence of negative charges (phosphates) and positive charges (amines). Protein self-assembly to form supramolecular structures may provide a template for silicic acid condensation. Phosphate ions can improve the silica aggregation owing to the serving ionic cross-linker [20].

Besides silaffins, LCPA can rapidly induce the condensation of the silicic acid; however, the presence of phosphate groups from silaffins is required. Additionally, polyamine acts likely as flocculation agent of nanocolloids [41].

Thus, silaffins as well as LCPA synergistically contribute to silica formation in diatom cell wall.

1.4.2.2 Morphogenesis of silica deposition valve (SDV)

Besides DNA replication, silica deposition vesicle/valve (SDV) formation has been considered as a key phenomenon in the diatom cell cycle. The mechanism still remains unclear. Many studies have indicated that the silica deposition vesicle (SDV) was formed in the specialized membrane-bound compartment, called silicalemma (SL), of diatom cell. Silica formation controlled by biomolecules in SL develops 3D-structures. It has been widely accepted that not only silica formation but also valve structural formation (SDV) is probably

controlled by biomolecules of the cells. Regarding this understanding, numerous realistic models of SDV structural formation have been assumed [35],[42],[43].

The high silicon concentration (and perhaps colloidal silica nanoparticles) is continuously carried into SL where silica nucleus is formed. The growth of silica nucleus builds 2D pore silica precipitation inside SL and finally develops 3D porous structures of SDV under the main regulation of biomolecules; however, the precise mechanism of 2D-patterning pore, 3D- silica porous structures formation as well as where silica forms has been a debatable issue. To date, some highlighted models have been suggested to clarify this phenomenon [16], [44].

1. The diffusion- limited aggregation has been considered as the model for SDV formation, especially of the rib-like costae formation in the case of centric diatom. According to this model, silica nanocolloids as nucleus may be formed in SiT system and transported together with silicic acid to the lipid membrane of SL where colloids may diffuse across the membrane. Organic liquids inside SL could potentially support the aggregation of colloids to stage bigger particles diffusing and organizing their position due to negative surface charges of particles [45]. However, this model still doesn't explain the diverse morphologies of diatom frustule. Moreover, the evidence of silica colloids formed in SiT system has not been cleared yet.

2. A second model has suggested that the phase separation of two different liquids regulates the patterning of the silica structure, (Figure 1-6). In this model, biomolecules firstly assemble via electrostatic charges to form the big organic "droplet" and concomitantly "colloidal" silica precipitates around the droplet. Afterwards, fragmentation of droplet may occur due to the different surface charge between silanol groups of silica surface and polyamine surface. Moreover, viscosity might be considered as a factor that can support phase separation [46]. This method might forecast the different morphology of SDV as well as diatom frustule guided by the different of silaffins assembly [47], [48].

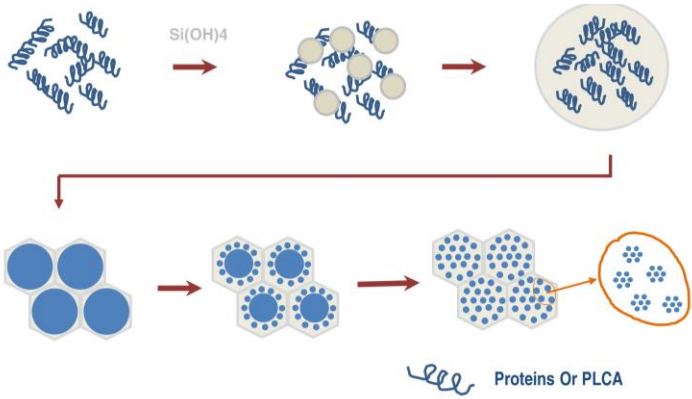

Figure 1-6: The drawing scheme of the mechanism of silicon oxide deposition in diatom cell wall by using phase separation model. Silicon oxide depicted at the position showed by the white grey colour, adapted [46]

3. Oppositely to the model 1, it has been proposed that silica deposition was only synthesized into SL by the induction of silica formation by silaffins proteins [49].

Besides the organic association in diatom cell wall, some inorganic elements were also detected such as aluminium, nickel, germanium, zinc. This inorganic matter perhaps influences not only silicic acid transportation but also patterning and silica morphogenesis. Moreover, other factors such as the presence of gaseous nitrogen, water pressure due to the sea depth and temperature could influence frustule morphogenesis [50], [51].

1.5 Diatom cell cycle

Diatom division can follow either sexual or asexual reproduction, which generally depend on cell volume. However, most diatom species follow asexual division (Figure 1-7) in which DNA replication and SDV formation play crucial roles [52].

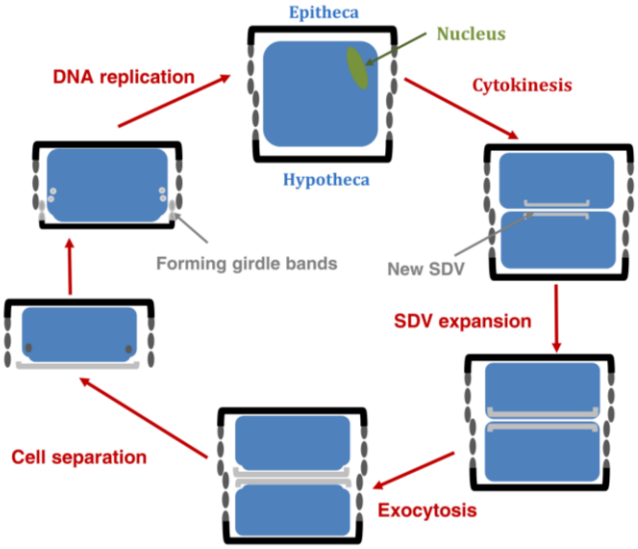

Figure 1-7: The scheme of diatom cell cycle (asexual). The cross section of diatom was illustrated, reproduced from [4].

The parent cell with protoplast and nucleus located at the end of the epivalve is a starting point of the new cell cycle. Diatom cell will grow to reach the required volume. The cell growth consists of the expansion of protoplast accompanied by the formation of girdle bands of hypotheca. In the same time, nucleus migrates from initial position to where the girdle bands attach to hypotheca. When the girdle band of hypotheca is complete, the process of mitosis is then initiated, followed by cytokinesis. Regarding the process of cytokinesis, the silicalemma (SL) located beneath cell membrane can be generated by the dictyosome-derived vesicle and fused to complete its formation. Silica precipitation can be formed during SL formation [53]. During cytokinesis, silica gradually is precipitated and fused till the new SDV completely matures. The SDV sibling valve formed by the same nucleus division separate in two protoplast daughters to form sibling daughter cells. Currently, the hypovalve of the parent cell is an epivalve of one daughter cell [2].

1.6 Biomaterials, bio-inspired and biomimetic materials

1.6.1 Biomaterial definition and classification

The definition of biomaterial issued by American National Institute of Health defines a biomaterial as "'any substance or combination of substances, other than drugs, synthetic or natural in origin, which can be used for any period of time, which augments or replaces partially or totally any tissue, organ or function of the body, in order to maintain or improve the quality of life of the individual" [54].

This definition has been considered as the most acceptable description.

Dealing an ethical issue, this definition could have many controversies about original human tissue/ organs transplanted from person to person. David F. Williams adapted this concept to be ''*A biomaterial is a substance that has been engineered to take a form which, alone or as part of a complex system, is used to direct, by control of interactions with components of living systems, the course of any therapeutic or diagnostic procedure, in human or veterinary medicine*.''[55]. Concerning with the D.F. Williams definition, cells as well as specific drug delivery systems supporting biological activities of cells or controlling some factors to maintain implanted material activity should be considered as a new biomaterial [56]. Thus, manmade or biological materials should be classified biomaterials.

Regarding the definition, biomaterials can be categorised into different groups based on their functions and how they interact with living systems.

Classically, biomaterials can be classified into four groups regarding their composition: metals and alloys, ceramics, polymers and composites.

Herein some selected examples about materials and their applications are listed following the classical grouping (table 1-2)

Table 1-2: Some examples of different biomaterial and their applications, modified [57]

Classification	Biomaterials	Applications	Refs
Polymer	Polyurethane	Wound dressing, heart valves, artificial hearts, tubing	[58]
Polymer	Silicon rubber	Catheters, drainages tube, flexible sheath	
Polymer	Poly caprolactone	Degradable bone fixation, soft tissue suture, bone void filler, soft tissue	
Polymer	Collagen	Hard and soft tissue	[57]
Metal	Titanium and its alloy	Fracture fixation, join replacement, stents	[59]
Metal	Stainless steel	Stents, orthopedic fixation devices	
Ceramic	Hydroxyapatite	Implant coating, bone filler, bone graft	[60]–[62]
Ceramic	Bio-glass	Bone cement, orthopedic implant as hip, knee, shoulder…	
Ceramic	Alumina	Orthopedic prostheses, joint replacement	
Ceramic	Zirconia	Dental crow, heart valves, joint replacement	
Composite	Collagen–hydroxyapatite composite	Bone graft	[61], [63]

Selections and uses of biomaterials should take into account role and site or implant.

1.6.1 Requirements of biomaterials

Depending on application, biomaterials should have different requirements, which are sometimes opposite. For examples, biomaterials for bone tissue engineering demand to be biodegradable to be replaced by the extra cellular matrix made by cells while heart valves must be bio-stable and wear resistant. In general, all biomaterials should possess physicochemical properties fulfilling specific requirements that depend on the application, one of those being the biocompatibility with the host.

Following D.F. Williams, 1987, biocompatibility may be defined "*…the ability of a biomaterial to perform its desired function with respect to a medical therapy, without eliciting any undesirable local or systemic effects in the recipient or beneficiary of that therapy, but generating the most appropriate beneficial cellular or tissue response in that specific situation, and optimising the clinically relevant performance of that therapy*" [64], [65].

1.6.2 Bioinspired and biomimetic materials from nature

Nature has certainly provided diversity of living and non-living systems proposing innumerable structures and materials that can be used or eventually provide inspiration for different desired functions. Biomimetic structures can be fabricated by a proper selection of nature sources, designed to fulfil desired application, understood and reinvented in the laboratory [66], [67].

Numerous drugs, materials and processes, phenomena as the self-cleaning of lotus leaves, the morpho-rhetenor phenomenon of butterfly, protein's self-assembly of Lanreotide, magnetotactic bacteria of microorganism or marine skeletal biominerals have been discovered from nature. Indeed, nature and its evolution could be an inspiring source to learn, adapt and develop sustainably [68]–[70].

For biomedical use, new candidate materials possessing specific properties are required. Learning, inspiration and imitation from nature may be a good solution to handle the need.

Classic examples of bio-inspiration are the architectures of Gaudi inspired to nature shapes [71].

The word "biomimetics" was firstly used by Otto Schmitt who studied the neural impulse propagation in squid nerves [72]. Nowadays, mimicking nature for tailored and desired applications of an artificial

device with man-made alternatives based on the profound understanding of the corresponding biological mechanisms or materials is termed biomimetics.
Biomimetics can be simply defined as “Biologically inspired design, adaptation, or derivation from nature” [73].

1.6.3 Silk fibroin biopolymer

Silk, a fibrous proteins, is present in specialized glands of spiders and several insects of the Lepidoptera family, like mites, butterflies and moths [74]. Each silk has quite different amino acid compositions, depending on origin and specific functions. However, generally speaking, silk proteins are rich of alanine, glycine, and serine amino acids. Silkworm silk comprises two proteins, an inner core made by fibroin, and an outer coating made by a family of proteins named sericins. For biomedical applications, only fibroin is generally used, due to some early adverse reaction attributed to sericins.
Structure of silk fibroin can be composed of different combination of elastic β-spirals, crystalline β-sheets, α-helices and spacer region components [75].
Silk fibroin from *Bombyx mori* cocoons has been widely proposed for various biomedical applications.
Fibroin’s amino acid composition of *Bombyx mori* mostly comprises glycine (43%), alanine (30%) and serine (12%). The molecule is an assembling of a heavy and a light chain. Light chain is made by 253 aminoacids that do not form crystalline domains, is hydrophilic and connects to the heavy chain by di-sulphide bonds. The heavy chain consists of 12 domains that form the crystalline regions in silk fibers, which are interspersed with primary sequence that is non-repetitive and thus forms fewer organized domains in the fibers. The crystalline domains in the fibers consist of Gly-X repeats, with X being Ala, Ser, Threonine (Thr) and Valine (Val). The formation of crystalline structures is due to the short lateral chains of the amino acids in these regions, which allow protein folding in β-sheet conformation [74].
Silk fibroin can have three conformations named silk I, silk II and silk III. Conformations of silk I, i.e., the water soluble structure that fibroin assumes in the silkworm gland, and of silk III, i.e., the structure that fibroin can build at the water–air interface in thin films have not been

fully clarified yet. Silk II has been viceversa long regarded as a prime example of the well-oriented β-sheet conformation [74], [76].
Silk fibroin is considered to be biocompatible. It can be degraded in vivo by proteolysis as a usual protein. Different processes have been reported to fabricate fibroin in different shapes, as films, sponges, gels, nets and so on [77].

1.7 Biomineralization and biomaterials

1.7.1 Biomineralization

The term “biomineralization” refers to processes of living organisms to produce minerals for specific purposes.
Biocalcification, i.e., the production of calcium minerals, is the most prevalent biomineralization process. In term of taxonomic distribution, calcium carbonate found in corals, mollusc shells, foraminifera is a biomineral based on calcification. Among biominerals containing calcium, calcium phosphate found in the hard tissue of mammalians and some algae is very common, about 25% of total biominerals [78], [79].
Besides calcification, silicification is another major example of biomineralization, especially in marine organisms.
Silicification was typically described in the formation of hydrated amorphous silica in most sponges and diatoms [27].
Moreover, biomineralization occurs in the production in nature of metal compounds of iron, barium, magnesium, strontium, germanium, etc. [73].
The mechanism for biomineralization has been suggested by using classical nucleation theory [67]. Initially, a core of inorganic minerals is formed due to an excess of their constituting ions, which form small clusters and grow to reach a critical size. At this point, the size of clusters is stable because the increasing surface energy is balanced by the decrease of bulk energy, which is related to the crystal lattice formation. In contrast, almost 60% of biominerals exist in the amorphous hydrated form, with biogenic silica being a featured example. The hydrated form can be the precursor of the crystalline form, as for the hydrated carbonate that transforms into the mature crystalline form [80],[81].

Composition, structure and mechanical properties of biominerals affect both biological activity and environment where they are produced.
Traditionally, biomineralization processes can be classified in two major groups depending upon the level of biological impact; biologically induced mineralization and biologically controlled mineralization [73], [78].

1. The term “biologically induced mineralization” regards mineral phases resulting from the interaction between biological activity and the environment. Character of biologically induced minerals is heterogeneity, which greatly depends on the environment where they are formed [82].
2. The concept of biologically controlled mineralization refers to mineralization processes, including nucleation, growth, morphology and final location that are strictly controlled by biological activity, i.e., activity of cells. These processes can be categorized into three groups; extra, inter and intracellular, depending on where they are located. The process often involves the interaction with biomacromolecules such as proteins or polysaccharides functioning as frame of the mineral deposition. Thus, certain materials based on biomimeralization are indeed tight composite of organic and inorganic phase [79], [83], [84].

1.7.2 Hard bone tissue and the role of silicon on bone maintenance

1.7.2.1 Hard skeletal tissue formation

The main mineral component of human body is calcium phosphate apatite, the inorganic component of hard tissues such as bones and teeth.
In human bone, calcium phosphate apatite, hydroxyapatite, constitutes up to 70% of bone volume [85]; it is formed and deposited in the extracellular matrix during biomineralization.
The formation of hard bone tissue can be simply divided into two main stages, including primary and secondary osteogenesis [86]. The primary stage of mineralization starts on forming calcification nodules, a nucleation of hydroxyapatite precipitation, which results from the interaction between the collagen-proteoglycan matrix (osteoid) and

calcium salt precursors. During the interaction, matrix mineralization forms a ‘woven’’ bone microstructure; however, the lamellae or crystals of hydroxyapatite are not formed yet [87],[88].

.

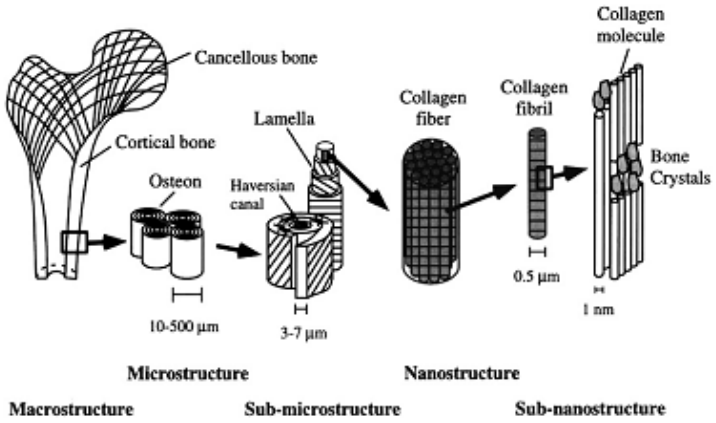

Figure 1-8: The hierarchical organization of bone structure ranging from nano to macro length scale [89]

The hierarchical structure of bone from nano to macro (Figure 1-8) forms as follows. Layered lamellae form from the mineralized and oriented collagen fibers and arrange in osteons surrounding blood vessels; finally, porous cancellous bone is generated from the assembly of the densely packed osteons [90], [91].

Different kinds of cells including osteoprogenitor cells, osteoblasts, osteocytes and osteoclasts are involved in the bone growth, maintenance and remodelling. Osteoprogenitor cells are able to differentiate in bone cells, osteoblasts. Osteoblasts synthesize and mineralize organic matrix (osteoid) of bone.

After mineralization of the extracellular matrix, osteoblasts remain trapped in the bone matrix and transform into osteocytes that are responsible for bone maintenance and remodelling. Furthermore, osteoclasts also derive from blood monocytes/macrophages. Bone remodelling occurs through the coordinated action of osteoclasts, osteoblasts, osteocytes, and bone lining cells together.

1.7.2.2 The role of silicon on bone formation and maintenance

The role of silicon on bone formation was first mentioned by Carlisle in early studies regarding experiments on animals with the discovery of the unusual high silicon level in connective tissue as tendons, bone, skin [92], [93]. Silicon has been considered as an important trace element playing a key role in bone formation, but nevertheless the mechanism of silicon biological effect remains unclear.

One theory proposed that Si acts as a primary nucleation centre [94] which may facilitate apatite formation. This theory might be supported by the observation of thin amorphous silica layers associated with calcification in crustacean cuticles at the early stage [95]. In addition, the role on bone formation of silicon-substituted calcium phosphates has been considered more effective than pure calcium phosphates [96], [97].

An important explanation for the silicon role claims that the presence of silicon improves collagen and proteoglycans synthesis. The improvement of bone osteoid in term of the structural integrity and mechanical strength is a critical point for bone formation as well as cardiovascular health [93], [98].

Another suggestion for the silicon role in bone formation is that absorption of copper and magnesium may be facilitated by a higher silicon intake. Besides, silicon perhaps alleviates aluminium toxicity owing to the combination of soluble silicon with Al^{3+} that prevents the negative effects of aluminium on collagen synthesis and structure. Both strategies are essential for bone growth and maintenance [99], [100].

Numerous in-vitro studies have focused on the effects of silicon on bone formation in osteoblast cultures. Particularly, silicon containing materials improved osteoblast proliferation, adhesion and differentiation [101], [102]; ortho-silicic acid promoted gene expression of alkaline phosphatase, osteocalcin and collagen I production from osteoblasts [103]; silicic acid induced up-regulation of bone morphogenetic protein 2 (BMP-2) [104]; moreover, nanosilica coating material enhanced the differentiation of human bone marrow mesenchymal stem cells (hBMSCs) [105].

Besides the significant benefits of silicon on bone formation, silicon deficiency depressed the growth and provoked skull deformities in rats, being also cause of skeletal abnormalities concerned with the

formation of the cartilage matrix and connective tissue, observed in chicks [106]. Furthermore, silicon can inhibit bone mass loss. Silicon has been suggested as a dietary supplement in premenopausal women [107]–[110].

1.7.3 Bone healing and tissue engineering

1.7.3.1 Bone healing

Bone healing can be defined as a process that restores the “original” bone tissue. Cells, growth factors, bone graft materials, biochemical and biomechanical factors influence the bone healing potential. Healing process comprises three overlapping stages: inflammation, repair and remodelling [111].

Inflammation

The development of hematoma occurs after bone damage within the first few hours. Then, a granulation tissue is formed within the fracture or defect site in order to prevent infection, thanks to the activity of inflammatory cells (macrophages, monocytes, lymphocytes cells) and fibroblasts. Moreover, cytokines and growth factors released by activity of these cells form new capillaries and induce the migration of mesenchymal cells [112]–[114].

Repair

The repairing stage follows inflammation with the formation of soft callus as cartilaginous template around the repair side, because of the activity of chondrocytes and fibroblasts. Together with cartilaginous matrix formation, vascular system continues growing, vessels increase in size and form branches, controlled by fibroblast proliferation and chondrocytes behaviour. Afterwards, the osteoid matrix starts to mineralize due to the dominant increase of osteoblasts differentiated by osteoprogenitors from many sources like periosteum and bone marrow. Mineralized bone progressively stabilizes and substitutes the soft callus. In the parallel, revascularization proceeds, providing oxygen for the differentiation of progenitor cells [111], [115].

Remodelling

The remodelling stage completes the bone healing process. The hard callus tissue restores its original shape by osteoclast activity. Osteoclasts demineralise inorganic matrix and degrade collagen; at the same time, osteoblasts form new bone. Coordination between osteoclasts and osteoblast balances the secretion of cytokines in order to maintain the stability of matrix [111].

1.7.3.2 Tissue engineering

The term tissue engineering (TE), firstly introduced in 1988 by Langer and Vacanti, was defined as "an interdisciplinary field of research that applies the principles of engineering and the life sciences towards the development of biological substitutes that restore, maintain, or improve tissue function" [116].

The idea of tissue engineering is to regenerate tissues to restore their original characteristics in term of biological, chemical, physical and mechanical properties. To reach the goal, the combination of biology, materials science, engineering, physics, chemistry, and medicine in an integrated manner is required [117], [118].

Cells, scaffolds and growth factors (bioactive factor) are three main elements of tissue engineering. The integration of the above three components is critical to regenerate anatomically and physiologically correct tissue. It means that the cells–matrix interactions and intercellular communications must be profoundly understood to achieve successful results.

Bone tissue engineering scaffolds

The matrix for cell growth in-vivo must be 3D, with proper architecture and physical properties, supply nutrients and growth factors that are needed for cell proliferation and extracellular matrix (ECM) production. The scaffolds must be a temporary template for cells for the restoration of the tissue [117],[119].

Scaffold materials must be biocompatible and scaffold must perform the required functions. Moreover, high porous structure with interconnected geometry is required in order to allow cell growth, penetration and distribution and to facilitate blood vessel development.

For bone tissue engineering scaffolds, optimal pore size ranges from 200 to 900 μm [120].

Together with biocompatibility and architecture, proper surface properties should promote initial cell adhesion and migration, while providing the right interaction with proteins to stimulate cell proliferation. Furthermore, osteoinduction, degradation rate and mechanical properties should be taken into deep attention [121], [122].

Materials such as ceramics and polymers have been used for the production of scaffold for bone tissue engineering. β-tricalcium phosphate (β-TCP), hydroxyapatite and biodegradable natural or synthetic polymers are commonly used [123]–[126], as well as their combination in composites [127], [128].

Owing to specific architecture of scaffolds for bone tissue, methodology and techniques for scaffold production should be consistent with the desired porosity, pore size, pore distribution and interconnectivity. Various processing techniques of scaffold fabrication have been used, such as solvent casting, melt based technologies, phase inversion, freeze drying, electrospinning, 3D printing [118], [120], [129].

Cells for bone tissue engineering

As previously presented, osteoblasts are indeed the fundamental choice due to their role on bone formation and maintenance. Cell can be taken directly from patients and expanded in vitro, or xenogeneic cells can be used; however, the proliferation capacity of osteoblasts is slow [130].

Many other cell sources have been suggested for tissue engineering, for example, human embryonic stem cells (ESCs), induced pluripotent stem cells (IPs), adipose-derived stem cells (ADSCs) peripheral blood–derived stem cells (PBs), mesenchymal stem cells (MSCs), etcetera. Amongst, MSCs have been accepted as a potential source for bone tissue engineering due to the ability to differentiate into bone cells [131],[132].

Growth factors and supplements

The process of bone formation involves a variety of hormones, cytokines and growth factors, that act as signalling molecules [133] binding to cell receptors in order to support different functions such as cell migration, proliferation and differentiation. Bone morphogenetic protein (BMP), insulin-like growth factor (IGF), and vascular endothelial growth factor as common growth factors have been used in bone tissue engineering. Growth factors may be combined with the scaffold or immobilized on the scaffold [134]. The use of growth factor for bone tissue is beneficial; however, their use is restricted by their high cost.

In addition, osteoinductive materials such as, hydroxyapatite, clays, silica or titanium oxide incorporated into scaffolds has been demonstrated to improve cell differentiation as well as bone formation [132], [135].

1.8 Diatomite and strategies for biological applications

1.8.1 Diatomite

Diatomite or diatomaceous earth is the siliceous sedimentary rock resulting from the deposit and accumulation of the cell wall of dead diatoms. Owing to the original formation, diatomite is finely porous and lightweight with density from 0.32 to 0.64 kg/l. Generally, dry diatomite comprises 80-90% of silica (sometime up to 95%). Some common components as alumina, hematite as well as organics are present [136].

Based on physical properties and original formation, diatomite has been used in various fields such as construction, chemical and pharmaceutical industries as an absorptive carrier. Moreover, diatomite has been suggested as filler component in dentistry [137], [138].

1.8.2 Diatomite and diatom strategies for biological applications

Besides the traditional applications mentioned above, diatomite has been proposed as promising drugs delivery system and molecular catalysis applications thanks to the hierarchical 3D pore structures of diatom frustules; however, pre-treatment process of diatomite to

purify, enrich diatoms content, remove contaminants and functionalize surface is necessary before use [139], [140].
Mimicking diatom biosilicification is a challenging task for a bone tissue engineering dedicated, biomimetic approach [1],[141].
The interaction between biopolymer (peptides) and silicon in diatoms determines and controls silica formation and organization; it could be exploited for drug delivery applications or for protein/enzyme immobilization or to fabricate biosensors and microfluidic devices [142]–[145].
Moreover, hybrid organic/inorganic biomaterials could found appropriate applications for the design of scaffolds for bone regeneration [146]. Amongst, hybrid silica/collagen compounds have received deep attention due to the ability of self- assemble proteins [147], [148].

1.9 Objectives and outline

Seeking a new candidate or improving current materials for proper applications is an important task of material science and engineering. The integration of advanced technology in various fields has provided us many opportunities for search, observation, deeper understanding and learning natural phenomena in order to create man-made materials that can be used for desired applications.
Silica or silicon is one of the most abundant compounds of the earth crust, especially in silicon oxide or silicate forms. Amongst, siliceous structures made by biosilicification of numerous organisms as in the formation of in marine sponge or diatom skeleton, are the most interesting example owing to their morphology and 3D pore structure.
Biosilicification, i.e., the skeleton formation in many marine organisms may be translated and transferred to the role of silicon on human skeletal formation.
The main aim of this work was to take inspiration from the natural source of silicon, diatoms, for the fabrication of bone tissue scaffold containing silicon as bioactive component.

Chapter 2

Processing and Characterization of Diatom Nanoparticles and Microparticles as Potential Source of Silicon for Bone Tissue Engineering

This chapter describes the purification and characterization of diatomite and preparation and characterization of diatoms particles. Two different methods of purification were used and compared in order to assess their influence on characteristics of diatom particles. The silicon released from the diatoms particles has been evaluated and their compatibility with cells has been determined with cell cultures in vitro.

Chapter 3

Enhancing bioactive properties of silk fibroin with diatom particles for bone tissue engineering applications

Based on the results of toxicity and silicon release, this chapter reports the fabrication and characterization of 3D composite scaffold of silk fibroin with micro and nanoparticles of diatoms. Scaffolds were prepared with the salt leaching method. The effect of the addition of diatom micro and nanoparticles on scaffold architecture and mechanical properties as well as on activity, proliferation and early bone formation markers with MG63 osteoblast-like cells lines was evaluated.

Chapter 4

Osteoinductive Silk fibroin/ Diatom Particles Scaffolds for Bone Tissue Regeneration

Herein, we checked the ability of diatom/fibroin composite scaffolds to induce differentiation of osteoprogenitor cells using human mesenchymal stem cells. Based on the results of the previous chapter, we evaluated two different scaffolds, silk fibroin loading a mixture of micro and nano diatom particles and pure silk fibroin, and two different culture conditions.

Chapter 2: Processing and Characterization of Diatom Nanoparticles and Microparticles as Potential Source of Silicon for Bone Tissue Engineering

Part of this chapter has been published in:

Journal of Materials Science and Engineering C,

Authors: Thi Duy Hanh Le, Walter Bonani, Giorgio Speranza, Vincenzo Sglavo, Riccardo Ceccato, Devid Maniglio, Antonella Motta, Claudio Migliaresi

"Processing and Characterization of Diatom Nanoparticles and Microparticles as Potential Source of Silicon for Bone Tissue Engineering"

No 59. (2016), pages: 471–479

Abstract

Silicon plays an important role in bone formation and maintenance, improving osteoblast cell function and supporting mineralization. Often, bone deformation and long bone abnormalities have been associated with silica/silicon deficiency. Diatomite, a natural deposit of diatom skeletons, is a cheap and abundant source of biogenic silica. The aim of the present study is to validate the potential of diatom particles derived from diatom skeletons as silicon-donor materials for bone tissue engineering applications. Raw diatomite (RD) and calcined diatomite (CD) powders were purified by acid treatments, and diatom microparticles (MPs) and nanoparticles (NPs) were produced by fragmentation of purified diatoms under alkaline conditions. The influence of processing on the surface chemical composition of purified diatomites was evaluated by X-ray photoelectron spectroscopy (XPS). Diatom NPs were also characterized in terms of morphology and size distribution by transmission electron microscopy (TEM) and dynamic light scattering (DLS), whilst diatom MPs morphology was analyzed by scanning electron microscopy (SEM). Surface area and microporosity of the diatom particles were evaluated by nitrogen physisorption methods. Release of silicon ions from diatom-derived particles was demonstrated using inductively coupled plasma optical emission spectrometry (ICP/OES); furthermore, silicon release kinetic was

found to be influenced by diatomite purification method and particle size. Diatom-derived microparticles (MPs) and nanoparticles (NPs) showed limited or no cytotoxic effect in vitro depending on the administration conditions.

2.1 Introduction

Silicon is the main component of silica formed exo- and endo-skeletons in some marine organisms [48]. The skeleton of unicellular marine organisms such as sea sponges and diatoms consists of hydrated amorphous silica which is gradually formed by immobilization and internalization of monosilicic acid in a process addressed as biosilicification [2], [149], [150].

Nevertheless, silicon is also involved in the biomineralization processes in mammals. Calcification involves many stages including formation of calcium phosphate under the direct regulatory control of several biological systems and in presence of elemental traces such as silicon, zinc and magnesium [86],[151]. Silicon is believed to be an essential element for bone development, although its role is not completely understood [110], [152]. For instance, silicon has been associated with the precipitation of calcium phosphate in the early stage of bone mineralization [95]. In addition, the presence of silicon at the inorganic/organic interface regulates the interaction between collagen and proteoglycans improving the quality of the extracellular matrix (ECM) [98]. Silicon can induce stem cell differentiation in osteoblasts and osteocytes [101],[105],[108]; furthermore, silicon directly inhibits osteoclast formation and bone resorption [153].

Use of degradable amorphous silica particles has been proposed to improve mineralization in bone regeneration applications besides other inorganic materials such as hydroxyapatite, tri-calcium phosphate, glass ceramic or zirconia [154],[155]. However, bioactivity of particles significantly depends on size, shape and surface properties [156]–[159]. Recent studies have been focused on possible applications of amorphous silica nanoparticles as dietary supplement for bone regeneration [160], [161]. Additionally, silica has been successfully incorporated with hydroxyapatite to enhance osteoconductivity of scaffolds for bone tissue regeneration [162], [163]. Silk or collagen scaffolds loaded with amorphous silica particles have been successfully proposed to improve osteoinductivity [135],

[147], [164]. So far a variety of amorphous silica sources have been considered. Often silica particles are of synthetic origin and are produced using chemicals and surfactants whose residues might have toxic effects [156]. So, there is a quest for abundant and reliable alternative sources of amorphous silica.

Diatomite, also known as diatomaceous earth, is the marine sediment of silica diatom skeleton remains. Diatomite is an inexpensive and unlimited source of biogenic silica. Thanks to their peculiar morphology and porosity, diatom skeletons derived from diatomite have been proposed for uses in photonics, drug delivery and molecular catalysis applications [8], [165], [139]. We think that diatomite could be a promising natural source of amorphous silica also for bone tissue engineering applications. Biomedical uses of biogenic silica have been preconized by Wang et al. [150], but to date diatomite-derived silica particles have never been used as a part of tissue engineering scaffolds. We believe that diatom microparticles and nanoparticles could be useful as bioactive silicon-donor additives for degradable engineered scaffolds and bone defect fillers.

However, raw diatomite contains some local contaminations such as clays and other inorganic and organic compounds that require purification before any medical use and the yield of diatomite purification processes depend on diatom type and source [166].

Here, raw diatomite (RD) and calcined diatomite (CD) powders were purified in strong acid conditions, and diatom nanoparticles (NPs) and microparticles (MPs) were subsequently produced by treating the skeletons in alkaline solution. NPs and MPs morphology, elemental composition and specific surface area were determined. Silicon ion released by diatom particles dissolution has been evaluated with dissolution experiments and cytotoxicity tests of diatom particles have been performed.

2.2 Materials and Methods

2.2.1 Materials

Powder form of raw diatomite materials (RD) used in this study was provided by Phu Yen mineral joint stock company (Phu Yen province, Viet Nam). RD powder was passed through a metallic sieve (mesh size 250 µm) to remove aggregates and macroscopic contaminations.

Phosphate buffer solution (PBS), sodium hydroxide (NaOH), hydrochloric acid (HCl) and Triton X-100 were purchase from Sigma-Aldrich (St. Louis, MO, USA). All reagents and solvents were used as received without further purification.

2.2.2 Raw diatomite purifications

2.2.2.1 Acid-purified raw diatomite powder

RD powder underwent acid treatment to remove inorganic contaminations; purification protocol modified from [167]. Briefly, RD powder was dried overnight in oven at 102ºC, passed through a metallic sieve (mesh size 125 µm) to remove larger aggregates, and then acid-treated with 1M HCl solution at 55ºC (in the proportion of 100 mg of powder per ml of HCl solution) for 24 hours under continuous stirring to remove the inorganic contamination. Afterwards, the obtained slurry was concentrated with a paper filter; the remaining solid part was washed and allowed to sediment in deionized water (DI water). The process was repeated for 10 times. Finally, the sediment was dried in oven at 102ºC and sieved through a 63 µm pore size sieve to obtain acid-purified RD (hereinafter AD) consisting of single diatoms.

2.2.2.2 Acid-purified calcined diatomite powder

Raw diatomite powder (RD) was heated at 650ºC in air for 3 hours to reduce organic contaminations [168]. Calcined diatomite powder (CD) was then passed through a metallic sieve (mesh size 125 µm), then treated with acid, as explained before, to obtain acid-purified CD (hereinafter named CAD).

2.2.3 Diatom microparticles and nanoparticles from purified diatoms

Diatom microparticles and nanoparticles were produced from purified diatoms powders (both AD and CAD) by mechanical fragmentation in alkaline conditions [28],[39]. Briefly, AD and CAD powders were suspended in 0.1M NaOH solution (typically, 10 mg of diatomite powder per ml of alkaline solution was used), and suspension was vigorously stirred for 2 weeks at room temperature (RT) to break

diatoms. Afterward, the alkaline suspension was kept at RT for one week to allow sedimentation.
The unsettled colloidal suspension was collected separately and centrifuged at 15000 rpm for 30 minutes to retrieve diatom nanoparticles (here named AD-NPs and CAD-NPs). The obtained NPs were subsequently washed in DI water and centrifuged (15000 rpm for 30 minutes) for 3 times to remove any NaOH traces. The settled solid fraction was also collected, re-suspended in DI water and centrifuged as above to recover trapped NPs.
Finally, the remaining settled fraction was collected and washed with DI water to obtain diatom microparticles (named AD-MPs and CAD-MPs, depending on the source of purified diatomite).

2.2.4 Diatomite, purified diatomite and diatom particles characterization

Composition and mineral contamination of the RD powder, AD and CAD purified powders were characterized by X-ray diffraction (XRD) with a high resolution powder diffractometer (Rigaku PMG/VH, Tokyo, Japan), with Bragg-Brentano geometry in the range 2θ from 5.0 - 60.0 degrees using CuKα radiation (λ =1.5405981 Å). Surface atomic composition of diatomite powders before and after purification was analyzed by X-ray photoelectron spectroscopy (XPS) with a Scienta Gammadata ESCA 200 (Uppsala, Sweden), equipped with monochromatic Al-Kα radiation source (hν = 1486 eV).
A Field-Emission Scanning Electron Microscope (Supra 40, Zeiss, Germany) was used for the observation of diatomite powders, diatoms morphology and microparticles size distribution using type II secondary electrons (SE2).
Back scattered electrons (BSE) combined with Energy-Dispersive X-ray analysis (EDAX) were used to detect elemental composition of diatom and contaminations using a FEI/Philips XL30 Environmental Scanning Electron Microscope (FEI, Hillsboro, Oregon, USA) equipped with Falcon X-Ray Microanalysis System.
Nanostructure of diatom skeleton wall was obtained by Transmission electron microscopy (TEM). Purified diatom skeletons were embedded in epoxy resin, and then the slurry was placed in a copper pipe (external diameter 3mm) and cured at 80°C to crosslink the epoxy resin. A 1 mm thick slice was cut from the pipe. The slice was

mechanically polished on both sides to reach a thickness of 100 µm. Afterwards, a copper grid 125 mesh for TEM was glued to one side of the disc to support the sample during final thinning under ion beam. The thin disc was then dimpled to reach a thickness of 20 µm.

The final thinning to reach the electron transparency was performed with ion milling in a Gatan Duo Mill apparatus using Argon ions and an accelerating voltage of 6 KV. A TEM (Phillips CM12) was used to observe nanostructure of sample. The instrument was equipped with EDS allowing investigating chemical composition. Here we present TEM micrographs of a diatom skeleton fragment as well as chemical composition of the skeleton wall at different locations measured by EDS.

The hydrodynamic radius of diatom NPs in both DI water and PBS was determined by Dynamic Light Scattering (DLS) using a Malvern 110 Zetasizer Nano ZS instrument (Malvern, United Kingdom), equipped with a He–Ne a 5 mW laser at 633 nm). Morphology and chemical analysis of the NPs were also confirmed by transmission electron microscopy with a CM12 TEM, (Philips, Eindhoven, Netherlands) - accelerating voltage 120 KeV - combined with Energy Dispersive X-Ray spectrometer (EXDS).

Surface area and pore size distribution microparticles and nanoparticles were evaluated by physisorption measurements. Nitrogen physisorption experiments were performed at the liquid nitrogen temperature (77 K) using a Micromeritics ASAP 2010 system (Norcross, GA, USA). All the samples were degassed below 1.3 Pa at 25 °C prior to the measurement. The Specific Surface Area (SSA) values were calculated by the BET equation in the interval $0.05 \leq (p/po) \leq 0.33$ [169]. Pore size distribution was calculated using the BJH method applied on both branches of the physisorption isotherms [170].

2.2.5 Silicon release from diatom particles in DI water

Aliquots of the diatomite-derived NPs and MPs prepared above were dispersed in DI water (100 µg of particles per ml of water) and stored at 37°C to allow for particles dissolution and silicon release. Three replicates for each experimental group (AD-MPs, AD-NPs, CAD-MPs and CAD-NPs) were extracted at predetermined time points (4, 8 and 24 hours; 2, 3, 4, 7 and 14 days). Samples were centrifuged at 15000

rpm for 30 mins, and supernatant were collected and stored at –20ºC. Before measurement, the frozen samples were thawed at RT, vortexed and diluted for silicon quantification. Silicon concentration was determined by inductively coupled plasma/optical emission spectroscopy using a Ciros Vision ICP-OES (SPECTRO Analytical Instruments, Germany). A sodium silicate solution (Sigma-Aldrich) was used as standard to build a calibration curve for silicon concentration.

2.2.6 Cytotoxicity test

Cytotoxicity of diatomite-derived NPs and MPs was evaluated following the ISO 10993-5 8.3 standard both with direct contact and elution methods. Embryonic Swiss mouse fibroblast cells (3T3) were expanded and cultured at 37ºC with 5% CO_2 in high glucose medium (DMEM) (Euroclone, Pero, Italy), supplemented with 10% fetal bovine serum (Gibco, NY, USA), 2mM L-glutamine, 1mM sodium pyruvate and 0.1% antibiotics (Gibco, NY, USA). The medium was changed every 2 days until cells confluence, then cells were detached with 0.1% trypsin and re-suspended in culture medium. Later, 3T3 cells were plated in polystyrene 48-well plate at a density of 5.10^3 cells/cm^2 and incubated under standard culture conditions.

A reduced culture medium was prepared with Dulbecco's Modified Eagle basal medium without phenol red with 10% heat-inactivated serum, 1 mM sodium pyruvate, 2 mM L-glutamine and 0.1% antibiotics.

Diatom particles (AD-MPs, AD-NPs, CAD-MPs and CAD-NPs) were disinfected with 70% ethanol solution and then collected by centrifugation at 15000 rpm for 30 minutes.

For the evaluation of cytotoxicity in elution mode, diatom particles extracts were prepared by soaking diatom particles in reduced medium for 4 days at 37 ^{0}C (particles concentration 100, 200, and 500 µg/ml). When cells reached about 70-80% of confluence, culture medium was removed and replaced with conditioned media containing diatom particles extracts. Cells were then cultured in conditioned medium with extracts for 24 hours.

For the evaluation of cytotoxicity in direct contact mode, diatom particles (AD-MPs, AD-NPs, CAD-MPs and CAD-NPs) were directly re-dispersed in reduced medium at designed concentrations (100,

200, and 500 µg/ml). In this mode diatom particles were directly supplied to the cells. 3T3 cells were culture in presence of diatom particles for 24 hours.
Lactate dehydrogenase assay (LDH) (TOX7, Sigma-Aldrich) was used to evaluate the cytotoxicity impact of particles extracts and particles themselves on the cells, following manufacturers' instructions. Cells cultured in reduced medium and treated for 30 min with 0.05% Triton X-100 were used as positive controls. Cell cultured in reduced medium without any diatom sample were used as negative control. Absorbance was measured using a Tecan Infinite 200 microplate reader (Tecan Group, Männedorf, Switzerland) at 490 nm, background absorbance was measured at 690 nm. Results were presented as mean ± standard deviation (n = 5).

2.3 Results and discussion

2.3.1 Purification of the raw diatomite powder

Raw diatomite powder (RD) and calcined diatomite powder (CD) were acid-treated with 1M HCl solution to reduce inorganic contaminants.
The yield of the purification process was about 75% in the case of acid-purified diatomite (AD) and 65% for the acid-treated calcined diatomite powder (CAD); that is, 25 to 35 % of the initial RD weight was lost during the different sieving steps, washed away or dissolved during the acidic treatment.

2.3.2 Characterization of raw diatomite and purified-diatomite

SEM analysis of RD powder revealed whole diatom skeletons surrounded by broken diatom fragments, small aggregates and impurities due to many sources of organic and inorganic contaminations (Figure 2-1 A). In Figure 2-1B and C it is possible to see that the different sieving steps and the acid treatment significantly reduced diatom fragments and small aggregates both for acid-purified diatomite (AD) and for acid-treated calcined diatomite powder (CAD). However, in both cases it was possible to spot damage diatom skeletons and large diatom fragments.
X-Ray diffraction analysis (Figure 2-1D) demonstrated the presence of mineral contaminants including illite, halloysite, muscovite, and quartz both in the RD as well as in the purified diatomite powders (AD

and CAD). Yet, a reduction of the intensity of the characteristic peaks after purification indicated a decreased amount of quartz and halloysite contaminations (Figure 2-1 D and E).

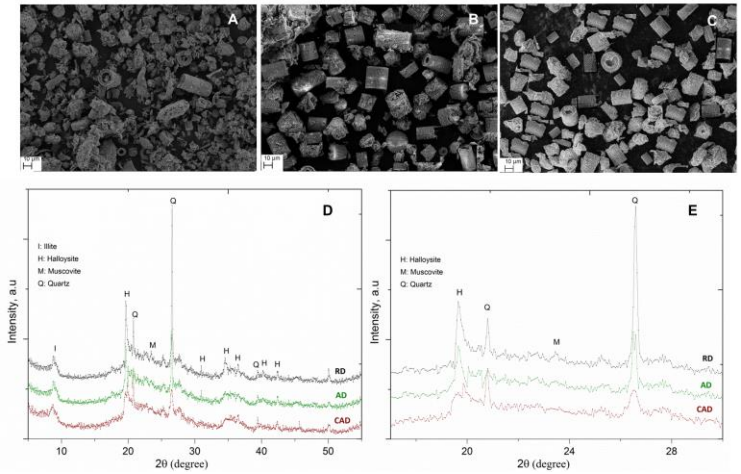

Figure 2-1: Morphology and mineral composition of raw diatomite (RD) and purified diatomite (AD and CAD) powders. A) SEM micrograph of diatomite powder (RD), B) and C) SEM micrographs of acid-purified raw diatomite (AD) and acid-purified calcined diatomite (CAD), respectively, D) X-Ray spectra of diatomite powders before and after purification showing clay mineral contaminations including illite (I), halloysite (H), muscovite (M) and crystalline silica (Quartz-Q), E) Detail of the X-Ray spectra in correspondence of the Quartz peak at 2θ = 26.5.

Chemical description of the material surfaces as well as the surface composition of RD powder and purified diatomite powders (AD and CAD) were obtained by XPS analysis.

The characteristic wide spectra of diatomite powders (Figure 2-2) established that the surface composition of diatomite powders was formed by a rather rich list of elements. The main elements were oxygen, carbon and silicon, aluminium, iron and magnesium were present to a lower extent. The elements concentrations together with the chemical bond interpretation are summarized in table 2.1

While analyzing the high-resolution spectra of the main component elements, it is possible to understand how the material changes in relation to specific treatments. This is shown in Figure 2.3 where the

C1s core lines of samples RD, AD and CAD are presented. As it can be seen in Figure 2-3, there is a rather strong change of the core line upon sample treatment. In particular the cleaning procedure leads to a total reduction of the C1s intensity due to the elimination of the main part of the organic contaminants with a significant decrease of the carbon content, from 20.6% to 8.5% and 6.1% in AD and CAD samples, respectively.
In the meanwhile, purified materials AC and CAD resulted to be enriched in silicon, oxygen, aluminum and iron.

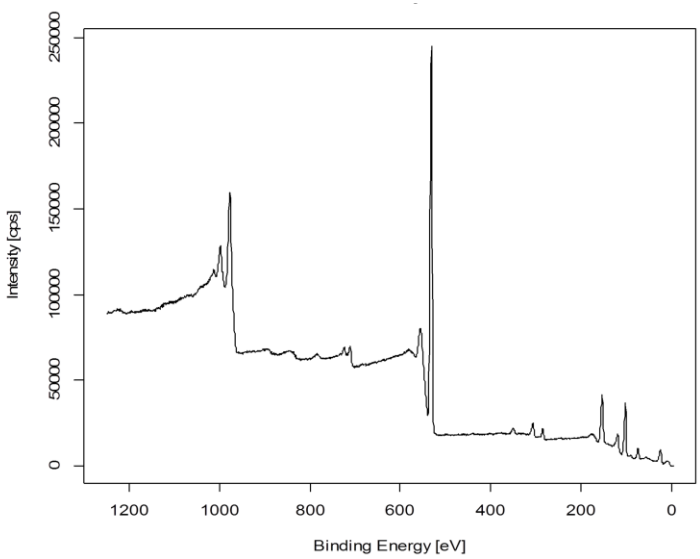

Figure 2-2: The whole XPS spectra of diatomite powders

Also the calcinations processing influenced the C1s line shape. In this case there was an increase of the intensity of the C1s oxidized components which fall in the range 286eV – 290eV for CAD material.

Table 2-1: Elemental composition of raw diatomite powder (RD) and purified diatomite powders (AD) and (CAD) as determined by X-ray photoelectron spectroscopy (XPS).

Atom %	Si2p	O1s	C1s	Al2p	Fe2p	Mg2p
RD	13.2 ± 1.0	58.9 ±1.7	20.6 ± 1.8	1.7 ± 0.2	2.9 ± 0.2	1.9 ± 0.1
AD	18.4 ± 0.5	62.8 ± 0.6	8.5 ± 0.2	4.7 ± 0.5	4.8 ± 0.4	1.2 ± 0.2
CAD	20.8 ± 0.7	64.0 ± 0.9	6.1 ± 0.3	4.2 ± 0.3	3.7 ± 0.3	1.6 ± 0.2

The effect of the purifications was mirrored also by the O1s core lines reported (Figure 2-3). The reduction of the hydrocarbon contaminants upon purifications leads to an increase of the total oxygen concentration. Slight decrease of the total oxygen abundance is induced by the calcination, in agreement with the decrease of the carbon concentration in the CAD sample.

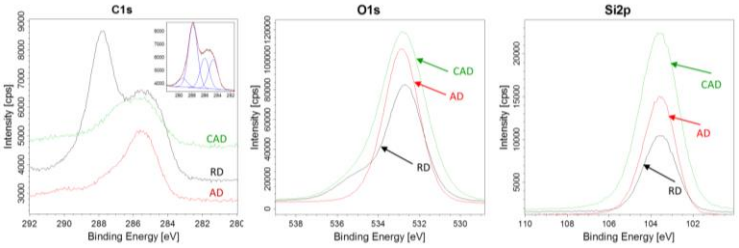

Figure 2-3: High energy resolution C1s, O1s and Si2p core lines obtained by XPS for raw diatomite powder (RD) and purified diatom powders (AD) and (CAD). In the inset is shown the deconvolution of the C1s core line in Gaussian components. Both purification procedures lead to a drastic reduction of the C1s intensity at 288 eV due to the elimination of the organic contaminants.

As for carbon, also in the case of oxygen sample treatments induce a modulation of the chemical bond intensities. In particular the removing impurities process induces an increase of the intensity of the component associated to the SiO_2 bonds in agreement with the increase of the Si concentration while the component located at high

binding energy and associated to H_2O decreases. Also Si2p core line showed a similar trend (Figure 2-3). The Si core line was fitted using just one component which represents silicon in SiO_2 chemical configuration. Apart the core line intensity the sample treatments does not have any effect on this chemical bond.

While removing small aggregates and diatom fragments, purification processes of RD powder did not change the morphology of diatom skeletons. At the same time, the results from XPS and XRD analyses and SEM observation demonstrated the efficiency of both process of diatomite purifications.

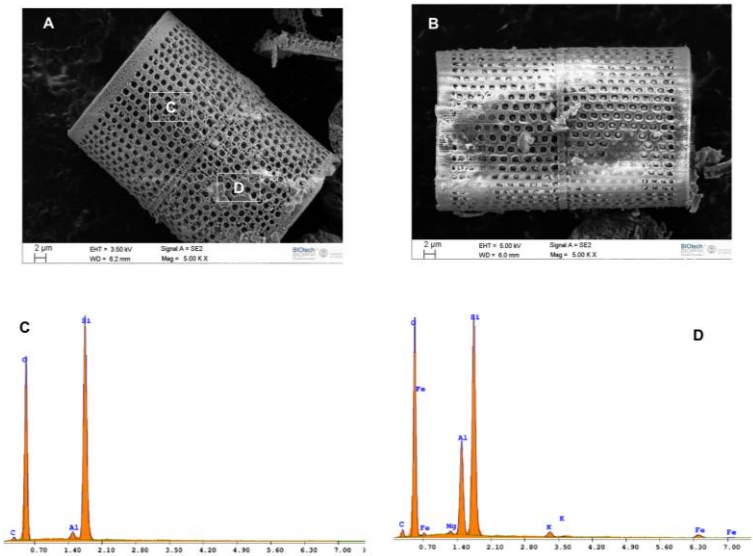

Figure 2-4: Morphology and elemental composition of diatom skeletons isolated from acid-purified calcined diatoms (CAD) obtained by Energy Dispersive X-ray Analysis (EDAX) A) SEM micrograph of a single diatom skeleton of CAD and B) CD samples, C) elemental composition of the clean diatom wall, D) elemental composition of an impurity/defect of the diatom skeleton. The patterned diatom wall presents a silicon/oxygen composition with low carbon and aluminium content, impurity shows high aluminium content and relevant iron/potassium/magnesium contaminations.

No significant differences in morphology are appreciable between calcined and not calcined diatom skeletons. The morphology of single

diatom skeletons observed by SEM illustrated the typical morphology of the Aulacoseira diatom group, cylindrical-body shape with diameter of 5 – 20 µm, length of 10 – 40 µm, and a wide circular opening on one side (Figure 2-4A and B).

EDAX observation of single diatom skeletons (Figure 2-4 C) indicated the presence of silicon, oxygen, carbon and aluminum, in agreement with Abramson et al.[8] and Koning et al. [171]. Composition of contaminant particles adhering to the skeleton revealed the presence of iron, potassium and magnesium (Figure 2-4 D).

For a deeper understanding of diatom frustule structure, single skeletons were also investigated by high magnification with SEM and TEM to observe their structure. The wall of diatom frustule presented the typical honeycomb porous structure with the densely populated pores layer ranging 400 - 800nm, which overlaps another pores layer with pore size about 200nm (Figure 2-5)

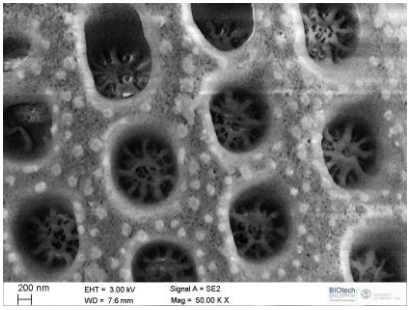

Figure 2-5: High magnification of SEM showed the porous structure of diatom cell wall encompassing patterned porous structure with different pores size.

TEM observation revealed rows of aligned nanometric strips of biogenic silica consisting of a regular array of silica nanoparticles (fFigure 2-6). Moreover, biogenic silica strips were organized in lamellar-like structures with different orientations depending on the specific location along the diatom skeleton. Silica nanoparticles deposition and formation of the biogenic silica strip are regulated by the presence of organic molecules [172].

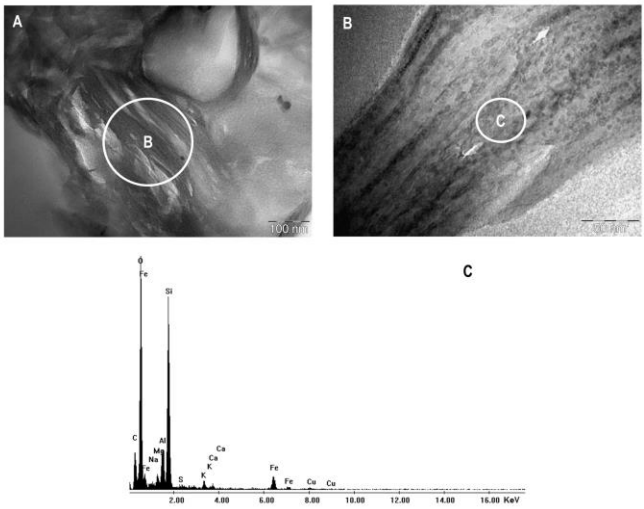

Figure 2-6:TEM observation of diatom fragments and chemical composition by EDS: A) different orientation of lamellar structure built up from biogenic silica strips, B) Micrograph shows parallel silica strips comprising small nanoparticles, (C) EDS demonstrated elemental composition of silica precipitates detected a chemical composition based on silicon, oxygen and aluminium with traces of iron, calcium and potassium. The presence of carbon and oxygen was also contributed by epoxy resin.

Thus, it could be assumed that association between organic substance and inorganic still remains at the nanoscale on the diatom skeleton structure. This is an agreement with the presence of carbon components in diatom skeleton before and even after purifications.

2.3.3 Diatomite nanoparticles preparation and morphology

Diatom nanoparticles and microparticles were produced from purified diatomite powders (both AD and CAD) by mechanical fragmentation in alkaline conditions. Nanoparticles were separated by microparticles by sedimentation and recovered from the unsettled colloidal suspension by high speed centrifugation. The yield of the process was around 15% in weight with respect to the weight of purified diatomites (AD and CAD) both for AD-NPs and fro CAD-NPs.

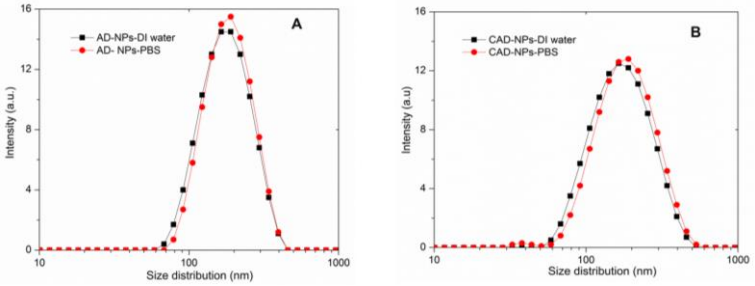

Figure 2-7: Size distribution of two different nanoparticles measured by dynamic light scattering (DLS) in DI water and PBS A) Size distribution of AD-NPs, B) Size distribution of CAD-NPs.

Dynamic Light Scattering (DLS) demonstrated that purified NPs presented a broad size distribution both in DI water and PBS; no relevant difference in particle agglomeration was observed between different solvents (Figure 2-7A and B). Particle diameters ranged from 70 to 300 nm with an average size around 170 nm (Table 2-2). No statistical differences were found between different samples.

Table 2-2: Average size of diatom nanoparticles measured by dynamic light scattering (DLS) in DI water and in PBS

Nanoparticles	Average Diameter (nm)	
	DI water	PBS
AD-NPs	171 ± 68	185 ± 66
CAD-NPs	161 ± 79	172 ± 84

TEM micrograph of AD-NPs and CAD-NPs (Figure 2-8A and B) showed irregular particles with a size of 50 nm or more. Interestingly, the irregular particles seemed to be generated by the aggregation of smaller biogenic silica nanoparticles about 10 nm in size.
In fact, it is well known that biogenic silica nanoparticles are formed by precipitation of biogenic colloidal silica by the action of silaffins in presence of silicic acid and some metallic ions in aquatic environment.

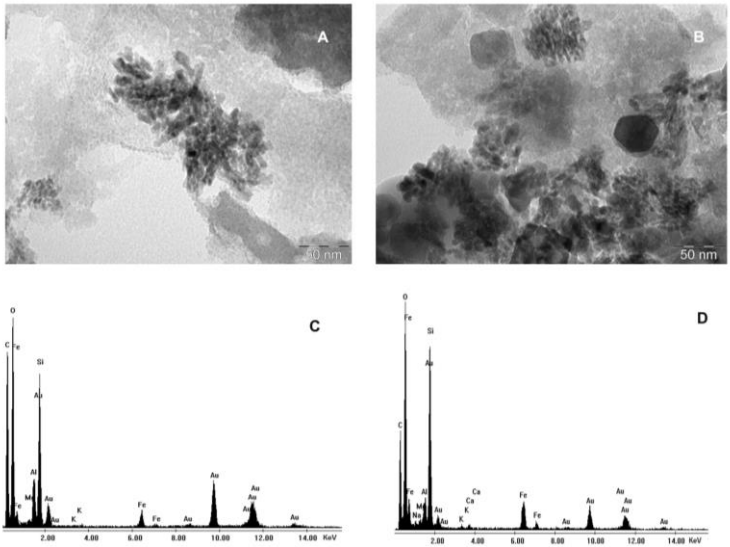

Figure 2-8: Morphology and elemental composition of nanoparticles obtained from acid-purified diatomite (AD-NPs) and acid-purified calcined diatomite (CAD-NPs). A) and B) TEM micrographs of AD-NPs and CAD-NPs, C) and D) elemental composition of AD-NPs and CAD-NPs determined by EDS. The presence of carbon was mainly contributed by ethanol solvent suspended NPs.

These observations are partially in contrast with DLS measurements (table 2-2) that reported nanoparticles ranging from 70 to 300 nm. Probably diatom nanoparticles were partially aggregated in DI water as well as in PBS. EDS spectra for both NPs types showed similar elemental compositions consisting of silicon, oxygen, aluminium and traces of iron and magnesium (Figure 2-8 C and D). No differences were found about the presence of elemental composition of diatom nanoparticles and diatom skeleton nanostructure presented previously.

The reduction of H_2O at the surface of diatom, the slight changed energy of Si – O based on wider energy core line of oxygen as well as silicon, and the oxidation of carbon after calcination could affect resulting NPs composition and also their surface chemical properties.

2.3.4 Diatoms microparticles morphology

Diatom microparticles were produced from purified diatomite powders (both AD and CAD) and were formed via mechanical fragmentation of diatom skeletons in alkaline conditions. Microparticles were separated by sedimentation and the yield of the process was around 80% in weight with respect to the initial weight of purified diatomites (AD and CAD) both for AD-MPs and CAD-MPs.

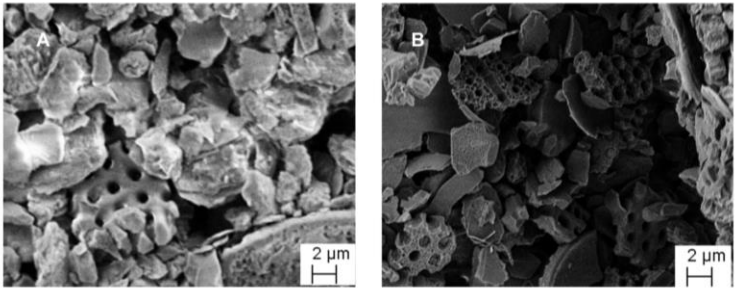

Figure 2-9: SEM morphology of diatom microparticles. A) Diatom microparticles produced from acid-purified raw diatomite (AD-MPs), B) Diatom microparticles from acid-purified calcined diatomite (CAD-MPs).

SEM micrographs revealed irregularly-shaped, highly porous MPs with size ranging from 1 to 10 µm (Figure 2-9). Clearly, the MPs consisted of micrometric fragments of skeleton diatom wall; and SEM observation did not show any significant morphological difference between AD-MPs and CAD-MPs.

2.3.5 BET surface area of nanoparticles and microparticles

All samples display isotherm curves that can be classified as Type IIb isotherms, according to the IUPAC classification (Figure 2-10) [173]. The presence of a Type H3 hysteresis loop allows to identify the samples as aggregates of plate-like particles with non-rigid slit-shaped pores, whose dimensions fall mainly in the micropore dimensions (< 2 nm in diameter), again according the IUPAC classification.

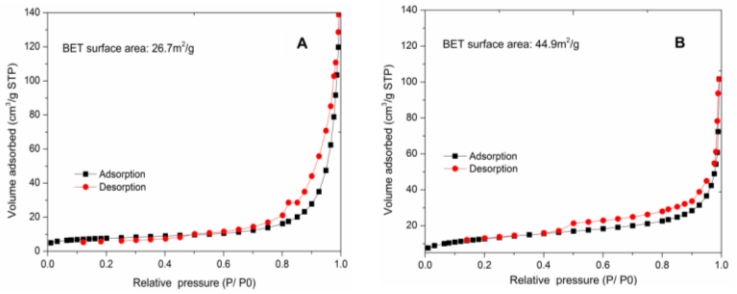

Figure 2-10: Nitrogen physisorption isotherms of (A) diatom microparticles AD-MPs and (B) nanoparticles AD-NPs prepared from acid-purified raw diatomite powders.

The results are in agreement with those reported in literature for clays [174]. Corresponding surface area values, obtained from BET model, are ranging from 25m^2/g from diatom AD-MPs to 45 m^2/g for diatom AD-NPs, typical values for this class of solids. Differences between micro- and nano-particle samples can be obtained from the analysis of the derived t-plot, where the adsorbed amount of analysis gas is plotted against the standard multilayer thickness at the corresponding P/P0 values. Within the limits of this method, pore areas due to the presence of micropores can be determined; as a result, the nanoparticle samples displayed a higher amount of micropores (about 40% of the whole specific surface area) than the microparticle samples (less than 15% of the whole specific surface area). This result represents the most evident difference between NPs and MPs; in fact, the pore distribution curves, obtained from BJH method, are quite similar for both samples, as already evidenced by physisorption isotherms, with an approximately monomodal distribution displaying a mode of the curves falling in 2-4 nm diameter range.
BET surface area results, TEM and SEM observations suggest that biogenic silica nanoparticles and microsilica particles were successfully produced from diatom whole skeletons.

2.3.6 Silicon ion release from dissolution of diatom particles in DI water

The release of silicon ion from diatom particles dissolution in DI water was determined by ICP/OES analysis of the supernatants showed in Figure 2-11.

The kinetics of silicon release from diatoms particles showed an initial fast release followed by a lowering of the rate as the incubation time increased. In particular, in the first 4 days the released silicon ranged from 87% to 92% of its final value.

After 4 days, silicon content, in AD-NPs supernatant was around 3 times higher than in CAD-NPs supernatant in spite of the comparable silicon content in the two particle groups. Instead, released silicon was 15.6 ppm and 11.1 ppm for AD-MPs and CAD-MPs, respectively.

Solubility of materials based on amorphous biogenic silica has been a controversial topic and a widespread conception [175]. Dissolution can be affected by many experimental factors including solvent characteristics such as ion strength, dissolution temperature and aging mechanisms of the diatomite deposits [176], [177].

Nitrogen physisorption analyses determined that diatom NPs presented a specific surface area larger than diatom MPs, and a large part of this difference was related to the contribution of nanosize porosity. Most likely, this difference in surface area between diatom MPs and NPs can partially explain why AD-NPs solubilize faster than AD-MPs.

Moreover, dissolution of diatom particles can be influenced by many diatom particles characteristics, such as surface chemistry and structure, morphology, composition and microstructure. For example, the density of hydrophilic silanol groups (-Si-O-H) at the surface of biogenic silica is believed to be an important factor for the control of the dissolution of diatom particles.

Zhuravlev [178] found that silanol groups of amorphous silica decreased more than 50% with respect to the initial amount after calcination at 600 °C. This probably means that the partial removal of hydroxyl group at the surface of diatoms during to calcination can transform hydrophilic silanol groups into hydrophobic siloxanes (≡Si-O-Si ≡) and reduce the density of silanol groups.

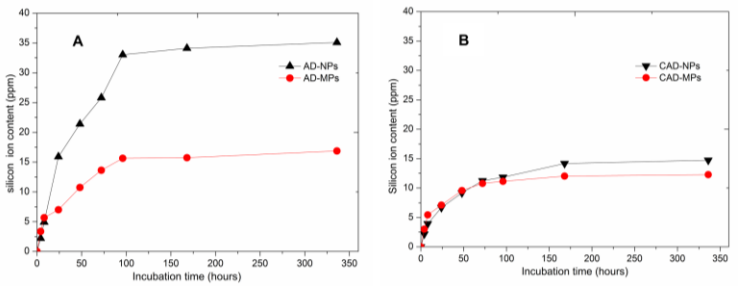

Figure 2-11: Silicon release profile from diatom nanoparticles and microparticles quantified by inductively couple plasma/optical emission spectroscopy (ICP/OES). A) Particles derived from acid-purified raw diatomite (AD-NPs and AD-MPs), B) Particles derived from acid-purified calcined diatomite (CAD-NPs and CAD-MPs).

As a consequence, different amounts of silanol group at the surface of two types of diatomite NPs could also contribute to explain differences in silicon release kinetics. We suppose that NPs derived from acid-purified raw diatomite should (AD-NPs) presented more surface silanol groups than NPs derived from calcined diatomite (CAD-NPs). For this reason, AD-NPs should dissolve faster than CAD-NPs, thus leading to faster silicon release.

2.3.7 Cytotoxicity of diatom particles

Toxic effect of diatom particles on 3T3 cells membrane integrity determined by LDH assay showed a significant dependency on the diatomite purification routes and dose. Toxic effect of AD particles was generally larger than CAD particles for both elution method (Figure 3-12A) and direct contact method (Figure 3-12 B). In the elution mode, either no toxicity or negligible toxicity was observed at all concentrations for CAD particles. AD particles showed limited cytotoxicity at all the concentrations (Figure 3-12A).

Similar results were found in direct contact mode (Figure 3-12 B). No cytotoxic effects were noted for CAD-NPs and CAD-MPs, except for CAD-MPs at the highest concentration (500 µg/ml). In addition, in direct contact mode AD-NPs resulted slightly cytotoxic just at the highest concentration, while AD-MPs presented the highest values of cytotoxicity for all the concentrations. However, the relative cytotoxicity never exceeded the value of 30%.

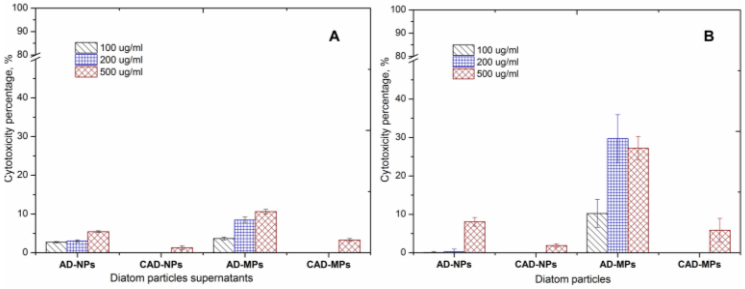

Figure 3-12: Percentage of cytotoxicity of the different groups of diatom particles on 3T3 cells determined with LDH assay; A) Elution method and B) Direct contact method. Cell cultured in reduced medium without any diatom sample were used as negative control (0% cytotoxicity), while cells treated with 0.05% Triton X-100 surfactant were used as positive control (100% cytotoxicity).

Considering dose dependency, cytotoxic effects generally increased following the increase of dose for both NPs and MPs.

The presence high silanol groups in AD-supernatant could explain higher toxicity of AD-NPs and AD-MPs in comparison to CAD counterparts in the elution mode due to faster release kinetics. Residual organic contaminants in AD samples could also contribute to the relatively higher cytotoxicity of AD samples [179], [156].

2.4 Conclusion

Tissue engineering strategies often relies on polymeric porous matrices loaded with calcium phosphate based ceramics to support and drive bone regeneration. However, it has also been shown that bone formation and maintenance occur under the regulatory control of various signals and elements; silicon for example is believed to be a critical factor in the early stages of mineralization. For this reason, there is a great interest in new silicon-donor ceramics. Diatomite is a cheap and abundant source of biogenic silica and we showed that it can be easily converted to silica particles with controlled size and chemistry.

Here, raw diatomite and calcined diatomite powders were purified by acid treatment, and silica-based diatom microparticles (MPs) and nanoparticles (NPs) were produced by fragmentation of purified

diatomite under alkaline conditions. We demonstrated that the resulting diatom particles can undergo degradation in aqueous environment, thus actively releasing silicon ions. Furthermore, we found that silicon release kinetic was influenced by diatomite purification method and particle size. Diatom-derived MPs and NPs showed limited or no cytotoxic effect in vitro, in particular particles derived from calcined diatomite. The possibility to easily suspend nano and microparticles particles in water and in ethanol, their limited cytotoxicity and their silicon release ability make diatom-derived particles a candidate as bioactive filler for polymeric scaffolds for bone tissue engineering.

Acknowledgements

This study was funded by Erasmus Mundus (2012-2015) project from European commission. We are grateful to prof. Matteo Leoni of University of Trento for XRD analysis.

Chapter 3: Enhancing bioactive properties of silk fibroin with diatom particles for bone tissue engineering applications

Part of this chapter has been submitted in:
Journal of Tissue Engineering and Regenerative Medicine
Title "Enhancing bioactive properties of silk fibroin with diatom particles for bone tissue engineering applications"
Authors: Thi Duy Hanh Le, Volha Liaudanskaya, Walter Bonani, Antonella Motta, Claudio Migliaresi

Abstract

Many studies have highlighted the role of silicon in human bone formation and maintenance. Silicon, in fact, is considered to nucleate the precipitation of hydroxyapatite and to reduce the bone resorption. For this reason, we have combined silk fibroin with silicon releasing diatom particles, as potential material for bone tissue engineering applications. Sponges of fibroin loaded with different amounts and sizes of diatom particles were prepared by solvent casting-particulate leaching method, and their morphology, porosity, and mechanical properties were evaluated. The biological effect of diatom addition was assessed on human osteosarcoma cell line MG63, a suitable osteoblast-like model, through cell adhesion, metabolic activity and proliferation assays. In addition, alkaline phosphatase activity (ALP), osterix and collagen type I production in MG63 cell line were assessed as markers of early bone formation to demonstrate a pro-mineralization potential of scaffolds
Results of the studies showed that addition to fibroin of diatoms particles improved the osteogenic properties of osteoblast-like cells compared with the pure silk fibroin.

3.1 Introduction

Tissue engineering consists in the combined use of scaffold and cells to induce tissue regeneration and repair [116]. Besides being biocompatible, scaffold materials must be biodegradable, possibly match mechanical properties and architecture of the target tissue to regenerate/repair, transfer and translate the biomechanical and biochemical signals from/to cells. Scaffolds that have been proposed for bone regeneration comprise ceramic materials, polymers and their composites [29], [147], [128], [180]–[184], [62]. Among biological polymers, silk fibroin has been proposed, partly thanks due to its excellent biocompatibility and controllable biodegradability, tunability of mechanical properties and of shape/architecture, as sponge, fiber, thin film or injectable gel [185]–[194].

Loading silk fibroin sponges with proper supplements or growth factors that support osteogenesis can significantly improve osteoinductive properties of silk fibroin [195]–[197].

Various materials were proposed for osteoinduction, such as inorganic ceramics, metals and polymers [154], [155], [198]–[200].

Silicon is an abundant element in nature, which exists in oxidized form as water-soluble including silicic acid and sodium silicates and insoluble form as silicate and silica.

Silicon is a minor constituent of the bone, less than 1% of bone dry weight, however it is considered to be crucial for bone formation [110],[152] being nucleating agent for the precipitation of hydroxyapatite [94]. Moreover, silicon facilitates the reduction of bone resorption due to regulation of osteoprotegerin (OPG) and receptor activator of NF-kB ligand (RANKL) markers expression [108],[153]. Numerous in vitro experiments proved beneficial effect of silicon on bone formation, for instance, silicon doped ß- tricalcium phosphate enhances differentiation of mesenchymal stem cells into bone tissue as well as osteoblast's activity [182]; soluble silicon upregulates alkaline phosphatase and propyl hydroxylase enzymes activity, active components of bone remodeling and maturation [105], [103]; In addition, the presence of soluble silicon at inorganic-organic interface plays a key role in the formation of cross-linking between collagen and proteoglycans during bone formation to improve the connection of extracellular matrix formation [98],[95]; Furthermore, silicic acid

induces upregulation of bone morphogenetic protein 2 (BMP-2) and collagen type I expression [104], [201].

Silicon containing materials, such as polymers composites with platelet silicate nanoclay, bio-glass as well as amorphous silica particles [195], [202], [203] have been proposed for bone tissue engineering.

In the last years, attention has been addressed to bio-silica as promising osteoinductive additive [150], [204]. Bio-silica, is mostly hydrated amorphous silica, can be naturally formed by biosilicification of silaffin proteins (in diatoms) in presence of the silicic acid of the environment [10], [21].

The application of bio-silica synthesized from silicatein enzyme was recently suggested for bone tissue engineering [204]. In our previous study, we proved that diatom particles derived from diatom skeleton are non-toxic and can be used as silicon-releasing agent [205].

To our knowledge, bio-silica of diatom skeleton was never used as additive for engineered scaffolds for bone tissue engineering applications.

Herein, the aim of the presented study was to investigate the in vitro osteoinductive properties of silk fibroin sponges loaded with diatom micro- and nanoparticles as silicon donors. We evaluated the effect of diatom-loaded (at different size and concentration) silk fibroin sponges versus pure silk fibroin sponges through the cell metabolic activity, proliferation, adhesion and the expression of bone specific markers such as alkaline phosphatase activity, collagen type 1 and osterix in MG63 human osteoblast-like cell line.

3.2 Materials and Methods

3.2.1 Materials

Reagents including phosphate buffer solution (PBS), sodium hydroxide (NaOH), hydrochloric acid (HCl), lithium bromide (LiBr), Triton X-100, sodium chloride (NaCl), glutaraldehyde solution, sodium cacodylate trihydrate, formalin, bovine serum albumin (BSA), 4, 6 diamidino-2-phenyindole, dilactate (DAPI), polyethylene glycol (PEG) and ethanol were purchased from Sigma-Aldrich (St. Louis, MO, USA).

Diatom nanoparticles (DNPs) and microparticles (DMPs) were obtained from purified diatom skeletons isolated from diatomaceous

powder (Phu Yen mineral joint stock company, Phu Yen province, Viet Nam) as reported in [205]. DNPs size was in the range of 50 nm to 300 nm as measured by dynamic light scattering (DLS) and DMPs ranged from 1 to 10 µm as estimated by Scanning Electron Microscopy (SEM).
Silk fibroin (SF) was isolated from Bombyx mori silkworm cocoons (Cooperativa Sociolario, Como, Italy).

3.2.2 Scaffold preparation

Silk cocoons were treated twice in alkaline water baths at 98 ^{0}C for 1.5 hours with 1.1 g/l and 0.4 g/l Na_2CO_3, respectively. Degummed silk was then washed several times in de-ionized (DI) water and dried at room temperature (RT). Fibroin was then dissolved in 9.3M LiBr (1 g of fibroin in 10 ml of LiBr solution) at 65 ^{0}C for 2.5 h. The solution was dialyzed against DI water for 3 days at RT in a Slide-A-Lyzer dialysis cassette (3.5K MWCO, Pierce, Rockford, IL, USA) to remove LiBr salt and then against a 25% wt. PEG solution (Mn: 10000 KDa) to concentrate SF solution up to 7.8 – 8.3% wt. The fibroin concentration was measured by absorbance spectroscopy using a NanodropTM spectrophotometer (Thermo Fisher Scientific, Wilmington, DE, USA).
Before any further use, silk fibroin solution was filtered using a ceramic filter (porosity < 5 µm) to eliminate impurities.
Diatom nanoparticles (DNPs) and microparticles (DMPs) obtained following reference [205], were dispersed in DI water, added to aqueous silk fibroin solutions in different proportions and the resulting suspensions were mixed for homogenization for 10 min.
The final concentration of silk fibroin in the solution was 6.2% wt. while the total concentration of diatom particles (DPs) was set to 0.8% and 3.2% wt. with respect to the dry fibroin content.
Pure SF as well as SF composite sponges with different proportions of DNPs and DMPs were prepared as follows.
5 ml of aqueous silk fibroin and diatom particles suspensions were transferred to 60 mm petri dishes, and 11 g of NaCl (salt crystals with size ranging from 425 to 1180 µm) were slowly poured into the petri dishes and left at RT till the formation of a stable hydrogel. NaCl salt was then removed by repetitive washings in deionized (DI) water and samples were then frozen at -80 ^{0}C and freeze-dried overnight.

Before use, dried sponges were hydrated with DI water, cut to 2 x 6 mm of height vs diameter cylinders and sterilized in autoclave at 1 bar, 121 ^{0}C for 45 minutes.
Name codes and compositions of the different samples are summarized in Table 3-1.

Table 3-1: Composition of the silk fibroin/diatom particles scaffolds

Sample name	DNPs, wt. %	DMPs, wt. %
SF	0.0	0.0
SF-N0.8	0.8	0.0
SF-M0.8	0.0	0.8
SF-(N+M)0.8	0.4	0.4
SF-N3.2	3.2	0.0
SF-M3.2	0.0	3.2
SF-(N+M)3.2	1.6	1.6

3.2.3 Scaffolds characterization

A Field-Emission Scanning Electron Microscope (Supra 40, Zeiss, Germany) was used to observe the architecture and morphology of fabricated scaffolds. Prior analysis, samples were coated with Pt/Pd (BIO-RAD, SEM coating unit PS3, Assing S.p.a, Rome, Italy).
The presence of diatom particles as well as their distribution was detected using back scattered electrons (BSE). Samples were coated with carbon before observation.
Fourier Transform Infrared FTIR (Spectrum, Perkin Elmer, US) analysis was used to analyze sponge and diatom particles powder.
Porosity of sponges was determined using the liquid displacement method. Sponges were submerged in a known volume of hexane (V1) for 8 minutes. The total volume of hexane with sponges (V2) was measured. Afterward sponges were removed and the residual volume of hexane (V3) was recorded. The porosity of sponges was calculated by the equation:

$$\%\ Porosity = \frac{V1 - V3}{V2 - V3} \times 100\%$$

Water content of the dry scaffold was determined by using DI water absorption. In details, the dry scaffold known its weight was continuously soaked drop by drop DI water till completely wet state that defined its weigh did not change. The wet samples then weighed. The percentage of water content was given by the equation

$$\%\ \text{Water content} = \frac{m_{wet} - m_{dry}}{m_{wet}} \times 100\%$$

Young's modulus of wet cells unseeded scaffolds was evaluated by compression tests performed at 37 ^{0}C, displacement rate 1mm/min up to 80% of strain, using Bose ElectroForce 3200.

3.2.4 Cell culture

MG63 human osteosarcoma cell line (passage 102, Istituto Zooprofilattico Brescia, Italy) was used to perform the in vitro studies. Cells were subcultured in 175 mm^2 culture flasks as monolayer at 37 ^{0}C under 5% CO_2 in Minimum Essential Medium (MEM) supplemented with 10% foetal serum bovine (FBS), 1mM non-essential amino acid, 100 units/ mL antibiotic, 2mM glutamine and 1mM sodium pyruvate. Medium was changed every third day till the cells reached 90-95% confluence.

Sponges were placed into 48 well plates, washed with PBS and then conditioned with culture media for 20 minutes. Cells were seed at two different concentrations; 9x10^3 and 4.5 x10^3 per mm^2 of sample; A confined drop method was used to seed each concentration on the top of each sponge and then after 2 hours additional 400 µl of medium was added to each well. After 24 hours of incubation, seeded sponges were transferred into new plates. Cells were cultured up to 14 days.

3.2.4.1 Cell proliferation and metabolic activity

Evaluation of in vitro cell metabolic activity and proliferation was performed 3 and 7 days after cell seeding.

Cellular metabolic activity was measured with Alamar Blue® (Invitrogen, Oregon, USA) assay following the manufacture instructions. In brief, the culture medium was removed and replaced with equal volume of fresh medium with 10% of Alamar Blue® reagent at each experimental time point. Samples were incubated for 2 hours with light protection, after that 100 µl of surnatant was taken from each sample in triplicates and transferred to 96-well plate and

the signal was measured with fluorescent plate reader machine (560 nm excitation and 590 emission; Safire, Tecan, Austria).
The proliferation rate of MG63 cells in the sponges was determined with DNA quantification assay with Quant-iT PicoGreen® dsDNA Assay Kit (Invitrogen, Molecular Probes, Oregon, USA) following the manufacturer's instructions. In brief, total DNA content was collected with 0.5ml of Triton-X 0.05%, after a short wash in PBS, and stored at -20 ^{0}C until further analysis. Prior assay all samples were thawed at room temperature, sonicated for 20 seconds (cycle: 1, amplitude 40%), then diluted till the test sensitive concentration. Fluorescent intensity of PicoGreen-DNA complex was measured in 96-well black plates with a plate reader (Safire, Tecan, Austria). A calibration curve was built up by using the DNA standard provided with the assay to correlate the fluorescent intensity to the concentration of DNA.

3.2.4.2 Cells morphology and adhesion

Adhered cells morphology was evaluated with FE-SEM microscope. At each experimental time point, samples were fixed with 2.5% glutaraldehydrate in cacodylic buffer 0.1 M, incubated for 20 minutes at 4 ^{0}C, then rinsed 3 times in cacodylic 0.1 M buffer, finally dehydrated in a graded series of ethanol/water solutions (70, 80, 90, 95 %) and twice in pure ethanol for 10 minutes per time. At last, samples were freeze-dried and, prior, FE-SEM visualization, sputter coated with a thin Pt/Pd layer.

3.2.4.3 Live and dead assay

Cells viability was evaluated at days 3 and 7 after seeding with confocal microscopy after staining with calcein AM and propidium iodide (PI) (Invitrogen, Oregon, USA). In brief, samples were incubated for 20 min at 37 °C with calcein (1 ul of calcein per 1ml of MEM), washed in PBS, exposed to the second staining with propidium iodide (100 ul of PI per 1ml of PBS), double washed in PBS and immediately visualized with confocal microscope (A1, Nikon).

3.2.4.4 Immunocytochemistry

Specific markers expression of bone formation due to osteoblast's activity was evaluated with immunocytochemistry against collagen type I and osterix. At established experimental time points, samples

were washed with PBS and then fixed with 4% of PFA for 30 min at room temperature (RT). Subsequently samples were blocked and permeabilized with buffer containing 1% of BSA and 0.3% of triton X in PBS for 1 hour at RT, followed by staining with the diluted (1:200 in 1% of BSA/ PBS buffer) primary antibody against collagen type I (ab6308- rabbit) and osterix (ab94744 - abcam, Cambridge, UK) for 1.5 hours and washed 3 times with PBS for 5 minutes each. Then, samples were incubated with secondary antibodies (anti-rabbit Alexa Fluor 568, Molecular Probes, Grand Island, NY), diluted 1:500 in PBS for both osterix and collagen type I for 1 hour, triple washed with PBS, and finally, stained with DAPI solution (1:1000) for 5 minutes at RT. Before visualization with confocal laser microscope, samples were washed with PBS.

3.2.4.5 Alkaline phosphatase quantification

The alkaline phosphatase (ALP) activity was measured on the cell lysates. At each experimental time point, cell culture medium was removed and samples were washed 3 times with PBS before adding 0.5 ml of Triton X – 0.05% in PBS per well. Samples were incubated for 30 minutes at room temperature (RT) and then frozen at -20 ^{0}C until all samples were collected. Before measurement, samples were thawed at RT and then sonicated in ice-cold water bath for 20 seconds (cycle: 1, amplitude 40%) with a Virsonic ultrasonic cell disrupter (Virtis, Warmister, PA). ALP activity was measured following the manufacturer's instructions (ab83371 ALP assay Fluorometric, Cambrige, UK) with a standard curve in the range from 0.0 to 0.4 nmol 4-MUP. ALP concentration was measured by fluorescent intensity at 360/ 440 nm (Ex/ Em) using a TECAN (Austria) microplate reader according to the standard curve data.

3.2.4.6 Statistical analysis

All biological tests were performed on three samples with triplicate measurement for each sample whereas porosity and Young's modulus were done on four samples. Data are presented as mean± standard error. One way or two way of variance (ANOVA, originPro 8.5.1) was used to evaluate significant difference among the control (silk fibroin scaffold) and composite scaffolds. The significant difference of two data sets was defined at $p<0.05$.

3.3 Results and discussion

3.3.1 Sponge characterization

Architecture and morphology of composite SF/DPs scaffolds as well as silk fibroin scaffolds are shown in Figure 3-1. Scaffolds have a porous structure, with large (up to 400 microns) and small randomly distributed and interconnected pores, with no appreciable differences between silk fibroin and composite SF/ DPs sponges.
Micrographs (Figure 3d-f) displayed on the surface of all scaffolds the presence of microspheres with estimated size ranging from 1 to 10μm, with microspheres distribution and density depending on the sample composition. In particular, the density of microspheres progressively increased at increasing diatom particles concentration.

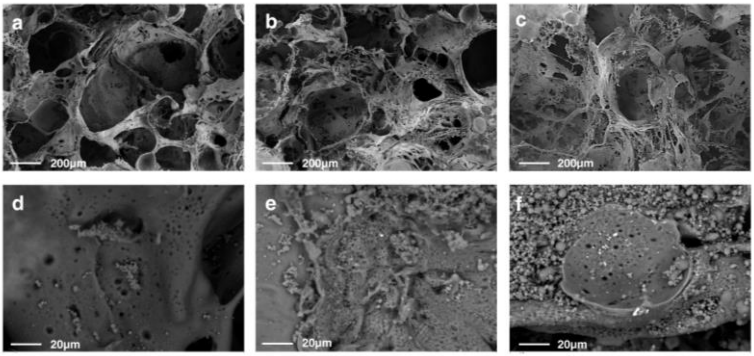

Figure 3-1: a-c) Scanning electron microscopy (SEM) images presented three different scaffold architectures of SF– silk fibroin, SF-(N+M) 0.8–composite comprising of 0.8% diatom particles mixed diatom nanoparticles (DNPs) and diatom microparticles (DMPs) and SF-(N+M) 3.2 – composite with 3.2% of diatom particles mixture of DNPs and DMPs, d-f) high magnification of SEM to observe difference of their structures.

Microspheres formation could be due to the assembling of silk fibroin in aqueous solution in micelles and then into microspheres, triggered by the presence of diatom particles, especially at lower concentration of silk fibroin. The microspheres formation by the addition of DPs could depend on the difference of surface energy between DPs and silk fibroin during the dry process that may tend to increase self-assembly of protein. Moreover, the interaction between silicic acid

from diatom particles and the hydroxylated amino acids of silk fibroin may cause modifications in the protein assembling, similarly to what has been observed for collagen proteins modifications. Silk microspheres formation was described in literature earlier [206], [207].

Diatom particles distribution was analysed with backscattered electron (BSE) of FE-SEM images, diatom particles are visible as white spots, whereas silk fibroin matrix is grey. As predicted, no white domains were revealed in silk fibroin scaffold (Figure 3-2) while the micro white spots distribution is observed in SF/ DPs composite comprising of diatom microparticles and the mixture of micro particles and nanoparticles. DNPs were not detected with FE-SEM due to the limitation of magnification. Moreover, DPs in composite scaffolds might be randomly covered by silk fibroin. Diatom particles embedded on the surface of composite sponges may increase the surface roughness, except for diatom particles covered by silk fibroin.

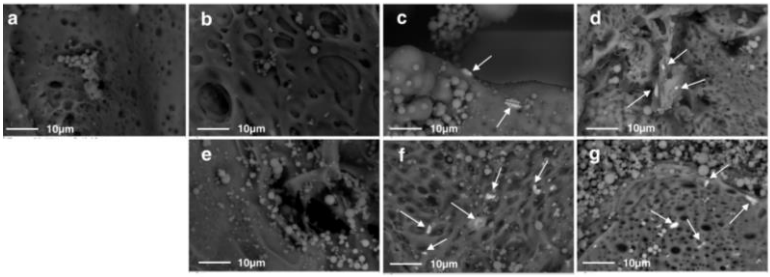

Figure 3-2: Diatom distribution of all groups scaffolds detected by using BSE of FE- SEM : a) SF- silk fibroin, b) SF-N0.8 – composite with 0.8% of diatom nanoparticles (DNPs), c) SF-M0.8 – composite with 0.8% of diatom nanoparticles (DMPs), d) SF-(N+M)0.8 – composite comprising of 0.8% diatom particles mixed (DNPs) and (DMPs), e) SF-N3.2 – composite with 3.2% of DNPs, f) SF-M3.2 – silk fibroin added 3.2% of DMPs and g) SF-(N+M)3.2 – composite with 3.2 % of DPs mixture of DNPs and DMPs, respectively. Arrows presented diatom particles placed in scaffolds.

The protein secondary conformation and the effect of the diatoms particles addition on samples conformation were evaluated by infrared spectroscopy. Pure fibroin sponges as well all the composite samples showed adsorption bands at around 1622 cm^{-1} (amide I), 1518 cm^{-1} (amide II), 1260 cm^{-1} (amide III), and the shoulder at 1265

cm^{-1} confirmed ß-sheet is the main secondary conformation (Figure 3-3). Shoulder at 1690 cm^{-1} suggested that this ß-form is of antiparallel type [185]. The addition of diatoms nano and micro particles did not cause structural conformation modifications to SF, probably due to the major effect of NaCl salt on the protein organization. The feature peak related to Si-O-Si/ Si- OH of biosilica around 1030 cm^{-1} [28] was not visible in the composite matrices curves, probably due to the particles dispersion into the bulk. Furthermore, the signal of this peak might be decreased due to DPs by silk fibroin covering or embedding superficial diatom particles.

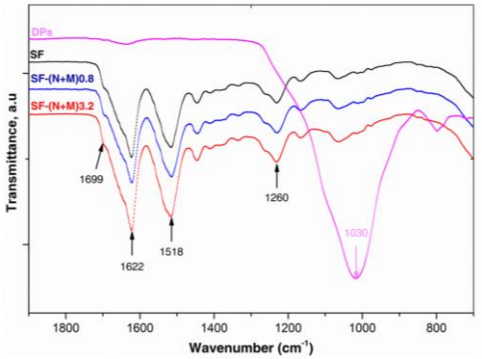

Figure 3-3: FTIR spectra of 3 different scaffolds including SF– silk fibroin, SF-(N+M)0.8 – composite comprising of 0.8% diatom particles mixed diatom nanoparticles (DNPs) and diatom microparticles (DMPs) and SF-(N+M)3.2 – composite with 3.2% of diatom particles mixture of DNPs and DMPs.

Porosity of all samples, measured with the liquid displacement method, ranged for all scaffolds from 85 to 87% (Table 3-2). However, the addition of the diatom particles appears to modify the assembling and structure of the scaffolds that present in the case of composites many areas (finding that is common to all samples) with fibrillar and less dense packing.

Table 3-2: Porosity of all scaffold groups was determined by the hexane replacement

Groups	SF	SF-N0.8	SF-M0.8	SF-(M+N)0.8	SF-N3.2	SF-M3.2	SF-(M+N)3.2
Porosity, %	87.3 ±1.1	86.1 ±1.5	86.0 ±1.4	84.9 ±1.9	86.2 ±18	86.7 ±1.7	86.0 ±1.9

Young's modulus of wet scaffolds was calculated from the linear region of stress-strain curves. The results (Figure 3-4) showed that elastic modulus of composite SF/ DPs scaffolds with low and high DPs concentration was reduced around 40% in comparison with silk fibroin scaffold. The decrease of the compressive elastic modulus of the composite scaffolds is in contrast with the well-known effect of the addition of micro or nanofillers on polymer materials, and can be explained on the basis of the modification of the polymer structure that has been commented when illustrating the SEM micrographs of Figure 3-1.

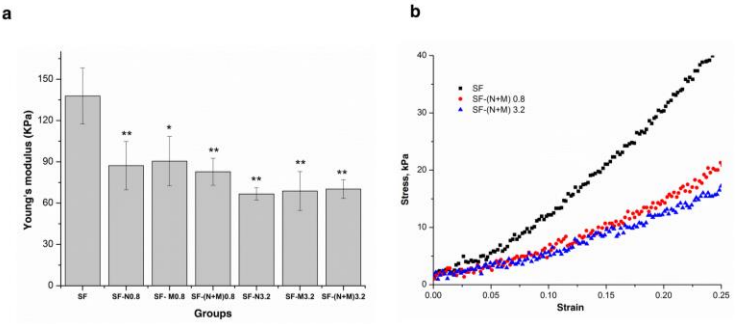

Figure 3-4: Compressive elastic moduli elastic modulus of composite scaffolds and b) the selected of stress-strain curve in the linear region of silk fibroin (SF), silk fibroin loading 0.8 (SF-(N+M)0.8) and 3.2% (SF-(N+M)3.2) of mixture diatom particles.

3.3.2 Evaluation of in vitro cells bioactivity in various scaffold formulations

3.3.2.1 Metabolic activity and proliferation

The results of the conducted assays are presented in Figure 3-5. Metabolic activity is a complex process of cells behaviour, which will depend on variety of factors. Here we used Alamar Blue assay to evaluate cells activity combined with DNA quantification, to detect the proliferation rate. Based on the results of Alamar Blue assay (Figure 3-5), there was no effect of DPs at low concentration on cell metabolic activity at day 3 for both concentrations of the cells seeded, however slight increase in the cells activity was observed in scaffolds with higher DPs concentration. Notably, at day 7 after seeding, a significant increase in metabolic activity was observed in scaffold groups loaded with DPs compared to silk fibroin scaffolds, especially at low concentration of the cell seeded.

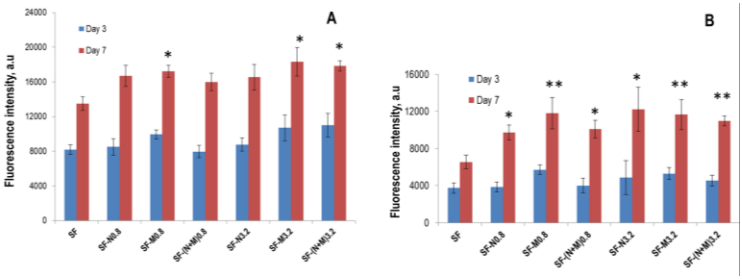

Figure 3-5: Cell metabolic activity performed by Alamar Blue® at two different cell seeded initially at A) 9.10^3 cells/ mm^2 and b) $4.5.10^3$ cell/mm^2 for all groups including SF–silk fibroin, SF-N0.8 – composite with 0.8% of diatom nanoparticles (DNPs), SF-M0.8 – composite with 0.8% of diatom nanoparticles (DMPs), SF-(N+M)0.8 – composite comprising of 0.8% diatom particles mixture of (DNPs) and (DMPs), SF-N3.2 – composite with 3.2% of DNPs, SF-M3.2 – silk fibroin added 3.2% of DMPs and SF-(N+M)3.2 – composite with 3.2 % mixture of DNPs and DMPs, respectively. Statistically significant difference compared with the control at the same time of culture was representative at * ($p<0.05$), ** ($p<0.01$).

We hypothesize that the release of silicon from diatom particles dissolution could contribute to the increase of cell metabolic activity and proliferation rate, through the activation of molecular mechanisms to maintain osteoblastic activity, as previous studies reported [103]. The presence of soluble Si could be involved in the expression of IGF-I factor by osteoblasts that contributed to the improvement of cell proliferation, as well as the inhibition of cell death [208]. Moreover, the changes in sponge microstructure with addition of diatom particles might enhance MG63 osteoblastic activity as well.

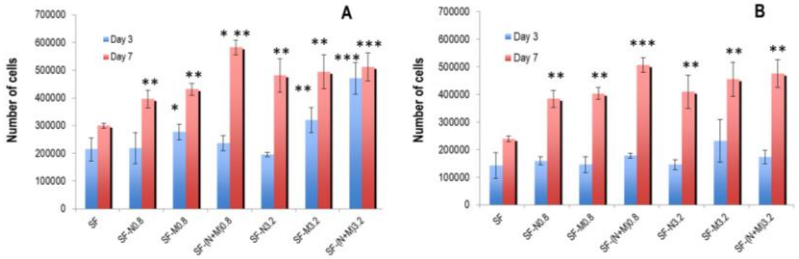

Figure 3-6: Cell proliferation quantified by PicoGreen Kit of two different cell seeded initially at A)9.10^3 cells/ mm2 and b)$4.5.10^3$ cell/mm^2 for all group scaffolds including SF–silk fibroin, SF-N0.8 – composite with 0.8% of diatom nanoparticles (DNPs), SF-M0.8 – composite with 0.8% of diatom nanoparticles (DMPs), SF-(N+M)0.8 – composite comprising of 0.8% diatom particles mixture of (DNPs) and (DMPs), SF-N3.2 – composite with 3.2% of DNPs, SF-M3.2 – silk fibroin added 3.2% of DMPs and SF-(N+M)3.2 – composite with 3.2 % mixture of DNPs and DMPs, respectively. Statistically significant difference compared with the control at the same time of culture was representative at * ($p<0.05$), ** ($p<0.01$) and *** ($p<0.001$)

The effect of different scaffold formulations on cell proliferation was investigated with DNA quantification assay (Figure 3-6). In general, cell proliferation rate on SF/DPs scaffolds increased in comparison to silk fibroin scaffolds. At day 3, significant upregulation in cell number was found in SF- M3.2, SF-(N+M)3.2 samples, in particular SF-(N+M)3.2 scaffolds in which cell number doubled with respect to the control group. However, cell proliferation in all scaffolds at low concentration of the cells seed did not show the change. After 7 days of incubation, the noticeable increase in cell number was detectable

in all groups of composite scaffolds for both low and high concentrations of initial cells seeded. Results show that addition of diatom particles in silk fibroin sponges significantly increases cell proliferation rate.

Cell proliferation results were consistent with cell metabolic activity, which supports the initial hypothesis of silicon effect on faster bone formation. These findings could provide a basic proof of the improvement of the silk fibroin bioactive properties with diatom particles supplementation. Specifically, an up-regulation of cell proliferation rate will be crucial to reach faster bone formation and as consequence maturation and matrix mineralization.

3.3.2.2 Cells viability and distribution

The cell viability and cell distribution on scaffolds were assessed with confocal laser microscopy (CLM); results are presented in Figure 3-7

Confocal images show significant improvement of cell adhesion in all composite SF/DPs samples 7 days after seeding at high initial concentration as well as the low one, except for SF-(N+M)0.8 at the low initial concentration. However, at day 3 cells adhered on pure SF and SF composite scaffolds with lower particles content are still in round shape and clustered. Higher diatoms concentration induced changes in adhered cells morphology, that had more spindle shape, and started to connect each other even at the first experimental time point. After 7 days of culture, all composite scaffolds displayed higher cell adhesion and interconnections.

The result of cell viability is consistent with cell metabolic activity and cell proliferation.

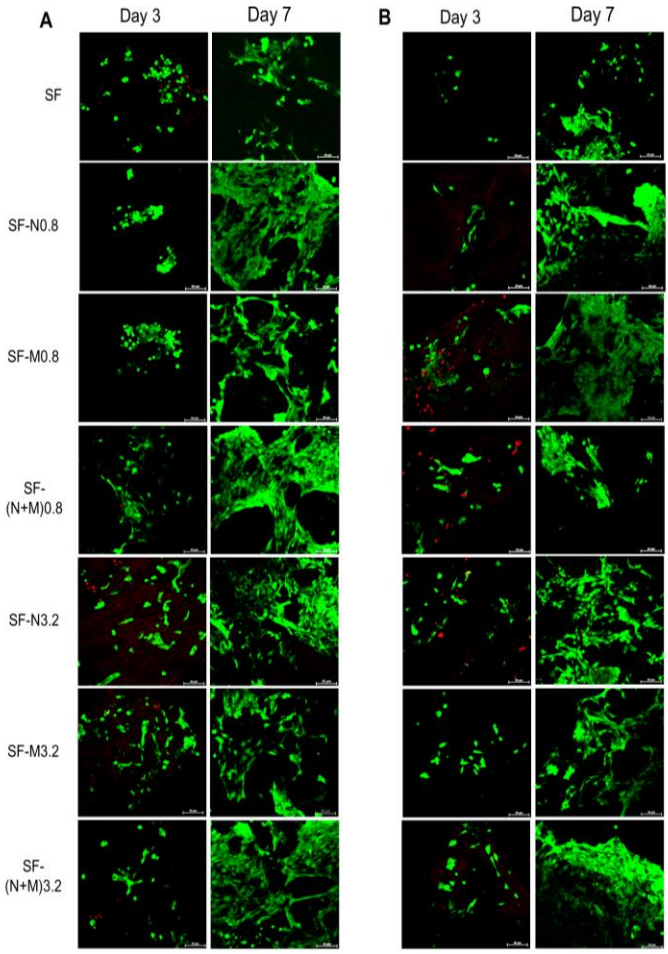

Figure 3-7: Confocal scanning laser microscopy images of cell live/ dead stained with calcein AM/ PI after day 3 and 7 of culture of two concentration of the cells initially seeded A) 9.10^3 and B) $4.5\ 10^3$ cell/ mm^2 in different scaffolds including SF–silk fibroin, SF-N0.8 – composite with 0.8% of diatom nanoparticles (DNPs), SF-M0.8 – composite with 0.8% of diatom nanoparticles (DMPs), SF-(N+M)0.8 – composite comprising of 0.8% diatom particles mixed (DNPs) and (DMPs), SF-N3.2 – composite with 3.2% of DNPs, SF-M3.2 – silk fibroin added 3.2% of DMPs and SF-(N+M)3.2 – composite with 3.2 % of DPs mixture of DNPs and DMPs, respectively (scale bar = 50μm).

3.3.2.3 Cell morphology and adhesion

Proper cell adhesion supports cell functionality, proliferation and survival, and this process can be disrupted during cell adhesion to different material surfaces, thus it is critical parameters to control in material evaluation. Cell adhesion on SF and SF/DPs scaffolds were evaluated with SEM micrographs, and results are presented in Figure 3-8

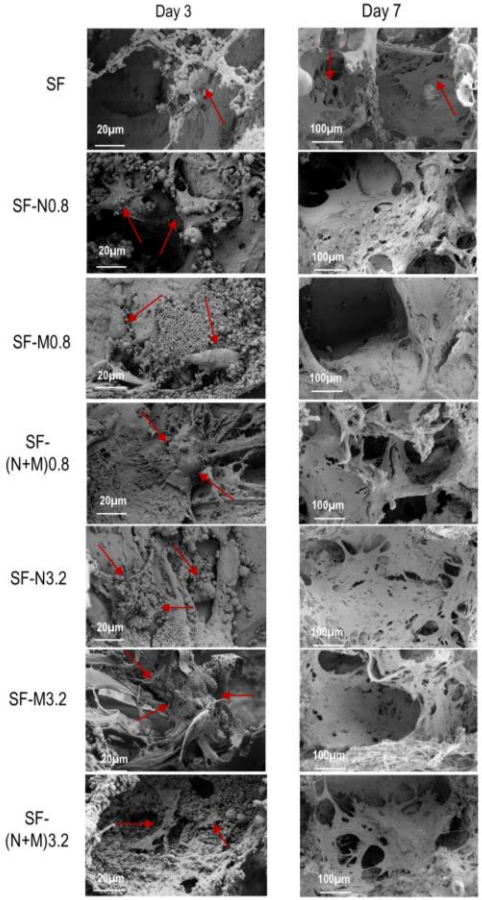

Figure 3-8: SEM micrographs of cell morphology (after day 3) and attachment on different scaffolds after 7 day of culture at the high concentration of cell seeded. Red arrows depict the position of cells.

As can be seen, cells seemed to change their morphology from the round to spindle shape and communicate together in all composite scaffolds in comparison with the round shape in pure silk fibroin at day 3. The cell number and distribution was more advanced in all scaffolds with DPs presence after 7 days of incubation. Moreover, cells in DPs/ silk fibroin scaffolds covered not only the surface of pore outer rings but also tended to migrate into the pores, whereas in silk fibroin scaffolds cells seemed to be distributed randomly without formation of homogeneous layers.

It was expected to observe cells migrating in scaffolds to proliferate in empty areas of scaffolds. The significant improvement in cell adhesion could confirm the role of soluble silicon reported in previous literature.

These results also support the DNA quantification assay on the amount of cells in the visible areas of all scaffolds.

An enhancement of cell adhesion could be one of reasons that explains an increase of cells metabolic activity as well as proliferation rate, besides the direct effect on the molecular level of soluble silicon released by diatom particles dissolution on cell proliferation and metabolic activity, mentioned above.

3.3.3 Bone formation markers

3.3.3.1 Immunocytochemistry

Osterix is an important transcription factor which triggers and controls osteoblasts differentiation and continues to play an essential role in bone maintenance [209], [210]. Moreover, osterix overexpression plays a crucial role in early bone formation by upregulating alkaline phosphatase activity and osteocalcin expression, and stimulates the calcification of new forming bone into mature tissue [211]–[213].

Osterix expression was evaluated with CLM, and results are presented in Figure 3-9.

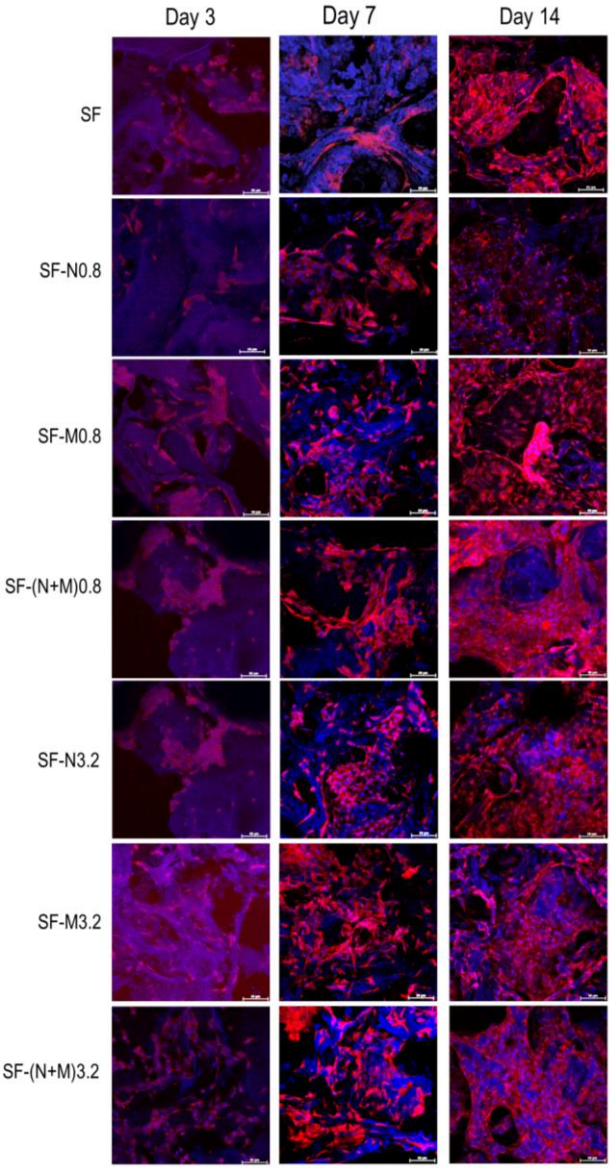

Figure 3-9: Confocal scanning laser microscopy images of samples stained with specific antibody for observation of the signal and organization of Osterix (red) after day 3, 7 and 14 of culture and DAPI for nuclei (blue) of all scaffolds (scale bar = 50 µm)

Osterix signal increases appreciably with incubation time and with the amount of added particles. After 3 days the signal is more evident in the sample containing 3.2 % of particles, at 7 days in all composites with respect to the pure fibroin scaffold, and differences flatten at the last experimental time point. The up-regulation of osterix expression, as well as its distribution in SF/DPs scaffolds, indicates an increased osteogenic activity, which could result in the enhancement of early bone formation by osteoblasts with addition of diatom particles.

Collagen type I is the major component of bone ECM and compose about 80% of total protein content [214].

We detected the expression of collagen type I already at early time points, mainly around the cell nuclei up to 7 days, this meaning that it could be protocollagen. In particular, the expression of collagen type I precursor in scaffolds with DPs was significantly higher than in the control (silk fibroin scaffold only), especially in SF-(N+M)3.2 composite. A significant increase can be observed after 7 days of incubation together with the assembly of collagen into a network especially for the higher DPs content scaffold (Figure 3-10).

The above results on collagen type I production and assembling are coherent with the previous findings on cells proliferation and metabolic activity.

Moreover, the presence of soluble silicon stimulates the propyl hydroxylase enzyme activity, which is strongly correlated with bone formation and maturation, this supporting the hypothesis that the silicon released from DPs dissolution might trigger collagen type I synthesis by MG63 besides the effect of cell proliferation. Additionally, the interaction between collagen and proteoglycans [103] might improve the deposition and organization of collagen type I fibers produced by osteoblast-like cells. At last, the presence of silicic acid released from diatom particles during cell culture at low concentration might promote the collagen type I production as well as self–assembly of collagen type in fibrils due to the interaction between collagen and silicon's possibility [148].

The obtained experimental data suggest that DPs, in particular at higher concentration, boost cell proliferation rate at early time points and up-regulate the early bone markers osterix and collagen type I production and organization.

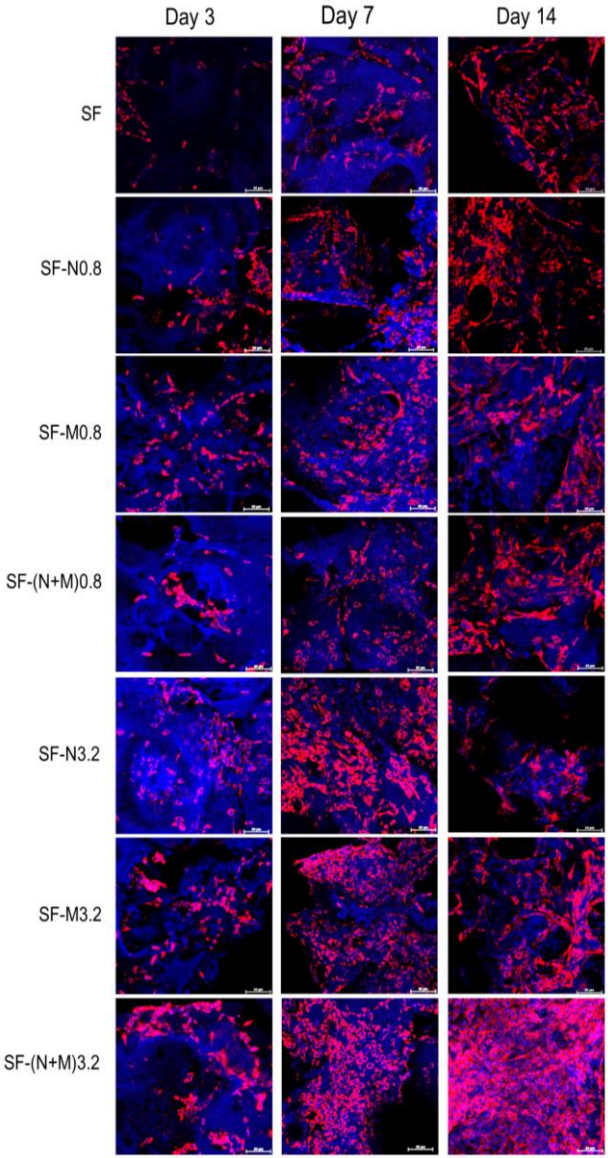

Figure 3-10: Confocal scanning laser microscopy images of samples stained with specific antibody for observation of the signal and organization of collagen type I (red) occurred after day 3, 7 and 14 of incubation and DAPI for nuclei (blue) of all scaffolds (scale bar = 50μm).

3.3.4 Alkaline phosphatase quantification

Alkaline phosphatase (ALP) is the central player in the process of osteogenesis. ALP level and activity are considered as a classical early osteogenic marker, particularly used in in vitro experiment as predictor of bone maturation and mineralization process [215], [216]. The results of ALP activity in MG63 seeded in SF or composite scaffolds within 14 days of culture are presented in Figure 3-11. ALP production increased with incubation time for all scaffolds, being always higher for composites with respect to the pure fibroin material. A sudden increase could be detected in composite scaffolds at 7 days, and even more at 14 days of incubation, where the values are three times higher than for pure fibroin.

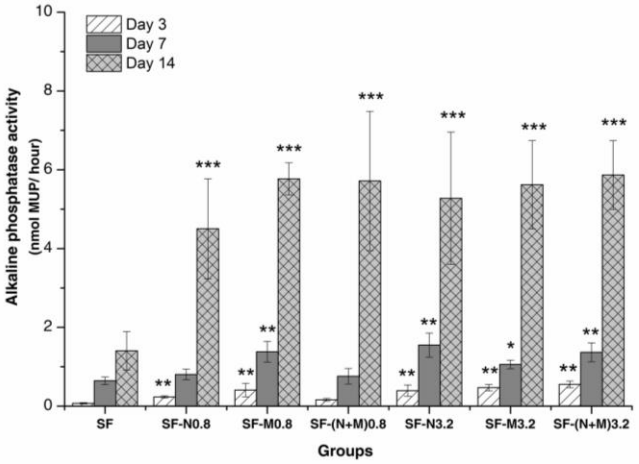

Figure 3-11: The effect of scaffold formulations on alkaline phosphatase (ALP) activity induced by MGG3 during 3, 7 and 14 days of culture showed the upgrading of ALP activity with the presence of diatom particles (DPs) on scaffolds, compared with silk fibroin scaffold – SF. Significant difference was representative at * ($p<0.05$), ** ($p<0.01$) and *** ($p<0.005$), compared with the control at the same time of culture.

The noticeable up-regulation of total ALP amount in composite SF/DPs scaffolds could be explained by the known bioactivity of silica as an osteogenic agent. Moreover, the release of silicon from DPs

dissolution might participate in enhancing ALP production in osteoblasts, which can be combined with the significant increase of cell proliferation with the addition of diatoms. The obtained results are in agreement with the previous findings about the soluble silicon function on osteoblastic differentiation, especially the increase of alkaline phosphatase activity.

3.4 Conclusion

In conclusion, we demonstrated the improvement of bioactivity of 3D fibroin scaffolds loaded with diatom particles for bone regeneration application. As reported, scaffold characterization, including morphology, porosity, elastic modulus as well as structure by FTIR and biological evaluation of diatom particles/ silk fibroin scaffold were performed and compared to silk fibroin scaffold.

Significant up-regulation of collagen type I and osterix signals as well as amount of ALP enzyme were detected.

Based on above results on the biological activities of- from osteoblast-like MG63 cell line, we conclude that diatom particles can supplement silk fibroin scaffolds to support osteoblast activity, adhesion and proliferation.

We propose the addition of DPs to silk fibroin sponges, as a method to induce osteogenesis and to promote early bone formation.

So far, the combination of silk fibroin and DPs can be considered as a new system for bone tissue engineering

Chapter 4: Osteoinductive Silk fibroin/ Diatom Particles Scaffold for Bone Tissue Regeneration

This chapter was collaborated with Dr. Volha Liaudanskaya

Abstract

Loss of bone function constitutes a serious disability for a high number of patients, especially osteoporosis in older people. To date, bone regeneration remains a very challenging method to recover the lost function, but still requires materials and procedures not consolidated yet. We have demonstrated that diatom particles can be used as osteogenic additives to improve the bioactivity of silk fibroin scaffolds. Here, we investigated the osteoinduction promoted by diatom particles in silk fibroin scaffolds to induce bone tissue regeneration.

The addition of diatoms improved ALP induction, earlier formation of fibronectin and production of collagen type I in human mesenchymal stem cells cultures, compared to a control system.

4.1 Introduction

Bone healing is an active process to recover skeletal formation in human body after suffering from fracture or disease. This process can be facilitated by three main components of tissue engineering including scaffold materials, cells and bioactive factors [217]. Up to date, for bone graft application, biomaterials are required to be not only osteoconductive but also osteoinductive to strongly support and induce cell differentiation in osteogenic cells for the synthesis of new bone [218], [219].

As already told, silk fibroin is an excellent candidate for bone tissue engineering due to biocompatibility and controllable biodegradability, tunable mechanical properties and manufacturability, being moreover osteoconductive [123], [189], [192]. However, silk alone has limited osteoinductive properties for bone formation [220]. Therefore, the incorporation of appropriate inorganic particles able to promote

osteoinduction in SF scaffolds could help to achieve a successful bone regeneration pathway.

Amongst various inorganic osteoinductive particles such as titanium oxide, calcium phosphate, hydroxyapatite particles [146],[202], biomaterials containing silicon can trigger bone formation due to silicic acid released from them. In the previous chapter, we elucidated that diatom particles, as a potential source of silica incorporated in silk fibroin, up-regulate bioactivity of osteoblast-like cell and promote earlier new bone formation.

The induction of osteogenesis by a bone graft is a critical point for a fast and successful bone healing process [221]–[223].

The aim of present study was to evaluate the induction of osteogenesis, i.e. osteoinduction, of silk fibroin loaded diatom-particles scaffolds. Herein, scaffold osteinductive ability was evaluated with human mesenchymal stem cells (hMSC), in two different culture media including expansion and osteogenic differentiation medium.

4.2 Materials and methods

4.2.1 Materials

Silk fibroin solution, diatom particles and method of scaffold fabrication have been presented in the chapter 3. In this chapter, we fabricated two groups of porous scaffolds fabricated by a salt leaching method: silk fibroin alone (the negative control) and silk fibroin loaded with 3.2% by weight of diatom nanoparticles/microparticles (SF-(N+M)3.2).

Scaffolds were cut into cylinders 2 x 6 mm of height vs. diameter, and autoclaved at 1 bar, 121˚C for 45 minutes before use.

Reagents including phosphate buffer solution (PBS), sodium hydroxide (NaOH), hydrochloric acid (HCl), lithium bromide (LiBr), Triton X-100, sodium chloride (NaCl), formalin, bovine serum albumin (BSA), 4, 6 diamidino-2-phenyindole, dilactate (DAPI), polyethylene glycol (PEG) and ethanol were purchased from Sigma-Aldrich (St. Louis, MO, USA).

4.2.2 Cell culture

Human mesenchymal stem cells (hMSC) were subcultured in 175 mm^2 culture flasks coated with collagen in Dulbecco's Modified Eagle

Medium (DMEM) supplemented with 20% of foetal bovine serum (FBS), 1% of penicillin/ Streptomycin (P/S), at 37˚C with 5% CO_2 . Medium was changed every three days till cells reached around 80% of confluence.

Before seeding cells, scaffolds were placed into a 48-wells plate and conditioned with 400µl of expansion medium for 30mins, then dried under hood for 1.5 hours. Afterwards, aliquots of media (30µl) containing 10^5 cells were seeded on the top of each scaffold, incubated under hood for 1.5 hours, and then added with 400 µl of expansion medium into each well. After 24 hours, seeded scaffolds were transferred into a new plate and added with two different media: DMEM with 10% of FBS, 0.1µM of dexamethasone (Sigma- Aldrich), 10mM of ß-glycerophosphate, 50µM Ascorbic acid (differentiated media) and expansion medium. Cells were cultured up to 21 days. Both differentiation and expansion media were carefully changed every three days until the testing point.

4.2.3 In vitro experiment

4.2.3.1 Cell proliferation

The proliferation rate of MG63 cells in the sponges was determined with DNA quantification by using Quant-iT PicoGreen® dsDNA Assay Kit (Invitrogen, Molecular Probes, Oregon, USA) following the manufacturer's instructions. In brief, total DNA content was collected with 0.5ml of Triton-X 0.05%, after the short wash in PBS. All the DNA samples were stored at -20 ^{0}C before quantification. Prior assay, all samples were thawed at room temperature and sonicated for 20 seconds (cycle: 1, amplitude 40%). After, DNA was diluted to the suitable concentration and PicoGreen was used for quantification. Fluorescent intensity of PicoGreen-DNA complex was measured in 96-well black plates with a plate reader (Safire, Tecan, Austria). A calibration curve was built up by using the DNA standard provided with the kit to correlate the fluorescent intensity to the concentration of DNA in the studied samples.

4.2.3.2 Immunocytochemistry

Immunocytochemistry against fibronectin and collagen I was used to evaluate the potential differentiation of hMSCs. At every tested time points of cell culture, samples were taken, washed with PBS (without

Ca^{2+} and Mg^{2+}) and then fixed with 4% of formalin for 30 min at room temperature (RT). Subsequently, samples were blocked and permeabilized with buffer containing 1% of BSA and 0.3% of triton X in PBS for 1 hour at RT, stained with the diluted (1:200 in 1% of BSA/ PBS buffer) primary antibody against collagen type I (Meridian Life Science, Saco, ME, USA) and fibronectin (ab23751 - abcam, Cambrige, UK) overnight at 4^0C and triple washed with PBS for 10 minutes each. Then, samples were incubated with secondary antibodies (anti-rabbit Alexa Fluor 568, Molecular Probes, Grand Island, NY) diluted 1:500 in PBS for both fibroinectin and collagen type I for 1 hour, followed by triple washing with PBS. Finally, the samples were incubated with DAPI solution (1:1000) for 10 minutes at RT. Samples were washed with PBS before visualization acquired with the confocal laser microscope.

4.2.3.3 Alkaline phosphatase quantification

The alkaline phosphatase (ALP) activity was measured on the cell lysates. At each experimental time point, cell culture medium was removed and samples were washed 3 times with PBS before adding 0.5 ml of Triton X – 0.05% in PBS per well. Samples were incubated for 30 minutes at room temperature (RT) and then frozen at -20^0C until all samples were collected. Before measurement, samples were thawed and sonicated on ice for 20 seconds (cycle: 1, amplitude 40%) with a Virsonic ultrasonic cell disrupter (Virtis, Warmister, PA). ALP activity was measured following the manufacturer's instructions (ab83371 ALP assay Fluorometric, Cambrige, UK) with a standard curve in the range from 0.0 to 0.4 nmol 4-MUP. ALP concentration was measured by fluorescent intensity at 360/ 440 nm (Ex/ Em) using TECAN (Austria) microplate reader according to the standard curve data.

4.2.3.4 Statistical analysis

All biological tests were performed on three samples with triplicate measurement for each sample. Data are presented as mean ± standard error. One way or two way of variance (ANOVA, originPro 8.5.1) was used to evaluate significant difference among the control (silk fibroin scaffold) and composite scaffolds. The significant difference of two data sets was defined at $p<0.05$.

4.3 Results and discussion

4.3.1 Cell proliferation

Human mesenchymal stem cells require an appropriate cell numbers to differentiate. Cell proliferation was determined by using DNA quantification assay presented in Figure 4-1. In general, the addition of diatom particles did not show any effects on hMSCs proliferation in both media; though, a statistically significant increase of cell number was found in composite scaffold loaded with diatom particles at day 21 in expansion medium.

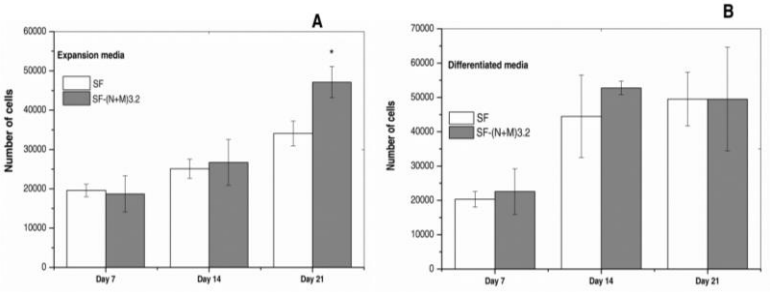

Figure 4-1: Cell proliferation in expansion and differentiated medium up to 21 day of culture of two scaffold groups, pure silk fibroin (SF) and silk fibroin loading 3.2% of diatom particles mixed nanoparticles and microparticles. Statistically significant difference compared with the control at the same time of culture was representative at * ($p<0.05$).

A slight difference of the cell proliferated behaviour was showed in different media. Particularly, the numbers of retained cells in two groups of scaffolds progressively increased during the cell growth in the expansion medium while differentiation medium enhanced the hMSCs proliferation up to day 14 of culture, with no further increase detected at day 21. Surprisingly, the number of retained cells in all scaffolds in both media was, in fact, smaller than that of cell seeded, 10^5 cells, at the starting point.

However, the effect of silicon released from composite scaffolds was quite evident in the expansion medium, as previous literature reported [224]. In the differentiation medium the effect is less clear, since osteogenic differentiating agents such as dexamethasone could trigger the proliferation rate of hMSCs.

4.3.2 Immunocytochemistry

Fibronectin (FN) is a major component of extracellular matrix, which is a crucial factor inducing bone cell differentiation. FN is the earliest proteins synthesized by osteoblast [225],[226]. Moreover, the presence of insoluble FN may facilitate physiological processes of bone healing including angiogenesis, thrombosis, inflammation [227]. FN expression was examined by CLM, and results are presented in Figure 4-2.

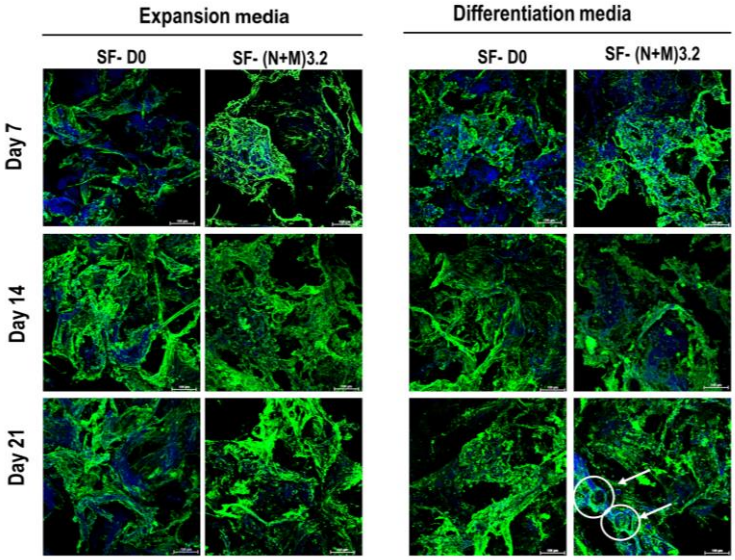

Figure 4-2: Confocal scanning laser microscopy images of samples stained with specific antibody for observing fibronectin (green) synthesized after day 7, 14 and 21 of hMCSs incubation and DAPI for nuclei (blue) of two groups of scaffold; SF– pure silk fibroin, and SF-(N+M) 3.2 – silk fibroin loading 3.2 % of diatom particles combined of nanoparticles (DNPs) and microparticles DMPs (scale bar = 50µm) in two different medium. The arrows may show the region of bone lacunae.

In both media, results showed that FN was obviously observed at the first time point and highly expressed at day 14, but decreased at the last time point.

In particular, in expansion medium, FN expression in SF-(N+M)3.2, both signal and distribution at day 7, are higher if compared to the

negative control. No more difference of FN was observed in expansion medium at day 14 as well as day 21 of culture.
FN expression of pure and composite scaffold in differentiation medium behaves like expansion. The FN expression in the composite sample was higher than in pure silk fibroin at the day 7. However, FN expression in silk fibroin scaffold seemed to be higher in distribution and signal, compared to composite scaffold at day 14.

It is known that type I collagen accounts for 80% of bone ECM proteins, which can be synthesized by osteoblasts during the bone development [228].

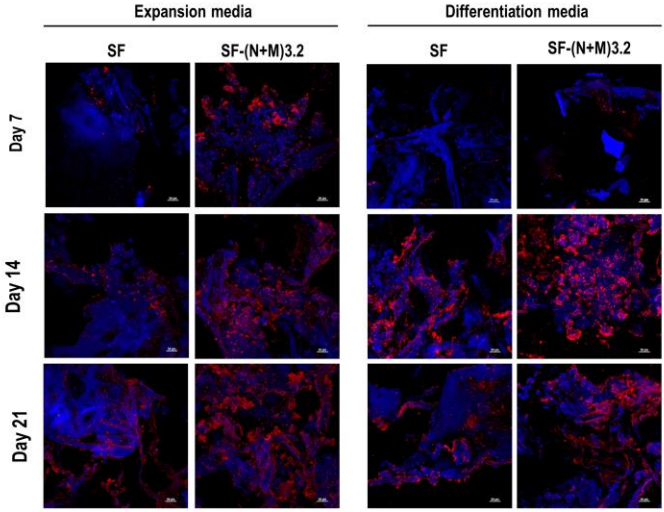

Figure 4-3: Confocal scanning laser microscopy images of samples stained with specific antibody for observing collagen type I (red) synthesized after day 7, 14 and 21 of hMCSs incubation and DAPI for nuclei (blue) of two groups of scaffold; SF– pure silk fibroin, and SF-(N+M) 3.2 – silk fibroin loading 3.2 % of diatom particle combined nanoparticles (DNPs) and microparticles DMPs (scale bar = 50µm) in two different medium.

The obtained results indicated that collagen I expression in term of distribution and signal in composite scaffolds is generally much

higher than in pure silk fibroin in both culture conditions. Distribution and signal seemed to be reduced in the day 21 (Figure 4-3).
The explanation could be that the silicon ion released from composite scaffold during cell culture is able to increase hMSCs proliferation and differentiation of hMSCs into osteoblasts, that significantly improved the synthesis of collagen type I [105], [224]. The result of collagen expression is in agreement with the strong effects of soluble silicon on the bone formation reported by the previous literature [103]. The decrease of collagen expression at day 21 could be due to the mineralization of collagen, that we have tried to evaluate.
However, the assay was unsuccessful because fibroin masked the signal.

4.3.3 Alkaline phosphatase quantification

It is known that alkaline phosphatase (ALP) plays an important role on the osteogenesis process which occurs during bone maturation amongst the major osteogenic hallmarks. Therefore, ALP behaviour has been used as biomarker to monitor bone formation process [216], [229].
As shown in the Figure 4-4, ALP production gradually increased during 21-day of culture in expansion medium. Moreover, as expected, the addition of diatom particles into silk fibroin scaffold induced higher ALP amounts.

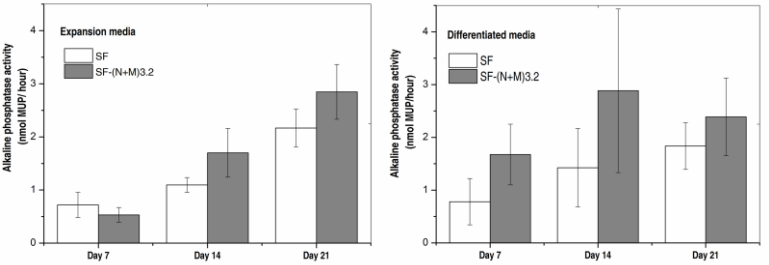

Figure 4-4: Quantification of alkaline phosphatase activity induced by hMSCs seeded into two different scaffolds; pure silk fibroin (SF) and silk fibroin loading 3.2% of diatom particles mixed nanoparticles and microparticles; up to 21 day in expansion and differentiated medium, respectively.

In differentiated medium ALP activity presented a maximum after 14 days, then decreasing at day 21, accordingly with the findings already reported about cell proliferation.
We hypothesize that the release of silicon from DPs dissolution may contribute to the ALP production. This has been previous reported in the case of osteoblasts [208]. Together with the activity of soluble silicon, differentiation media could also trigger earlier ALP production [224], [229].

4.4 Conclusion

Consequently, in this chapter, we preliminary demonstrated that the silk fibroin loaded diatom particles improved differentiation potential of hMSCs regarding earlier fibronectin and collagen type I formation as well as increased ALP production, compared to the control.
The conducted study could provide proofs for diatom particles application as promising osteoinductive additives for bone healing.

Final Conclusion

The novelty of our work is in the use of diatom particles–derived from natural fossil diatom skeletons as a silicon donor triggering bone formation in scaffolds suitable for bone tissue regeneration.

Thesis aimed to profoundly understand the produced materials throughout various methods such as electron scanning microscope (SEM), X-ray diffraction (XRD), X-ray photoelectron spectroscopy (XPS) and transmission electron microscope (TEM).

Diatom microparticles and nanoparticles were successfully produced. These particles showed potential biomedical use displaying limited or absence of toxicity in in-vitro up to 500 µg/ml of concentration as determined by lactate dehydrogenase (LDH) assays.

The silicon ion release from diatom particles dissolution that was evaluated by inductively coupled plasma optical emission spectrometry (ICP/OES), provided strongly supporting evidence for possible application of diatoms on bone regeneration as silicon donors.

In order to access bone tissue application, silk fibroin loaded with diatom particles with different amount and size was used to fabricate 3D scaffolds by using the salt leaching method. The effect of diatom particles on scaffold properties was studied in terms of morphology, porosity, structure, mechanical properties and biological main features.

In biological evaluations with osteoblast-like cells MG63, we found that silk/ diatom particles scaffold significantly enhanced cell metabolic activity (Alamar Blue® assay), proliferation rate (Quant-iT PicoGreen® dsDNA Assay), viability and distribution (calcein AM and propidium iodide staining). Furthermore, triggering of early bone formation determined throughout alkaline phosphatase induction (ALP fluorometric assay) and collagen type I and osterix expression (immunocytochemistry staining) was found in composite silk/ diatom particles scaffold in comparison to silk alone.

Following the obtained result in osteoblast-like cells, we investigated the effect of the developed silk/ diatom particles systems on human mesenchymal stem cells (hMSCs) cultures. We established that diatom particles addition improved ALP activity and collagen type I

expression and triggered earlier formation of fibronectin compared to pure silk fibroin.

In other words, silk/ diatom particles induced differentiation of human mesenchymal stem cells.

This work, overall, introduced a new promising biomaterial system for bone tissue regeneration.

In perspective, mineralization should be evaluated; moreover, further studies in vivo are necessary to fully prove the beneficial effect of the addition of diatom particles to silk fibroin scaffolds on bone healing. On the other hand, deeper studies about the interaction between diatom particles and silk fibroin at molecular level should be performed to better understand the effect of diatom particles addition on scaffold topography and silk conformation.

References

[1] R. Gordon, D. Losic, M. A. Tiffany, S. S. Nagy, and F.A.S. Sterrenburg, “The Glass Menagerie: diatoms for novel applications in nanotechnology,” *Trends Biotechnol.*, vol. 27, no. 2, pp. 116–127, 2009.

[2] Simpson, TL., Volcani, BE., *Silicon and Siliceous Structures in biology system*. 1981, Springer-Verlag, New York, Inc: USA.

[3] T. Brembu, P. Winge, A. Tooming-Klunderud, A. J. Nederbragt, K. S. Jakobsen, and A. M. Bones, “The chloroplast genome of the diatom Seminavis robusta: New features introduced through multiple mechanisms of horizontal gene transfer,” *Mar. Genomics*, vol. 16, pp. 17–27, 2014.

[4] N. Kröger and E. Brunner, “Complex-shaped microbial biominerals for nanotechnology.,” *Wiley Interdiscip. Rev. Nanomed. Nanobiotechnol.*, vol. 6, no. 6, pp. 615–27, 2014.

[5] B. Tesson and M. Hildebrand, “Extensive and intimate association of the cytoskeleton with forming silica in diatoms: control over patterning on the meso- and micro-scale.,” *PLoS One*, vol. 5, no. 12, p. e14300, 2010.

[6] E. G. Vrieling, T. P. M. Beelen, R. A. van Santen, and W. W. C. Gieskes, “Diatom silicon biomineralization as an inspirational source of new approaches to silica production,” *Prog. Ind. Microbiol.*, vol. 35, no. C, pp. 39–51, 1999.

[7] D. Losic, R. J. Pillar, T. Dilger, J. G. Mitchell, and N. H. Voelcker, “Atomic force microscopy (AFM) characterisation of the porous silica nanostructure of two centric diatoms,” *J. Porous Mater.*, vol. 14, no. 1, pp. 61–69, 2007.

[8] L. Abramson, S. Wirick, C. Lee, C. Jacobsen, and J. A. Brandes, “The use of soft X-ray spectromicroscopy to investigate the distribution and composition of organic matter in a diatom frustule and a biomimetic analog,” *Deep. Res. Part II Top. Stud. Oceanogr.*, vol. 56, no. 18, pp. 1369–1380, 2009.

[9] I. E. Pamirsky and K. S. Golokhvast, “Silaffins of diatoms: From applied biotechnology to biomedicine,” *Mar. Drugs*, vol. 11, no. 9, pp. 3155–3167, 2013.

[10] A. Scheffel, N. Poulsen, S. Shian, and N. Kröger, “Nanopatterned protein microrings from a diatom that direct silica morphogenesis.,” *Proc. Natl. Acad. Sci. U. S. A.*, vol. 108, no. 8, pp. 3175–3180, 2011.

[11] L. G. Frigeri, T. R. Radabaugh, P. a Haynes, and M. Hildebrand, “Identification of Proteins from a Cell Wall Fraction of the Diatom Thalassiosira pseudonana Insights into Silica Structure Formation,” *Mol. Cell. Proteomics*, vol. 5, no. 1, pp. 182–193, 2006.

[12] N. Kröger, G. Lehmann, R. Rachel, and M. Sumper, “Characterization of a 200-kDa diatom protein that is specifically associated with a silica-based substructure of the cell wall.,” *Eur. J. Biochem.*, vol. 250, no. 1, pp. 99–105, 1997.

[13] N. Kröger, R. Deutzmann, C. Bergsdorf, and M. Sumper, “Species-specific polyamines from diatoms control silica morphology.,” *Proc. Natl. Acad. Sci. U. S. A.*, vol. 97, no. 26, pp. 14133–14138, 2000.

[14] W. H. van de Poll, E. G. Vrieling, and W. W. C. Gieskes, “Location and expression of frustulins in the pennate diatoms Cylindrotheca fusiformis,

Navicula pelliculosa, and Navicula salinarum (Bacillariophyceae)," *J Phycol*, vol. 35, pp. 1044–1053, 1999.
[15] N. Kroger, C. Bergsdorf, and M. Sumper, "A new calcium binding glycoprotein family constitutes a major diatom cell wall component," *EMBO J.*, vol. 13, no. 19, pp. 4676–4683, 1994.
[16] M. Sumper and E. Brunner, "Learning from Diatoms: Nature's Tools for the Production of Nanostructured Silica," *Adv. Funct. Mater.*, vol. 16, no. 1, pp. 17–26, 2006.
[17] N. Kröger and R. Wetherbee, "Pleuralins are involved in theca differentiation in the diatom Cylindrotheca fusiformis.," *Protist*, vol. 151, no. 3, pp. 263–273, 2000.
[18] C. C. Lechner and C. F. W. Becker, "Silaffins in silica biomineralization and biomimetic silica precipitation," *Mar. Drugs*, vol. 13, no. 8, pp. 5297–5333, 2015.
[19] N. Kröger, R. Deutzmann, and M. Sumper, "Polycationic peptides from diatom biosilica that direct silica nanosphere formation.," *Science*, vol. 286, no. 5442, pp. 1129–1132, 1999.
[20] N. Kröger, S. Lorenz, E. Brunner, and M. Sumper, "Self-assembly of highly phosphorylated silaffins and their function in biosilica morphogenesis.," *Science*, vol. 298, no. 5593, pp. 584–586, 2002.
[21] N. Poulsen, M. Sumper, and N. Kröger, "Biosilica formation in diatoms: characterization of native silaffin-2 and its role in silica morphogenesis.," *Proc. Natl. Acad. Sci. U. S. A.*, vol. 100, no. 21, pp. 12075–12080, 2003.
[22] M. Sumper, R. Hett, G. Lehmann, and S. Wenzl, "A Code for Lysine Modifications of a Silica Biomineralizing Silaffin Protein," *Angew. Chemie*, vol. 119, no. 44, pp. 8557–8560, 2007.
[23] N. Poulsen and N. Kröger, "Silica morphogenesis by alternative processing of silaffins in the diatom Thalassiosira pseudonana," *J. Biol. Chem.*, vol. 279, no. 41, pp. 42993–42999, 2004.
[24] S. Wenzl, R. Deutzmann, R. Hett, E. Hochmuth, and M. Sumper, "Quaternary ammonium groups in silica-associated proteins," *Angew. Chemie - Int. Ed.*, vol. 43, no. 44, pp. 5933–5936, 2004.
[25] A. I. Manurung, A. R. Pratiwi, and D. Syah, "Isolation and Characterization of Silaffin that Catalyze Biosilica Formation from Marine Diatom C haetoceros gracilis," vol. 14, no. 3, pp. 119–122, 2007.
[26] N. Kröger, "Prescribing diatom morphology: toward genetic engineering of biological nanomaterials," *Curr. Opin. Chem. Biol.*, vol. 11, no. 6, pp. 662–669, 2007.
[27] C. C. Perry, "Silicification: The Processes by Which Organisms Capture and Mineralize Silica," *Rev. Mineral. Geochemistry*, vol. 54, no. 1, pp. 291–327, 2003.
[28] H. Ehrlich, K. D. Demadis, O. S. Pokrovsky, and P. G. Koutsoukos, "Modern views on desilicification: Biosilica and abiotic silica dissolution in natural and artificial environments," *Chem. Rev.*, vol. 110, no. 8, pp. 4656–4689, 2010.
[29] S. M. Oliveira, R. A. Ringshia, R. Z. Legeros, E. Clark, M. J. Yost, L. Terracio, and C. C. Teixeira, "An improved collagen scaffold for skeletal regeneration," *J. Biomed. Mater. Res. - Part A*, vol. 94, no. 2, pp. 371–379, 2010.
[30] D. J. Belton, O. Deschaume, and C. C. Perry, "An overview of the fundamentals of the chemistry of silica with relevance to biosilicification and technological advances," *FEBS J.*, vol. 279, no. 10, pp. 1710–1720, 2012.

[31] M. Hildebrand, B. E. Volcani, W. Gassmann, and J. I. Schroeder, “A gene family of silicon transporters.,” *Nature*, vol. 385, no. 6618, pp. 688–689, 1997.
[32] C. Göbel, B. Schuster, D. Baurecht, U. B. Sleytr, and D. Pum, “S-layer templated bioinspired synthesis of silica,” *Colloids Surf B Biointerfaces,* vol. 75, no. 2, pp. 565–572, 2010.
[33] A. O. Marron, M. J. Alston, D. Heavens, M. Akam, M. Caccamo, P. W. H. Holland, and G. Walker, “A family of diatom-like silicon transporters in the siliceous loricate choanoflagellates.,” *Proc. Biol. Sci.*, vol. 280, no. 1756, p. 20122543, 2013.
[34] K. Thamatrakoln and M. Hildebrand, “Analysis of Thalassiosira pseudonana Silicon Transporters Indicates Distinct Regulatory Levels and Transport Activity through the Cell Cycle,” *Eukaryot. Cell*, vol. 6, no. 2, pp. 271–279, 2007.
[35] M. Hildebrand, “Silicic Acid Transport and Its Control During Cell Wall Silicification in Diatoms,” *Biomineralization*, pp. 159–176, 2005.
[36] A. J. Milligan, “ A Proton Buffering Role for Silica in Diatoms,” *Science (80-.).*, vol. 297, no. September, pp. 2001–2003, 2002.
[37] G. Sapriel, M. Quinet, M. Heijde, L. Jourdren, V. Tanty, G. Luo, S. Le Crom, and P. J. Lopez, “Genome-Wide Transcriptome Analyses of Silicon Metabolism in Phaeodactylum tricornutum Reveal the Multilevel Regulation of Silicic Acid Transporters,” *PLoS One*, vol. 4, no. 10, p. 7458, 2009.
[38] K. Thamatrakoln and M. Hildebrand, “Silicon Uptake in Diatoms Revisited: A Model for Saturable and Nonsaturable Uptake Kinetics and the Role of Silicon Transporters,” *Plant Physiol.*, vol. 146, no. 3, pp. 1397–1407, 2008.
[39] A. Gélabert, O. S. Pokrovsky, J. Schott, A. Boudou, A. Feurtet-Mazel, J. Mielczarski, E. Mielczarski, N. Mesmer-Dudons, and O. Spalla, “Study of diatoms/aqueous solution interface. I. Acid-base equilibria and spectroscopic observation of freshwater and marine species,” *Geochim. Cosmochim. Acta*, vol. 68, no. 20, pp. 4039–4058, 2004.
[40] M. Hildebrand, “Diatoms, biomineralization processes, and genomics,” *Chem. Rev.*, vol. 108, no. 11, pp. 4855–4874, 2008.
[41] M. Sumper, “Biomimetic Patterning of Silica by Long-Chain Polyamines,” *Angew. Chemie*, vol. 116, no. 17, pp. 2301–2304, 2004.
[42] K. V. Kharitonenko, Y. D. Bedoshvili, and Y. V. Likhoshway, “Changes in the micro- and nanostructure of siliceous valves in the diatom Synedra acus under the effect of colchicine treatment at different stages of the cell cycle,” *J. Struct. Biol.*, vol. 190, no. 1, pp. 73–80, 2015.
[43] S. Hazelaar, H. J. van der Strate, W. W. C. Gieskes, and E. G. Vrieling, “Monitoring Rapid Valve Formation in the Pennate Diatom Navicula Salinarum (Bacillariophyceae),” *J. Phycol.*, vol. 41, pp. 354–358, 2005.
[44] M. Fujiwara, K. Shiokawa, I. Sakakura, and Y. Nakahara, “Silica hollow spheres with nano-macroholes like diatomaceous earth.,” *Nano Lett.*, vol. 6, no. 12, pp. 2925–8, 2006.
[45] J. Parkinson, Y. Brechet, and R. Gordon, “Centric diatom morphogenesis: a model based on a DLA algorithm investigating the potential role of microtubules,” *Biochim. Biophys. Acta*, vol. 1452, pp. 89–102, 1999.
[46] M. Sumper, “A phase separation model for the nanopatterning of diatom biosilica.,” *Science*, vol. 295, no. 5564, pp. 2430–2433, 2002.
[47] L. Lenoci and P. J. Camp, “Diatom structures templated by phase-separated fluids,” *Langmuir*, vol. 24, no. 1, pp. 217–223, 2008.

[48] M. Sumper and N. Kröger, “Silica formation in diatoms: the function of long-chain polyamines and silaffins,” *J. Mater. Chem.*, vol. 14, pp. 2059–2065, Jul. 2004.
[49] M. A. Grachev, V. V. Annenkov, and Y. V. Likhoshway, “Silicon nanotechnologies of pigmented heterokonts,” *BioEssays*, vol. 30, no. 4, pp. 328–337, 2008.
[50] M. Gehlen, L. Beck, G. Calas, A. M. Flank, A. J. Van Bennekom, and J. E. E. Van Beusekom, “Unraveling the atomic structure of biogenic silica: Evidence of the structural association of Al and Si in diatom frustules,” *Geochim. Cosmochim. Acta*, vol. 66, no. 9, pp. 1601–1609, 2002.
[51] E. G. Vrieling, Q. Sun, M. Tian, P. J. Kooyman, W. W. C. Gieskes, R.A van Santen, and N. A J. M. Sommerdijk, “Salinity-dependent diatom biosilicification implies an important role of external ionic strength.,” *Proc. Natl. Acad. Sci. U. S. A.*, vol. 104, no. 25, pp. 10441–10446, 2007.
[52] M. Brzezinski, R. Olson, and S. Chisholm, “Silicon availability and cell-cycle progression in marine diatoms ,” *Mar. Ecol. Prog. Ser.*, vol. 67, no. M, pp. 83–96, 1990.
[53] R.M. Crawford, " Valve formation in Diatom and the fate of silicalemma and plasmalemma," *Culture*, vol. 26, pp. 21–26, 1981.
[54] C. P. Bergmann and A. Stumpf. *Dental Ceramics. Microstructure, properties and degradation*. 2013.Springer-Verlag, Berlin Heidelberg, Germany.
[55] D. F. Williams, “On the nature of biomaterials,” *Biomaterials*, vol. 30, no. 30, pp. 5897–5909, 2009.
[56] K. E. Kasza, A. C. Rowat, J. Liu, T. E. Angelini, C. P. Brangwynne, G. H. Koenderink, and D. A. Weitz, “The cell as a material,” *Curr. Opin. Cell Biol.*, vol. 19, no. 1, pp. 101–107, 2007.
[57] F. Barrère, T. A. Mahmood, K. de Groot, and C. A. van Blitterswijk, “Advanced biomaterials for skeletal tissue regeneration: Instructive and smart functions,” *Mater. Sci. Eng. R Reports*, vol. 59, no. 1–6, pp. 38–71, 2008.
[58] M. S. Shoichet, “Polymer scaffolds for biomaterials applications,” *Macromolecules*, vol. 43, no. 2, pp. 581–591, 2010.
[59] G. Binyamin, B. M. Shafi, and C. M. Mery, “Biomaterials: A primer for surgeons,” *Semin. Pediatr. Surg.*, vol. 15, no. 4, pp. 276–283, 2006.
[60] T. V Thamaraiselvi and S. Rajeswari, “Biological Evaluation of Bioceramic Materials - A Review,” *Trends Biomater. Artif. Organs,* vol. 18, no. 1, pp. 9–17, 2004.
[61] L. L. Hench, “Bioceramics: From Concept to Clinic,” *J. Am. Ceram. Soc.*, vol. 74, no. 7, pp. 1487–1510, 1991.
[62] C. Gao, Y. Deng, P. Feng, Z. Mao, P. Li, B. Yang, J. Deng, Y. Cao, C. Shuai, and S. Peng, “Current Progress in Bioactive Ceramic Scaffolds for Bone Repair and Regeneration,” *Int. J. Mol. Sci.*, vol. 15, no. 3, pp. 4714–4732, 2014.
[63] A. Tathe, M. Ghodke, and A. Nikalje, “A brief review: biomaterials and their application,” *Int. J. Pharm. Pharm. Sci.*, vol. 2, no. 4, pp. 19–23, 2010.
[64] B. M. Holzapfel, J. C. Reichert, J. T. Schantz, U. Gbureck, L. Rackwitz, U. Nöth, F. Jakob, M. Rudert, J. Groll, and D. W. Hutmacher, “How smart do biomaterials need to be? A translational science and clinical point of view,” *Adv. Drug Deliv. Rev.*, vol. 65, no. 4, pp. 581–603, 2013.
[65] D. F. Williams, “On the mechanisms of biocompatibility,” *Biomaterials*, vol. 29, no. 20, pp. 2941–2953, 2008.

[66] S.K. Kim, *Fuctional marine Biomaterial. Properties and applications*. 2015.Woodhead Publishing,Cambridge,UK.
[67] G.H.Nancollas, *Biological mineralization and demineralization*.1982, Springer-Verlag, Berlin Heidelberg, Germany.
[68] N. Zeytuni and R. Zarivach, "Crystallization and preliminary crystallographic analysis of the Magnetospirillum magneticum AMB - 1 and M. gryphiswaldense MSR-1 magnetosome-associated proteins MamA," *Acta Crystallogr. Sect. F Struct. Biol. Cryst. Commun.*, vol. 66, no. 7, pp. 824–827, 2010.
[69] G. M. Whitesides and G. M. Whitesides, "Bioinspiration : something for everyone," 2015.
[70] C. Valéry, F. Artzner, B. Robert, T. Gulick, G. Keller, C. Grabielle-Madelmont, M.-L. Torres, R. Cherif-Cheikh, and M. Paternostre, "Self-association process of a peptide in solution: from beta-sheet filaments to large embedded nanotubes.," *Biophys. J.*, vol. 86, no. 4, pp. 2484–2501, 2004.
[71] A. E. Rawlings, J. P. Bramble, and S. S. Staniland, "Innovation through imitation: biomimetic, bioinspired and biokleptic research," *Soft Matter*, vol. 8, no. 25, p. 6675, 2012.
[72] J. F. V. Vincent, O. a. Bogatyreva, N. R. Bogatyrev, A. Bowyer, and A.-K. Pahl, "Biomimetics: its practice and theory," *J. R. Soc. Interface*, vol. 3, no. 9, pp. 471–482, 2006.
[73] H. Ehrlich, *Biological materials of marine origin. Invertebrates.* 2010. Springer Dordrecht Heidelberg London, New York, USA.
[74] C. Vepari and D. L. Kaplan, "Silk as a biomaterial," *Prog. Polym. Sci.*, vol. 32, no. 8–9, pp. 991–1007, 2007.
[75] J. Sirichaisit, V. L. Brookes, R. J. Young, and F. Vollrath, "Analysis of structure/property relationships in silkworm (Bombyx mori) and spider dragline (Nephila edulis) silks using raman spectroscopy," *Biomacromolecules*, vol. 4, no. 2, pp. 387–394, 2003.
[76] A. Motta, L. Fambri, and C. Migliaresi, "Regenerated Silk Fibroin Films: Thermal and Dynamic Mechanical Analysis," *Spectrum*, vol. 203, pp. 1658–1665, 2002.
[77] G. H. Altman, F. Diaz, C. Jakuba, T. Calabro, R. L. Horan, J. Chen, H. Lu, J. Richmond, and D. L. Kaplan, "Silk-based biomaterials," *Biomaterials*, vol. 24, no. 3, pp. 401–416, 2003.
[78] S. Weiner and P. M. Dove, "An overview of biomineralization processes and the problem of the vital effect," *Rev. Mineral.*, vol. 54, no. 1, pp. 1–29, 2003.
[79] S. Weiner, "Biomineralization: A structural perspective," *J. Struct. Biol.*, vol. 163, no. 3, pp. 229–234, 2008.
[80] L. Addadi, S. Raz, and S. Weiner, "Taking advantage of disorder: Amorphous calcium carbonate and its roles in biomineralization," *Adv. Mater.*, vol. 15, no. 12, pp. 959–970, 2003.
[81] G. De With and N. A.J. M. Sommerdijk, "$CaCO_3$ Formation Revealed by Cryo-TEM," *Science (80-.).*, vol. 587, no. March, pp. 2007–2010, 2009.
[82] R. B. Frankel and D. A. Bazylinski, "Biologically induced mineralization by bacteria," *Rev. Mineral. Geochemistry*, vol. 54, no. 1, pp. 95–114, 2003.
[83] D. A. Bazylinski and R. B. Frankel, "Biologically Controlled Mineralization in Prokaryotes," *Rev. Mineral. Geochemistry*, vol. 54, no. 1, pp. 217–247, 2003.
[84] L. A. Estroff, "Introduction: Biomineralization," *Chem. Rev.*, vol. 108, no. 11, pp. 4329–4331, 2008.

[85] M. J. Olszta, X. Cheng, S. S. Jee, R. Kumar, Y. Y. Kim, M. J. Kaufman, E. P. Douglas, and L. B. Gower, “Bone structure and formation: A new perspective,” *Mater. Sci. Eng. R Reports*, vol. 58, no. 3–5, pp. 77–116, 2007.
[86] E. Bonucci, “The Mineralization of Bone and Its Analogies with Other Hard Tissues,” *Adv. Top. Cryst. Growth*, pp. 145–184, 2013.
[87] M. E. E. Maitland and A. L. L. Arsenault, “A correlation between the distribution of biological apatite and amino acid sequence of type I collagen.,” *Calcif. Tissue Int.*, vol. 48, no. 5, pp. 341–52, 1991.
[88] F. Nudelman, K. Pieterse, A. George, P. H. Bomans, H. Friedrich, L. J. Brylka, P. A. Hilbers, G. de With, and N. A. Sommerdijk, “The role of collagen in bone apatite formation in the presence of hydroxyapatite nucleation inhibitors,” *Nat. Mater.*, vol. 9, no. 12, pp. 1004–1009, 2010.
[89] M. R. Rogel, H. Qiu, and G. A. Ameer, “The role of nanocomposites in bone regeneration,” *J. Mater. Chem.*, vol. 18, no. 36, p. 4233, 2008.
[90] S. Weiner, W. Traub, and H. D. Wagner, “Lamellar Bone : Structure – Function Relations,” vol. 255, pp. 241–255, 1999.
[91] J. Y. Rho, L. Kuhn-Spearing, and P. Zioupos, “Mechanical properties and the hierarchical structure of bone,” *Med. Eng. Phys.*, vol. 20, no. 2, pp. 92–102, 1998.
[92] E. M. Carlisle, “Silicon: a possible factor in bone calcification.,” *Science*, vol. 167, no. 3916, pp. 279–80, Jan. 1970.
[93] W. J. Landis, D. D. Lee, J. T. Brenna, S. Chandra, and G. H. Morrison, “Detection and localization of silicon and associated elements in vertebrate bone tissue by imaging ion microscopy,” *Calcif. Tissue Int.*, vol. 38, no. 1, pp. 52–59, 1986.
[94] S. B. Cho, F. Miyaji, T. Kokubo, K. Nakanishi, N. Soga, and T. Nakamura, “Apatite-forming ability of silicate ion dissolved from silica gels.,” *J. Biomed. Mater. Res.*, vol. 32, no. 3, pp. 375–81, 1996.
[95] N. B. Matsko, N. Žnidaršič, I. Letofsky-Papst, M. Dittrich, W. Grogger, J. Štrus, and F. Hofer, “Silicon: The key element in early stages of biocalcification,” *J. Struct. Biol.*, vol. 174, no. 1, pp. 180–186, 2011.
[96] N. Patel, S. M. Best, W. Bonfield, I. R. Gibson, K. a. Hing, E. Damien, and P. A. Revell, “A comparative study on the in vivo behavior of hydroxyapatite and silicon substituted hydroxyapatite granules,” *J. Mater. Sci. Mater. Med.*, vol. 13, no. 12, pp. 1199–1206, 2002.
[97] K. A. Hing, P. A. Revell, N. Smith, and T. Buckland, “Effect of silicon level on rate, quality and progression of bone healing within silicate-substituted porous hydroxyapatite scaffolds,” *Biomaterials*, vol. 27, no. 29, pp. 5014–5026, 2006.
[98] S. Heinemann, T. Coradin, and M. F. Desimone, “Bio-inspired silica–collagen materials: applications and perspectives in the medical field,” *Biomater. Sci.*, vol. 1, no. 7, p. 688, 2013.
[99] F. H. Nielsen, “Micronutrients in Parenteral Nutrition: Boron, Silicon, and Fluoride,” *Gastroenterology*, vol. 137, no. 5 SUPPL, pp. S55–S60, 2009.
[100] J. D. Birchall, “The interrelationship between silicon and aluminium in the biological effects of aluminium,” *Ciba Found Symp.,* vol 169, pp. 50-61, 1992 .
[101] S. Zou, D. Ireland, R. A. Brooks, N. Rushton, and S. Best, “The effects of silicate ions on human osteoblast adhesion, proliferation, and differentiation,” *J. Biomed. Mater. Res. B. Appl. Biomater.*, vol. 90, no. 1, pp. 123–130, Jul. 2009.
[102] G. Mestres, C. Le Van, and M. P. Ginebra, “Silicon-stabilized α-tricalcium phosphate and its use in a calcium phosphate cement:

characterization and cell response.," *Acta Biomater.*, vol. 8, no. 3, pp. 1169–79, 2012.
[103] D. M. Reffitt, N. Ogston, R. Jugdaohsingh, H. F. J. Cheung, B. A. J. Evans, R. P. H. Thompson, J. J. Powell, and G. N. Hampson, "Orthosilicic acid stimulates collagen type 1 synthesis and osteoblastic differentiation in human osteoblast-like cells in vitro," *Bone*, vol. 32, no. 2, pp. 127–135, 2003.
[104] T. Gao, H. T. Aro, H. Ylänen, and E. Vuorio, "Silica-based bioactive glasses modulate expression of bone morphogenetic protein-2 mRNA in Saos-2 osteoblasts in vitro.," *Biomaterials*, vol. 22, no. 12, pp. 1475–83, 2001.
[105] S. Amorim, A. Martins, N. M. Neves, R. L. Reis, and R. A. Pires, "Hyaluronic acid/poly- L-lysine bilayered silica nanoparticles enhance the osteogenic differentiation of human mesenchymal stem cells," *J. Mater. Chem. B*, vol. 2, no. 40, pp. 6939–6946, 2014.
[106] R. Schamberger, *Biochemistry of the Essential Ultratrace Elements*. 1984. Plenum Press, New York, USA.
[107] H. Rico, J. L. Gallego-Lago, E. R. Hernández, L. F. Villa, A. Sanchez-Atrio, C. Seco, and J. J. Gérvas, "Effect of silicon supplement on osteopenia induced by ovariectomy in rats.," *Calcif. Tissue Int.*, vol. 66, no. 6, pp. 53–55, 2000.
[108] G. R. Beck, S. W. Ha, C. E. Camalier, M. Yamaguchi, Y. Li, J. K. Lee, and M. N. Weitzmann, "Bioactive silica-based nanoparticles stimulate bone-forming osteoblasts, suppress bone-resorbing osteoclasts, and enhance bone mineral density in vivo," *Nanomedicine Nanotechnology, Biol. Med.*, vol. 8, no. 6, pp. 793–803, 2012.
[109] R. Jugdaohsingh, A. I. E. Watson, P. Bhattacharya, G. H. van Lenthe, and J. J. Powell, "Positive association between serum silicon levels and bone mineral density in female rats following oral silicon supplementation with monomethylsilanetriol," *Osteoporos. Int.*, vol. 26, no. 4, pp. 1405–1415, 2015.
[110] R. Jugdaohsingh, "Silicon and bone health.," *J. Nutr. Health Aging*, vol. 11, no. 2, pp. 99–110, 2009.
[111] J. A. Auer, "Principles of fracture treatment," *Equine Surg.*, pp. 1000–1029, 2006.
[112] L. C. Gerstenfeld, D. M. Cullinane, G. L. Barnes, D. T. Graves, and T. a. Einhorn, "Fracture healing as a post-natal developmental process: Molecular, spatial, and temporal aspects of its regulation," *J. Cell. Biochem.*, vol. 88, no. 5, pp. 873–884, 2003.
[113] P. M. Kou and J. E. Babensee, "Macrophage and dendritic cell phenotypic diversity in the context of biomaterials," *J. Biomed. Mater. Res. - Part A*, vol. 96 A, no. 1, pp. 239–260, 2011.
[114] L. Sorokin, "The impact of the extracellular matrix on inflammation," *Nat. Publ. Gr.*, vol. 10, no. 10, pp. 712–723, 2010.
[115] J. Lamovec, E. Možina, and B. Baebler, "Hyperplastic callus formation in osteogenesis imperfecta," *Ann. Diagn. Pathol.*, vol. 7, no. 4, pp. 231–235, 2003.
[116] R. Langer and J. V. Vacanti, "Tissue Engineering," Science., vol. 260, pp. 920–925, 1993.
[117] M. Teschner, "Tissue engineering of bone tissue," *Z. Orthop. Ihre Grenzgeb.*, vol. 137, no. 6, pp. Oa4–a7, 2002.
[118] A. J. Salgado, O. P. Coutinho, and R. L. Reis, "Bone tissue engineering: State of the art and future trends," *Macromol. Biosci.*, vol. 4, no. 8, pp. 743–765, 2004.

[119] D. W. Hutmacher, “Scaffolds in tissue engineering bone and cartilage,” *Biomaterials*, vol. 21, no. 24, pp. 2529–2543, 2000.
[120] A. R. C. Duarte, J. F. Mano, and R. L. Reis, “Preparation of starch-based scaffolds for tissue engineering by supercritical immersion precipitation,” *J. Supercrit. Fluids*, vol. 49, no. 2, pp. 279–285, 2009.
[121] M. P. Lutolf, P. M. Gilbert, and H. M. Blau, “Designing materials to direct stem-cell fate.,” *Nature*, vol. 462, no. 7272, pp. 433–41, 2009.
[122] K. J. Burg, S. Porter, and J. F. Kellam, “Biomaterial developments for bone tissue engineering.,” *Biomaterials*, vol. 21, no. 23, pp. 2347–2359, 2000.
[123] B. B. Mandal and S. C. Kundu, “Cell proliferation and migration in silk fibroin 3D scaffolds,” *Biomaterials*, vol. 30, no. 15, pp. 2956–2965, 2009.
[124] M. Mason, K. P. Vercruysse, K. R. Kirker, R. Frisch, D. M. Marecak, G. D. Prestwich, and W. G. Pitt, “Attachment of hyaluronic acid to polypropylene, polystyrene, and polytetrafluoroethylene,” *Biomaterials*, vol. 21, no. 1, pp. 31–36, 2000.
[125] J. C. Middleton and A. J. Tipton, “Synthetic biodegradable polymers as orthopedic devices.,” *Biomaterials*, vol. 21, no. 23, pp. 2335–2346, 2000.
[126] R. J. Kroeze, M. N. Helder, L. E. Govaert, and T. H. Smit, “Biodegradable polymers in bone tissue engineering,” *Materials (Basel).*, vol. 2, no. 3, pp. 833–856, 2009.
[127] F. Yang, W. Cui, Z. Xiong, L. Liu, J. Bei, and S. Wang, “Poly(l,l-lactide-co-glycolide)/tricalcium phosphate composite scaffold and its various changes during degradation in vitro,” *Polym. Degrad. Stab.*, vol. 91, no. 12, pp. 3065–3073, 2006.
[128] Y.-P. Guo, J.-J. Guan, J. Yang, Y. Wang, C.-Q. Zhang, and Q.-F. Ke, “Hybrid nanostructured hydroxyapatite–chitosan composite scaffold: bioinspired fabrication, mechanical properties and biological properties,” *J. Mater. Chem. B*, vol. 3, pp. 4679–4689, 2015.
[129] Q. Lv and Q. Feng, “Preparation of 3-D regenerated fibroin scaffolds with freeze drying method and freeze drying/foaming technique,” *J. Mater. Sci. Mater. Med.*, vol. 17, no. 12, pp. 1349–1356, 2006.
[130] C. A. Heath, “Cells for tissue engineering.,” *Trends Biotechnol.*, vol. 18, no. 1, pp. 17–9, 2000.
[131] A. R. Amini, C. T. Laurencin, and S. P. Nukavarapu, “Bone tissue engineering: recent advances and challenges.,” *Crit. Rev. Biomed. Eng.*, vol. 40, no. 5, pp. 363–408, 2012.
[132] E. Jimi, S. Hirata, K. Osawa, M. Terashita, C. Kitamura, and H. Fukushima, “The current and future therapies of bone regeneration to repair bone defects,” *Int. J. Dent.*, vol. 2012, pp. 1–8, 2012.
[133] F. R. A. J. Rose and R. O. C. Oreffo, “Bone Tissue Engineering: Hope vs Hype,” *Biochem. Biophys. Res. Commun.*, vol. 292, no. 1, pp. 1–7, 2002.
[134] E. Jabbarzadeh, T. Starnes, Y. M. Khan, T. Jiang, A. J. Wirtel, M. Deng, Q. Lv, L. S. Nair, S. B. Doty, and C. T. Laurencin, “Induction of angiogenesis in tissue-engineered scaffolds designed for bone repair: a combined gene therapy-cell transplantation approach.,” *Proc. Natl. Acad. Sci. U. S. A.*, vol. 105, no. 32, pp. 11099–11104, 2008.
[135] A. J. Mieszawska, N. Fourligas, I. Georgakoudi, N. M. Ouhib, D. J. Belton, C. C. Perry, and D. L. Kaplan, “Osteoinductive silk-silica composite biomaterials for bone regeneration,” *Biomaterials*, vol. 31, no. 34, pp. 8902–8910, Dec. 2010.

[136] L. E. Antonides, “Diatomite,” *U.S. Geol. Surv. Miner. Yearb. 1997*, pp. 1–6, 1997.
[137] M. Aivalioti, P. Papoulias, A. Kousaiti, and E. Gidarakos, “Adsorption of BTEX, MTBE and TAME on natural and modified diatomite,” *J. Hazard. Mater.*, vol. 207–208, pp. 117–127, 2012.
[138] W. Xiong and J. Peng, “Development and characterization of ferrihydrite-modified diatomite as a phosphorus adsorbent,” *Water Res.*, vol. 42, no. 19, pp. 4869–4877, 2008.
[139] M. S. Aw, S. Simovic, Y. Yu, J. Addai-Mensah, and D. Losic, “Porous silica microshells from diatoms as biocarrier for drug delivery applications,” *Powder Technol.*, vol. 223, pp. 52–58, 2012.
[140] M. Bariana, M. S. Aw, M. Kurkuri, and D. Losic, “Tuning drug loading and release properties of diatom silica microparticles by surface modifications,” *Int. J. Pharm.*, vol. 443, no. 1–2, pp. 230–241, 2013.
[141] P. J. Lopez, J. Desclés, A. E. Allen, and C. Bowler, “Prospects in diatom research,” *Curr. Opin. Biotechnol.*, vol. 16, no. 2, pp. 180–186, 2005.
[142] J. N. Cha, G. D. Stucky, D. E. Morse, and T. J. Deming, “Biomimetic synthesis of ordered silica structures mediated by block copolypeptides,” vol. 403, no. January, pp. 289–292, 2000.
[143] N. Poulsen, C. Berne, J. Spain, and N. Kröger, “Silica immobilization of an enzyme through genetic engineering of the diatom Thalassiosira pseudonana,” *Angew. Chemie - Int. Ed.*, vol. 46, no. 11, pp. 1843–1846, 2007.
[144] B. Delalat, V. C. Sheppard, S. Rasi Ghaemi, S. Rao, C. A. Prestidge, G. McPhee, M.-L. Rogers, J. F. Donoghue, V. Pillay, T. G. Johns, N. Kröger, and N. H. Voelcker, “Targeted drug delivery using genetically engineered diatom biosilica,” *Nat. Commun.*, vol. 6, p. 8791, 2015.
[145] C. Groger, K. Luzt, E. Brunne, “Biomolecular Self-assembly and its Relevance in Silica Biomineralization,” *Cell Biochemi Biophys*., vol 50, pp. 23–39, 2008.
[146] Y. Zhang, C. Wu, T. Friis, and Y. Xiao, “The osteogenic properties of CaP/silk composite scaffolds,” *Biomaterials*, vol. 31, no. 10, pp. 2848–2856, 2010.
[147] M. F. Desimone, C. Hélary, I. B. Rietveld, I. Bataille, G. Mosser, M. M. Giraud-Guille, J. Livage, and T. Coradin, “Silica-collagen bionanocomposites as three-dimensional scaffolds for fibroblast immobilization,” *Acta Biomater.*, vol. 6, no. 10, pp. 3998–4004, 2010.
[148] D. Eglin, K. L. Shafran, J. Livage, T. Coradin, and C. C. Perry, “Comparative study of the influence of several silica precursors on collagen self-assembly and of collagen on "Si" speciation and condensation,” *J. Mater. Chem.*, vol. 16, no. 43, p. 4220, 2006.
[149] H. C. Schröder, F. Natalio, I. Shukoor, W. Tremel, U. Schloßmacher, X. Wang, and W. E. G. Müller, “Apposition of silica lamellae during growth of spicules in the demosponge Suberites domuncula: Biological/biochemical studies and chemical/biomimetical confirmation,” *J. Struct. Biol.*, vol. 159, no. 3, pp. 325–334, 2007.
[150] X. Wang, H. C. Schröder, V. Grebenjuk, B. Diehl-Seifert, V. Mailänder, R. Steffen, U. Schloßmacher, and W. E. G. Müller, “The marine sponge-derived inorganic polymers, biosilica and polyphosphate, as morphogenetically active matrices/scaffolds for the differentiation of human multipotent stromal cells: Potential application in 3D printing and distraction osteogenesis,” *Mar. Drugs*, vol. 12, no. 2, pp. 1131–1147, 2014.

[151] E. M. Carlisle, “Silicon: A requirement in bone formation independent of vitamin D1,” *Calcif. Tissue Int.*, vol. 33, no. 1, pp. 27–34, Dec. 1981.
[152] K. D. Cashman, “Milk minerals (including trace elements) and bone health,” *Int. Dairy J.*, vol. 16, no. 11, pp. 1389–1398, 2006.
[153] C. T. Price, K. J. Koval, and J. R. Langford, “Silicon: A review of its potential role in the prevention and treatment of postmenopausal osteoporosis,” *Int. J. Endocrinol.*, vol. 2013, 2013.
[154] Y. F. Zhang, Y. F. Zheng, and L. Qin, “A comprehensive biological evaluation of ceramic nanoparticles as wear debris,” *Nanomedicine Nanotechnology, Biol. Med.*, vol. 7, no. 6, pp. 975–982, 2011.
[155] A. Tautzenberger, A. Kovtun, and A. Ignatius, “Nanoparticles and their potential for application in bone,” *Int. J. Nanomedicine*, p. 4545, 2012.
[156] D. Napierska, L. C. J. Thomassen, D. Lison, J. A. Martens, and P. H. Hoet, “The nanosilica hazard: another variable entity.,” *Part. Fibre Toxicol.*, vol. 7, no. 1, p. 39, 2010.
[157] T. H. Chung, S.H. Wu, M. Yao, C. W. Lu, Y.S. Lin, Y. Hung, C.Y. Mou, Y.C. Chen, and D. M. Huang, “The effect of surface charge on the uptake and biological function of mesoporous silica nanoparticles in 3T3-L1 cells and human mesenchymal stem cells,” *Biomaterials*, vol. 28, no. 19, pp. 2959–2966, Jul. 2007.
[158] D. M. Brown, N. Kanase, B. Gaiser, H. Johnston, and V. Stone, “Inflammation and gene expression in the rat lung after instillation of silica nanoparticles: Effect of size, dispersion medium and particle surface charge,” *Toxicol. Lett.*, vol. 224, no. 1, pp. 147–156, 2014.
[159] S. Quignard, G. Mosser, M. Boissière, and T. Coradin, “Long-term fate of silica nanoparticles interacting with human dermal fibroblasts,” *Biomaterials*, vol. 33, no. 17, pp. 4431–4442, 2012.
[160] G. R. Beck, S. W. Ha, C. E. Camalier, M. Yamaguchi, Y. Li, J.-K. Lee, and M. N. Weitzmann, “Bioactive silica-based nanoparticles stimulate bone-forming osteoblasts, suppress bone-resorbing osteoclasts, and enhance bone mineral density in vivo,” *Nanomedicine nanotechnology, Biol. Med.*, vol. 8, no. 6, pp. 793–803, Aug. 2012.
[161] S. W. Ha, J.A. Sikorski, M. N. Weitzmann, and G. R. Beck, “Bio-active engineered 50nm silica nanoparticles with bone anabolic activity: Therapeutic index, effective concentration, and cytotoxicity profile in vitro,” *Toxicol. Vitr.*, vol. 28, no. 3, pp. 354–364, 2014.
[162] I. R. Gibson, S. M. Best, and W. Bonfield, “Chemical characterization of silicon-substituted hydroxyapatite,” *J. Biomed. Mater. Res.*, vol. 44, no. 4, pp. 422–428, Mar. 1999.
[163] W. Xu, C. Ganz, U. Weber, M. Adam, G. Holzhüter, D. Wolter, B. Frerich, B. Vollmar, and T. Gerber, “Evaluation of injectable silica-embedded nanohydroxyapatite bone substitute in a rat tibia defect model.,” *Int. J. Nanomedicine*, vol. 6, pp. 1543–1552, 2011.
[164] M. L. Foglia, D. E. Camporotondi, G. S. Alvarez, S. Heinemann, T. Hanke, C. J. Perez, L. E. Diaz, and M. F. Desimone, “A new method for the preparation of biocompatible silica coated-collagen hydrogels,” *J. Mater. Chem. B*, vol. 1, no. 45, p. 6283, 2013.
[165] J. E. N. Dolatabadi and M. de la Guardia, “Applications of diatoms and silica nanotechnology in biosensing, drug and gene delivery, and formation of complex metal nanostructures,” *TrAC - Trends Anal. Chem.*, vol. 30, no. 9, pp. 1538–1548, 2011.
[166] I. Ruggiero, M. Terracciano, N. M. Martucci, L. De Stefano, N. Migliaccio, R. Tatè, I. Rendina, P. Arcari, A. Lamberti, and I. Rea,

"Diatomite silica nanoparticles for drug delivery," *Nanoscale Res. Lett.*, vol. 9, no. 1, p. 329, 2014.
[167] O. Şan, R. Gören, and C. Özgür, "Purification of diatomite powder by acid leaching for use in fabrication of porous ceramics," *Int. J. Miner. Process.*, vol. 93, no. 1, pp. 6–10, 2009.
[168] E. Gulturk, "Thermal and acid treatment of diatom frustules," *Manuf. Eng.*, vol. 46, no. 2, pp. 196–203, 2011.
[169] S. Brunauer, P. H. Emmett, and E. Teller, "Adsorption of Gases in Multimolecular Layers," *J. Am. Chem. Soc.*, vol. 60, no. 2, pp. 309–319, Feb. 1938.
[170] E. P. Barrett, L. G. Joyner, and P. P. Halenda, "The Determination of Pore Volume and Area Distributions in Porous Substances. I. Computations from Nitrogen Isotherms," *J. Am. Chem. Soc.*, vol. 73, no. 1, pp. 373–380, Jan. 1951.
[171] E. Koning, M. Gehlen, A. M. Flank, G. Calas, and E. Epping, "Rapid post-mortem incorporation of aluminum in diatom frustules: Evidence from chemical and structural analyses," *Mar. Chem.*, vol. 103, no. 1–2, pp. 97–111, 2007.
[172] M. Sumper and N. Kroger, "Silica formation in diatoms : the function of long-chain polyamines and silaffins," *J. Mater. Chem.,*14, pp. 2059–2065, 2004.
[173] K. S. W. Sing, D. H. Everett, R. A. W. Haul, L. Moscou, R. A. Pierotti, J. Rouquerol, and T. Siemieniewska, "Reporting physisorption data for gas/solid systems with special reference to the determination of surface area and porosity," *Pure Appl. Chem.*, vol. 57, no. 4, pp. 603–619, Jan. 1985.
[174] S. Kaufhold, R. Dohrmann, M. Klinkenberg, S. Siegesmund, and K. Ufer, "N_2-BET specific surface area of bentonites.," *J. Colloid Interface Sci.*, vol. 349, no. 1, pp. 275–282, Sep. 2010.
[175] R. Viitala, M. Jokinen, S. L. Maunu, H. Jalonen, and J. B. Rosenholm, "Chemical characterization of bioresorbable sol-gel derived SiO_2 matrices prepared at protein-compatible pH," *J. Non. Cryst. Solids*, vol. 351, no. 40–42, pp. 3225–3234, 2005.
[176] J. P. Icenhower and P. M. Dove, "The dissolution kinetics of amorphous silica into sodium chloride solutions: effects of temperature and ionic strength," *Geochim. Cosmochim. Acta*, vol. 64, no. 24, pp. 4193–4203, Dec. 2000.
[177] C. O. Metin, L. W. Lake, C. R. Miranda, and Q. P. Nguyen, "Stability of aqueous silica nanoparticle dispersions," *J. Nanoparticle Res.*, vol. 13, no. 2, pp. 839–850, 2011.
[178] L. T. Zhuravlev, "The surface chemistry of amorphous silica," *Colloids Surf.*, vol. 173, pp. 1–38, 2000.
[179] Z. Elias, O. Poirot, I. Fenoglio, M. Ghiazza, M. C. Danière, F. Terzetti, C. Darne, C. Coulais, I. Matekovits, and B. Fubini, "Surface reactivity, cytotoxic, and morphological transforming effects of diatomaceous earth products in Syrian hamster embryo cells," *Toxicol. Sci.*, vol. 91, no. 2, pp. 510–520, 2006.
[180] M. Stoppato, H. Y. Stevens, E. Carletti, C. Migliaresi, A. Motta, and R. E. Guldberg, "Effects of silk fibroin fiber incorporation on mechanical properties, endothelial cell colonization and vascularization of PDLLA scaffolds," *Biomaterials*, vol. 34, no. 19, pp. 4573–4581, 2013.
[181] Q. Z. Chen, A. Efthymiou, V. Salih, and A. R. Boccaccini, "Bioglass®-derived glass-ceramic scaffolds: Study of cell proliferation and scaffold

degradation in vitro," *J. Biomed. Mater. Res. - Part A*, vol. 84, no. 4, pp. 1049–1060, 2008.
[182] C. L. Camiré, S. Jegou Saint-Jean, C. Mochales, P. Nevsten, J. S. Wang, L. Lidgren, I. McCarthy, and M. P. Ginebra, "Material characterization andin vivo behavior of silicon substituted α-tricalcium phosphate cement," *J. Biomed. Mater. Res. Part B Appl. Biomater.*, vol. 76B, no. 2, pp. 424–431, 2006.
[183] S. Foppiano, S. J. Marshall, G. W. Marshall, E. Saiz, and A. P. Tomsia, "Bioactive glass coatings affect the behavior of osteoblast-like cells.," *Acta Biomater.*, vol. 3, no. 5, pp. 765–71, 2007.
[184] C. He, F. Zhang, L. Cao, W. Feng, K. Qiu, Y. Zhang, H. Wang, X. Mo, and J. Wang, "Rapid mineralization of porous gelatin scaffolds by electrodeposition for bone tissue engineering," *J. Mater. Chem.*, vol. 22, no. 5, p. 2111, 2012.
[185] X. Hu, K. Shmelev, L. Sun, E. Gil, S. Park, P. Cebe, and D. L. Kaplan, "Regulation of silk material structure by temperature- controlled water vapor annealing," *Biomacromolecules,* vol. 12, no. 5, pp. 1686–1696, 2012.
[186] E. S. Gil, S. H. Park, X. Hu, P. Cebe, and D. L. Kaplan, "Impact of Sterilization on the Enzymatic Degradation and Mechanical Properties of Silk Biomaterials," *Macromol. Biosci.*, vol. 14, no. 2, pp. 257–269, 2014.
[187] Y. Wang, D. D. Rudym, A. Walsh, L. Abrahamsen, H. J. Kim, H. S. Kim, C. Kirker-Head, and D. L. Kaplan, "In vivo degradation of three-dimensional silk fibroin scaffolds," *Biomaterials*, vol. 29, no. 24–25, pp. 3415–3428, 2008.
[188] L. Ghorbanian, R. Emadi, S. M. Razavi, H. Shin, and A. Teimouri, "Fabrication and characterization of novel diopside/silk fibroin nanocomposite scaffolds for potential application in maxillofacial bone regeneration," *Int. J. Biol. Macromol.*, vol. 58, pp. 275–280, 2013.
[189] D. Yao, S. Dong, Q. Lu, X. Hu, D. L. Kaplan, B. Zhang, and H. Zhu, "Salt-leached silk scaffolds with tunable mechanical properties.," *Biomacromolecules*, vol. 13, no. 11, pp. 3723–9, 2012.
[190] M. Fini, A. Motta, P. Torricelli, G. Giavaresi, N. Nicoli Aldini, M. Tschon, R. Giardino, and C. Migliaresi, "The healing of confined critical size cancellous defects in the presence of silk fibroin hydrogel," *Biomaterials*, vol. 26, pp. 3527–3536, 2005.
[191] Y. Wang, E. Bella, C. S. D. Lee, C. Migliaresi, L. Pelcastre, Z. Schwartz, B. D. Boyan, and A. Motta, "The synergistic effects of 3-D porous silk fibroin matrix scaffold properties and hydrodynamic environment in cartilage tissue regeneration," *Biomaterials*, vol. 31, no. 17, pp. 4672–4681, 2010.
[192] W. H. Elliott, W. Bonani, D. Maniglio, A. Motta, W. Tan, and C. Migliaresi, "Silk Hydrogels of Tunable Structure and Viscoelastic Properties Using Different Chronological Orders of Genipin and Physical Cross-Linking," *ACS Appl. Mater. Interfaces*, vol. 7, no. 22, pp. 12099–12108, 2015.
[193] D. N. Rockwood, R. C. Preda, T. Yucel, X. Wang, M. L. Lovett, and D. L. Kaplan, "Materials fabrication from Bombyx mori silk fibroin," *Nat Protoc*, vol. 6, no. 10, pp. 1612–1631, 2011.
[194] C. Foss, C. Migliaresi, and A. Motta, "The optimization of a scaffold for cartilage regeneration.," *Organogenesis*, vol. 9, no. 1, pp. 19–21, 2013.

[195] A. J. Mieszawska, J. G. Llamas, C. A. Vaiana, M. P. Kadakia, R. R. Naik, and D. L. Kaplan, “Clay enriched silk biomaterials for bone formation,” *Acta Biomater.*, vol. 7, no. 8, pp. 3036–3041, 2011.
[196] C. Correia, S. Bhumiratana, L.-P. Yan, A. L. Oliveira, J. M. Gimble, D. Rockwood, D. L. Kaplan, R. A. Sousa, R. L. Reis, and G. Vunjak-Novakovic, “Development of silk-based scaffolds for tissue engineering of bone from human adipose-derived stem cells,” *Acta Biomater.*, vol. 8, no. 7, pp. 2483–2492, 2012.
[197] E. Ko and S. W. Cho, “Biomimetic polymer scaffolds to promote stem cell-mediated osteogenesis,” *Int. J. Stem Cells*, vol. 6, no. 2, pp. 87–91, 2013.
[198] H. Liu, G. W. Xu, Y. F. Wang, H. S. Zhao, S. Xiong, Y. Wu, B. C. Heng, C. R. An, G. H. Zhu, and D. H. Xie, “Composite scaffolds of nano-hydroxyapatite and silk fibroin enhance mesenchymal stem cell-based bone regeneration via the interleukin 1 alpha autocrine/paracrine signaling loop,” *Biomaterials*, vol. 49, pp. 103–112, 2015.
[199] A. Verket, H. Tiainen, H. J. Haugen, S. P. Lyngstadaas, O. Nilsen, and J. E. Reseland, “Enhanced osteoblast differentiation on scaffolds coated with TiO_2 compared to SiO_2 and CaP coatings,” *Biointerphases*, vol. 7, no. 1–4, pp. 1–10, 2012.
[200] X. Huang, X. Teng, D. Chen, F. Tang, and J. He, “The effect of the shape of mesoporous silica nanoparticles on cellular uptake and cell function,” *Biomaterials*, vol. 31, no. 3, pp. 438–448, 2010.
[201] F. Maehira, Y. Iinuma, Y. Eguchi, I. Miyagi, and S. Teruya, “Effects of soluble silicon compound and deep-sea water on biochemical and mechanical properties of bone and the related gene expression in mice,” *J. Bone Miner. Metab.*, vol. 26, no. 5, pp. 446–455, 2008.
[202] A. K. Gaharwar, S. M. Mihaila, A. Swami, A. Patel, S. Sant, R. L. Reis, A. P. Marques, M. E. Gomes, and A. Khademhosseini, “Bioactive silicate nanoplatelets for osteogenic differentiation of human mesenchymal stem cells,” *Adv. Mater.*, vol. 25, no. 24, pp. 3329–3336, 2013.
[203] I. Izquierdo-Barba, M. Colilla, and M. Vallet-Regí, “Nanostructured mesoporous silicas for bone tissue regeneration,” *J. Nanomater.*, vol. 2008, no. 1, 2008.
[204] X. Wang, H. C. Schröder, Q. Feng, F. Draenert, and W. E. G. Müller, “The deep-sea natural products, biogenic polyphosphate (bio-polyp) and biogenic silica (bio-silica), as biomimetic scaffolds for bone tissue engineering: Fabrication of a morphogenetically-active polymer,” *Mar. Drugs*, vol. 11, no. 3, pp. 718–746, 2013.
[205] T. D. H. Le, W. Bonani, G. Speranza, V. Sglavo, R. Ceccato, D. Maniglio, A. Motta, and C. Migliaresi, “Processing and characterization of diatom nanoparticles and microparticles as potential source of silicon for bone tissue engineering,” *Mater. Sci. Eng. C*, vol. 59, pp. 471–479, 2016.
[206] L. P. Yan, J. M. Oliveira, A. L. Oliveira, S. G. Caridade, J. F. Mano, and R. L. Reis, “Macro/microporous silk fibroin scaffolds with potential for articular cartilage and meniscus tissue engineering applications,” *Acta Biomater.*, vol. 8, no. 1, pp. 289–301, 2012.
[207] U.J. Kim, J. Park, H. J. Kim, M. Wada, and D. L. Kaplan, “Three-dimensional aqueous-derived biomaterial scaffolds from silk fibroin,” *Biomaterials*, vol. 26, no. 15, pp. 2775–2785, 2005.

[208] E. J. Kim, S. Y. Bu, M. K. Sung, and M. K. Choi, “Effects of Silicon on Osteoblast Activity and Bone Mineralization of MC3T3-E1 Cells.,” *Biol. Trace Elem. Res.*, vol. 152, no. 1, pp. 105–12, 2013.
[209] S. Strecker, Y. Fu, Y. Liu, and P. Maye, “Generation and characterization of Osterix-Cherry reporter mice.,” *Genesis*, vol. 51, no. 4, pp. 246–58, 2013.
[210] K. Nakashima and B. De Crombrugghe, “Transcriptional mechanisms in osteoblast differentiation and bone formation,” *Trends Genet.*, vol. 19, no. 8, pp. 458–466, 2003.
[211] M. M. Ali, T. Yoshizawa, O. Ishibashi, A. Matsuda, M. Ikegame, J. Shimomura, H. Mera, K. Nakashima, and H. Kawashima, “PIASxbeta is a key regulator of osterix transcriptional activity and matrix mineralization in osteoblasts,” *J. Cell Sci.*, vol. 120, no. 15, pp. 2565–2573, 2007.
[212] K. M. Sinha and X. Zhou, “Genetic and molecular control of osterix in skeletal formation,” *J. Cell. Biochem.*, vol. 114, no. 5, pp. 975–984, 2013.
[213] T. Matsubara, K. Kida, A. Yamaguchi, K. Hata, F. Ichida, H. Meguro, H. Aburatani, R. Nishimura, and T. Yoneda, “BMP2 regulates osterix through Msx2 and Runx2 during osteoblast differentiation,” *J. Biol. Chem.*, vol. 283, no. 43, pp. 29119–29125, 2008.
[214] S. Viguet-Carrin, P. Garnero, and P. D. Delmas, “The role of collagen in bone strength,” *Osteoporos. Int.*, vol. 17, no. 3, pp. 319–336, 2006.
[215] A. Javed, H. Chen. F.P. Ghori, “Genetic and transcriptional control bone formation” *Oral Maxillofac Surg Clin North Am*, vol. 2456, no. 205, pp. 1–15, 2011.
[216] H. J. Prins, A. K. Braat, D. Gawlitta, W. J. A. Dhert, D. A. Egan, E. Tijssen-Slump, H. Yuan, P. J. Coffer, H. Rozemuller, and A. C. Martens, “In vitro induction of alkaline phosphatase levels predicts in vivo bone forming capacity of human bone marrow stromal cells.,” *Stem Cell Res.*, vol. 12, no. 2, pp. 428–40, 2014.
[217] W. S. Khan, F. Rayan, B. S. Dhinsa, and D. Marsh, “An osteoconductive, osteoinductive, and osteogenic tissue-engineered product for trauma and orthopaedic surgery: How far are we?,” *Stem Cells Int.*, vol. 2012, 2012.
[218] R. Dimitriou, E. Jones, D. McGonagle, and P. V Giannoudis, “Bone regeneration: current concepts and future directions.,” *BMC Med.*, vol. 9, no. 1, p. 66, 2011.
[219] M. M. Stevens, “Biomaterials for bone tissue engineering,” *Mater. Today*, vol. 11, no. 5, pp. 18–25, 2008.
[220] “Osteoinductive silk fibroin_titanium dioxide_hydroxyapatite hybrid for bone tissue engineering.” .
[221] T. Albrektsson and C. Johansson, “Osteoinduction, osteoconduction and osseointegration,” *Eur. Spine J.*, vol. 10, no. SUPPL. 2, pp. 96–101, 2001.
[222] P. Giannoudis, H. Dinopoulos, and E. Tsiridis, “Bone substitutes: An update,” *Injury*, vol. 36, (Suppl 3), pp. S20–S27, 2005.
[223] R. Bielby, E. Jones, and D. McGonagle, “The role of mesenchymal stem cells in maintenance and repair of bone,” *Injury*, vol. 38, no. SUPPL. 1, 2007.
[224] S. Reis, A. Castro, and M. H. Fernandes, “Bone Anabolic Effects of Soluble Si : In Vitro Studies with Human Mesenchymal Stem Cells and CD14 + Osteoclast Precursors,” 2015.

[225] R. E. Weiss and a. H. Reddi, “Appearance of fibronectin during the differentiation of cartilage, bone, and bone marrow,” *J. Cell Biol.*, vol. 88, no. 3, pp. 630–636, 1981.
[226] C. H. Tang, R. S. Yang, T. H. Huang, S. H. Liu, and W. M. Fu, “Enhancement of Fibronectin Fibrillogenesis and Bone Formation by Basic Fibroblast Growth Factor Via Protein Kinase C-Dependent Pathway in Rat Osteoblasts,” *Mol. Pharmacol.*, vol. 66, no. 3, pp. 440–449, 2004.
[227] E. L. George, E. N. Georges-Labouesse, R. S. Patel-King, H. Rayburn, and R. O. Hynes, “Defects in mesoderm, neural tube and vascular development in mouse embryos lacking fibronectin.,” *Development*, vol. 119, no. 4, pp. 1079–1091, 1993.
[228] C. Niyibizi and D. R. Eyre, “Structural characteristics of cross-linking sites in type V collagen of bone. Chain specificities and heterotypic links to type I collagen.,” *Eur. J. Biochem.*, vol. 224, no. 3, pp. 943–950, 1994.
[229] M. F. Pittenger, A. M. Mackay, S. C. Beck, R. K. Jaiswal, R. Douglas, J. D. Mosca, M. a Moorman, D. W. Simonetti, S. Craig, and D. R. Marshak, “Multilineage potential of adult human mesenchymal stem cells.,” *Science*, vol. 284, no. 5411, pp. 143–7, 1999.

Scientific Production

Manuscripts in International journals

T. D. H. Le, W. Bonani, G. Speranza, V. Sglavo, R. Ceccato, D. Maniglio, A. Motta, and C. Migliaresi, “Processing and characterization of diatom nanoparticles and microparticles as potential source of silicon for bone tissue engineering,” *Mater. Sci. Eng. C*, vol. 59, pp. 471–479, 2016.

T. D. H Le, V. Liaudanskaya, W. Bonani, A. Motta and C. Migliaresi “Enhancing bioactive properties of silk fibroin with diatom particles for bone tissue engineering applications” Tissue Engineering and Regenerative Medicine, Submitted paper.

Participation to Congresses, Schools

8-11thJuly 2015

11th International Symposium on Frontiers in Biomedical Polymers, Riva del Garda, Italy.

Oral presentation. Thi Duy Hanh Le, Walter Bonani, Giorgio Speranza, Devid Maniglio, Antonella Motta, Claudio Migliaresi: "Diatom particles: A potential Source of Biogenic Silica for Bone Regeneration"

6-8th July, 2015

Summer school on Tissue Engineering and Regenerative medicine, Riva del Garda, Italy.

10-13th June, 2014

Tissue Engineering & Regenerative Medicine International Society, European Chapter Meeting, Genova, Italy.

Poster. Thi Duy Hanh Le, Antonella Motta, Luca Dalbosco, Claudio Migliaresi: "The Drug Loading Capacity of Diatomite". Published abstract PP216: on-line Journal of Tissue Engineering and Regenerative Medicine, Volume 8, Issue Supplement s1, pages 334

8-12th July, 2013

Summer school on Tissue Engineering and Regenerative medicine, Riva del Garda,Italy.

Acknowledgement

First of all, I would like to thank One More Step Project (Erasmus Mundus programme) for funding my PhD period.

I would like to express my deepest gratitude to Prof. Claudio Migliaresi, my advisor, for providing me the opportunity to work at BioTech lab, study at University of Trento and complete my PhD thesis. I will never forget his support, guidance and patience that made my thesis work possible. I am extremely grateful and appreciate him for his motivation, enthusiasm, and immense knowledge in many fields.

My sincere thanks also go to Prof. Antonella Motta, my co-advisor, for the knowledge on cell biology, her experimental guidance, her constant encouragement and tolerance and her smile that makes her a special mentor. She has been actively interested in my work and has always been available to advise me.

I also would like to thank Dr. Devid Maniglio and Dr. Walter Bonani for many questions and suggestions that helped me to expand my view.

I truly want to express the warmest thank to Dr. Volha Liaudanskaya, my great colleague, for her friendship, positive thinking and her collaboration work, especially her passion for research. It has been luck for me to have a chance to work with her.

In addition, I thank all present and past members of Biotech during my PhD period; Dr.Tianjing Zhao, Dr. Filippo Benetti, Cristiano Carlomagno, Dr. Luca Dalbosco, Rosasilvia Raggio, Dr. Mariangela Fedel, Dr. Sun Wei, Dr. Sara M. Olivera, Natascia Cozza, Nicola Cagol, Dr. Wichuda Jankangram, Vu Thai Kim Thi, Dr. Eleonora Carletti, Dr. Luca Gasperini, Dr Qiang Quan, Dr. Cristina Foss and Dr. Matteo Stoppato, for sharing their knowledge, a great work environment, friendship, coffees and good time. My deeper appreciation is extended to Lorenzo Moschini, our technician, for his invaluable support in my experiments. I am also greateful to Prof. Sabine Fuchs for her talking and encouragement.

I also would like to thank staff of Erasmus Mundus Office; Marcella Orrù and Sara Rebecchi, and the secretary at Department of Industrial engineering, Sara Di Salvo, for their essential support and administrative issues.

I want to express my gratitude to Prof. Do Quang Minh, Ms. Minh, Ms. Nhi and Dr. Khanh Son - Nguyen from Ho Chi Minh City University of Technology, Viet Nam for valuable support whenever they could.

Specific thanks to Tuan Anh, Sang, Lam, Hien, Hoa, Toan, Nguyen, Linh, Tinh, Nguyet, Duc, Van Anh, Tam, Mr. Hung and Mr. Dung, who are always available to help, talk, and cook for me whenever I need. You are always in my heart.

Thanks to my friends; Lorenzo, Martina, Cristina, Luca, Giacomo, Thuy, Jacopo, Reza, Angela, Alessio; for sharing with me the kitchen, smiling and spreading happiness. They are an amazing source of memories.

Of course, I would like to thank many other people who I know and don't know.

And finally, I would like to express my thankfulness to my family: my grandmother, my parents, my brothers and sisters, my nephew and niece who always give me a constant and unconditional love and acceptance. That love inspired me spiritually throughout my PhD and my life in general.